



# Kent Academic Repository

**Ng, Kendrick (2020) *Design and synthesis of novel DNA-inspired amphiphiles*.  
Master of Research (MRes) thesis, University of Kent,.**

## Downloaded from

<https://kar.kent.ac.uk/86564/> The University of Kent's Academic Repository KAR

## The version of record is available from

<https://doi.org/10.22024/UniKent/01.02.86564>

## This document version

UNSPECIFIED

## DOI for this version

## Licence for this version

CC BY (Attribution)

## Additional information

## Versions of research works

### Versions of Record

If this version is the version of record, it is the same as the published version available on the publisher's web site. Cite as the published version.

### Author Accepted Manuscripts

If this document is identified as the Author Accepted Manuscript it is the version after peer review but before type setting, copy editing or publisher branding. Cite as Surname, Initial. (Year) 'Title of article'. To be published in *Title of Journal*, Volume and issue numbers [peer-reviewed accepted version]. Available at: DOI or URL (Accessed: date).

## Enquiries

If you have questions about this document contact [ResearchSupport@kent.ac.uk](mailto:ResearchSupport@kent.ac.uk). Please include the URL of the record in KAR. If you believe that your, or a third party's rights have been compromised through this document please see our [Take Down policy](https://www.kent.ac.uk/guides/kar-the-kent-academic-repository#policies) (available from <https://www.kent.ac.uk/guides/kar-the-kent-academic-repository#policies>).

**University of Kent**

**Faculty of Sciences**

**School of Physical Sciences (SPS)**

**Design and synthesis of novel DNA-inspired  
amphiphiles**

**By**

**Kendrick Kei-Lun Ng**

**Thesis for the Masters of Science by Research**

**Supervisor: Dr. Jennifer Hiscock**

## Abstract

Antimicrobial resistance has become a major threat to mankind during the last century, no new antimicrobials have been discovered and pharmaceutical companies are no longer investing in the development of new antimicrobials. Due to the overuse and misuse of antibiotics, bacteria are evolving faster than ever. Research has shown that conventional antibiotics, that target specific enzymes, are becoming less effective, whereas amphiphilic antibiotics are still functional. This study aims at developing the efficacy of a novel class of amphiphilic compounds. Building on the work of Hiscock et al., DNA inspired amphiphiles, adenine analogue and thymine, were synthesised and its properties in the solid state, gas phase and solution state were studied.

Analysis of the compounds shows that in the solid state, they tend to form extended structures with several binding modes and in the gas phase the low complex aggregates are visible, showing the strength of the interactions. In the solution state, the amphiphiles tend to form low complex species in DMSO, whereas in a H<sub>2</sub>O: EtOH 19:1 solution, the amphiphiles tend to form extended aggregates (> 100 nm). An investigation of 1:1 mixture of the adenine and thymine compounds was also carried out and the results show similar properties to the other compounds, however, the interactions between the amphiphiles were found to be weak. Antimicrobial screening of the amphiphiles and the mixture shows only the thymine inspired amphiphile inhibits bacterial growth. Based on these results, we can conclude the use of an analogue of adenine has impacted the strength of the complementary base pair interaction, therefore, the amphiphile will be resynthesised with a greater resemblance to adenine.

## Acknowledgments

First and foremost, I would like to thank my mother for all the love and support she has given me. I would also like to express my gratitude to my supervisor Dr. Jennifer Hiscock for all the guidance and help they have provided me throughout the year. Finally, I would like to thank the Hiscock group for all the help and keeping my time here interesting with strange conversations they have involved me in throughout the year.

# Contents Page

Abstract.....	2
Acknowledgments.....	2
Abbreviations.....	5
1. Introduction.....	7
1.1 Development.....	7
1.2 Non-covalent interactions.....	8
1.3 DNA.....	12
1.4 Amphiphiles.....	15
1.5 Project Aims.....	22
2. Results and discussion.....	23
2.1 Synthesis.....	23
2.2 Self-association in the solid state.....	25
2.2.1 Single-crystal X-Ray diffraction.....	25
2.3 Self-association in the gas phase.....	28
2.3.1 Electrospray ionisation mass spectrometry.....	28
2.4 Association in the Solution state.....	31
2.4.1 <sup>1</sup> H NMR quantification studies.....	32
2.4.2 <sup>1</sup> H NMR DOSY studies.....	34
2.4.3 <sup>1</sup> H NMR self-association studies.....	38
2.4.4 <sup>1</sup> H NMR titration studies.....	41
2.4.5 Dynamic light scattering (DLS) and zeta potential.....	48
2.4.6 Surface tension and critical micelle concentration (CMC).....	50
2.5 Low level in-silico modelling.....	51
2.6 Antimicrobial properties.....	53
2.7 Conclusion.....	55
3. Future works.....	55
4. Experimental techniques.....	57
4.1 General remarks.....	57
4.2 DLS studies.....	57
4.3 Zeta potential studies.....	57
4.4 High-resolution mass spectra studies.....	58
4.5 Self-association and association constant calculation.....	58
4.6 Single-crystal X-ray studies.....	58
4. Synthesis.....	58
5. References.....	61
6. Appendix.....	66
6.1 Characterisation NMR.....	66

6.2	Single crystal X-ray structures.....	82
6.3	Mass spectrum data.....	84
6.4	<sup>1</sup> H NMR quantitative studies.....	90
6.5	<sup>1</sup> H NMR DOSY studies .....	95
6.6	<sup>1</sup> H NMR self-association studies .....	98
6.7	<sup>1</sup> H NMR titration studies .....	102
6.8	DLS data .....	108
6.9	Zeta potential.....	116
6.10	Critical micelle concentration .....	119
6.11	Low level in-silico modelling .....	121

Publications not related to this work:

“Towards the Prediction of Global Solution State Properties for Hydrogen-Bonded, Self-Associating Amphiphiles” Lisa J. White, Stilyana N. Tyuleva, Ben Wilson, Helena J. Shepherd, Kendrick K.L. Ng, Simon J. Holder, Ewan R. Clark and Jennifer R. Hiscock, Chemistry-A European Journal, 2018.

“Predicting the efficacy of hydrogen-bonded, self-associating amphiphiles as both antimicrobial and anticancer agents” Nyasha Allen, Lisa J. White, Jessica E. Boles, Laura R. Blackholly, Kendrick K. L. Ng, Nova O. Dora, Dominique F. Chu, Rebecca J. Ellaby, Helena J. Shepherd, Ben Wilson, Michelle D. Garrett, Daniel P. Mulvihill and Jennifer R. Hiscock, 2019. (manuscript submitted for publication)

## Abbreviations

br s	broad singlet (NMR)
CDI	N,N'-Carbonyldiimidazole
CMC	Critical Micelle Concentration
$^{13}\text{C}$	Carbon (NMR)
d	doublet (NMR)
dd	doublet of doublets (NMR)
DCM	Dichloromethane
DLS	Dynamic Light Scattering
DMF	Dimethylformamide
DMSO	Dimethylsulfoxide
DMSO- $d_6$	Deuterated Dimethylsulfoxide
$d_H$	Hydrodynamic diameter
DOSY	Diffusion-ordered spectroscopy
<i>E.coli</i>	Escherichia coli
EDC	1-Ethyl-3-(3-dimethylaminopropyl) carbodiimide
ESI-MS	Electrospray Ionisation Mass spectrometry
EtOAc	Ethyl Acetate
EtOH	Ethanol
FTIR	Fourier transform infrared spectroscopy
HBA	Hydrogen bond acceptor

HBD	Hydrogen bond donor
HOSu	<i>N</i> -Hydroxysuccinimide
J	Coupling constant (NMR)
K <sub>a</sub>	Association constant
m	multiplet (NMR)
M.P	Melting Point
m/z	Mass to charge ratio
NMR	Nuclear magnetic resonance spectroscopy
q	quartet (NMR)
s	singlet (NMR)
<i>S.aureus</i>	<i>Staphylococcus aureus</i>
t	triplet (NMR)
TBA	Tetrabutylammonium

# 1. Introduction

## 1.1 Development

Jean-Marie Lehn coined the term supramolecular chemistry in 1987 during his Nobel Laureate lecture, he defined it as 'chemistry beyond the molecule'.<sup>1</sup> It is the study of the higher complex entities, formed by the result of non-covalent forces.<sup>2</sup> Supramolecular chemistry is considered a young discipline, however, its concepts date back to the beginning of modern chemistry.

Chemistry, as we know it today began when Friedrich Wöhler synthesised urea crystals from inorganic reactants.<sup>3</sup> At the time, this was regarded as impossible as it did not obey the laws of vitalism;<sup>4</sup> which states organic compounds could not be synthesised from inorganic components as it did not possess a certain energy required for life. Following this many other organic substances were synthesised without the use of organic reactants, disproving vitalism.<sup>5</sup> Organic chemistry developed over the next few decades, however, the way the atoms were bonded still remained a controversial topic until 1916, where Gilbert N. Lewis proposed covalent bonding using a theory called 'valence' using a dot and cross diagram (Figure 1).<sup>6</sup> Lewis theorised there were two types of covalent bonding; polar formed by the transfer of electrons and non-polar bonding formed by the sharing of electrons.<sup>7,8</sup>

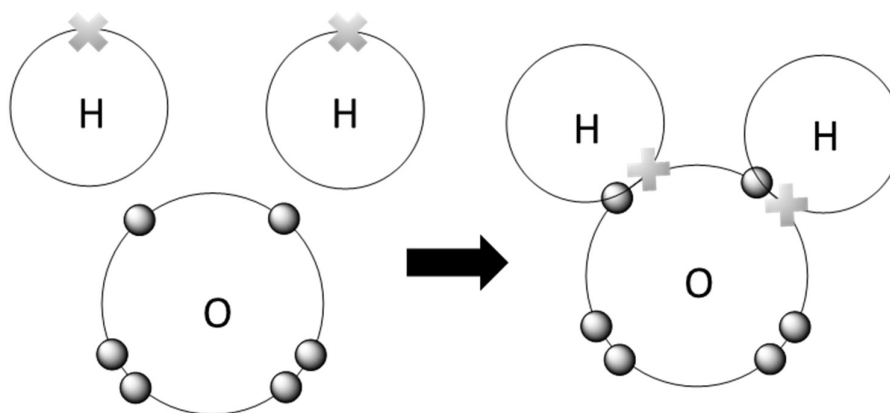


Figure 1 – Example of a dot and cross diagram to show a covalent bond in a water molecule.

## 1.2 Non-covalent interactions

The intermolecular non-covalent interactions were first suggested in 1873 by Johannes Diderik van der Waals; a force between molecules which is now known as van der Waals interactions.<sup>9-11</sup> This led to, Emil Fischer proposing the lock and key principle for enzymes in 1894,<sup>12</sup> stating that a specific substrate (key) is required to fit into the enzyme (lock), for the reaction to proceed (Figure 2).

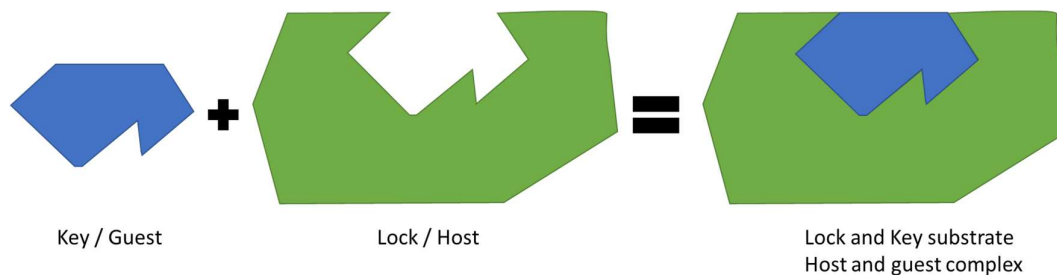


Figure 2 – Illustration of the lock and key principle. The components are complimentary allowing them to bind together to form the final complex.

Following this, Moore and Winmill hypothesised the presence of the hydrogen bond,<sup>13</sup> which was further supported by Latimer and Rodebush.<sup>14</sup> These concepts led to the synthesis of several host complexes that selectively bind to guest molecules; crown ether by Charles J. Pedersen,<sup>15</sup> macrocyclic cyclophanes by Donald J. Cram and cryptands by Jean-Marie Lehn (Figure 3).<sup>16,17</sup> Over the past decade, supramolecular chemistry has become one of the fastest-growing fields of chemistry and has contributed to the development of nanotechnology, winning another noble prize for James Fraser Stoddart in 2016.<sup>18,19</sup>

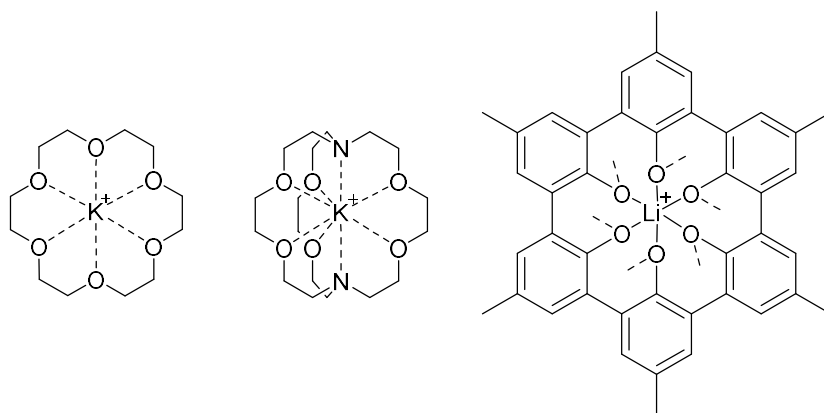


Figure 3 – The series of host-guest complexes developed by Pedersen (crown ether), Lehn (cryptate) and Cram (spherand) respectively.

Supramolecular complexes can self-organise or be preorganised. Preorganisation is where a molecule is designed to interact with a complementary molecule through non-covalent forces.<sup>20</sup> Whereas self-organisation is where the molecules assemble into higher ordered complex units through non-covalent interactions.<sup>21</sup> A supermolecule can both self-organise and be designed to preorganise.

The formation of a supramolecular complex is the result of a balance between electrostatic interactions and solvent interactions. There are many different types of non-covalent interaction, such as dipole-dipole interactions.<sup>22</sup> Dipole-dipole interactions are the weakest types of interactions with energies of < 5 kJ/mol and are formed by the attraction of one dipole to another (Figure 4A).<sup>23</sup> However, as the distance decreases the repulsive force between the electrons increase, therefore decreasing the energy and increasing the distance.<sup>24</sup>  $\pi$ - $\pi$  interactions occur between the electropositive and electronegative clouds on aromatic rings, they have energies of 0-50 kJ/mol.<sup>25</sup> There are three possible stacking configurations: edge to face (Figure 4B), face to face (Figure 4C) or offset stacking (Figure 4D).<sup>26</sup>

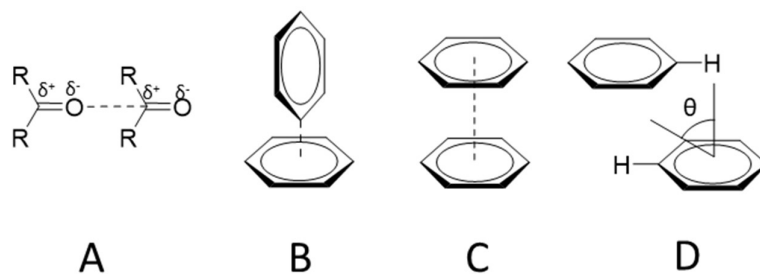


Figure 4 – Illustration of the non-covalent interactions A) dipole-dipole B)  $\pi$ - $\pi$  edge to face C)  $\pi$ - $\pi$  face to face D)  $\pi$ - $\pi$  offset.

The strongest type of non-covalent interaction is the ion-ion interaction, which is comparable in strength to the covalent bond, with energies of 100-350 kJ/mol and > 150 kJ/mol respectively. Other types of non-covalent interactions are the ion-dipole interactions which occur between a charged ion and a dipole on a polar molecule, the cation- $\pi$  interactions which occur between cations and electron rich aromatic ring systems and the anion- $\pi$  interaction which occurs between an anion and an electron deficient ring system (Figure 5).<sup>27-29</sup>

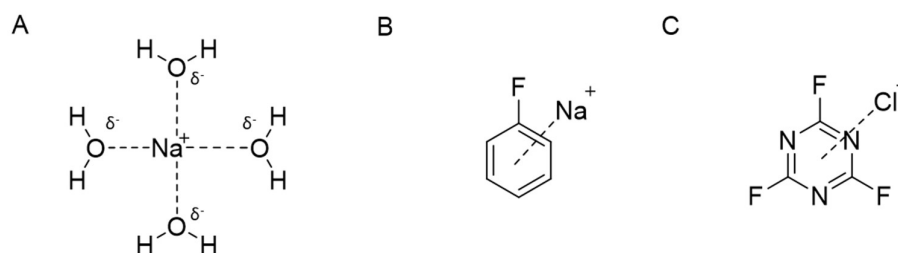


Figure 5 – Illustrations of non-covalent interactions A) ion-dipole B) cation-  $\pi$  C) anion-  $\pi$ .

Another non-covalent interaction is the hydrogen bond, the physical properties of the hydrogen bond have been studied extensively.<sup>30-32</sup> It has an energy range of 4-165 kJ/mol, which can be further categorised into weak electrostatic (< 20 kJ/mol), electrostatic (20-60 kJ/mol) or covalent interactions (> 60 kJ/mol).<sup>33-35</sup> The average bond lengths for electrostatic interactions are > 1.5 Å while covalent interactions are between 1.2-1.5 Å.<sup>36</sup> Hydrogen bonds can adopt many different geometries, such as: linear, bent, bifurcated (accepting and donating), trifurcated and three-centred bifurcated (Figure 6).<sup>37</sup> Hydrogen bonds are formed through hydrogen bond acceptor (HBA) groups, for example, oxygen, nitrogen and sulphur, interacting with electrostatically positive

acidic hydrogen atoms acting as hydrogen bond donating (HBD) groups. Although non-covalent interactions are weak compared to covalent bonds, the additive effect of many non-covalent interactions can stabilise molecular structures.

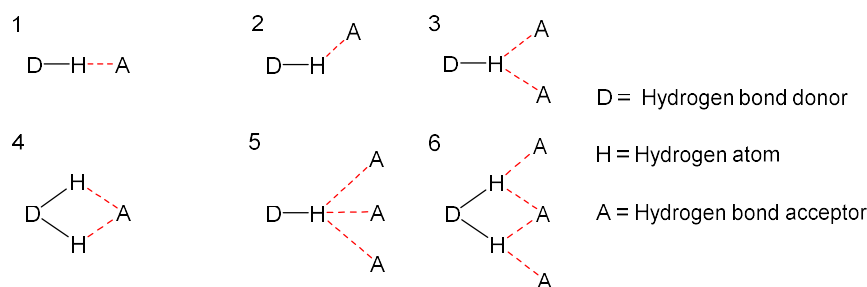


Figure 6 – Examples of the geometries a hydrogen bond can adopt 1) linear 2) bent 3) accepting bifurcated 4) donating bifurcated 5) trifurcated 6) three-centred bifurcated.

Natural systems contain many examples of supramolecular complex formation, which are vital for life. Proteins are an excellent example of supramolecular complexes. Enzymes catalyse all the chemical reactions in the body and antibodies bind to foreign particles to help protect it.<sup>38,39</sup> These molecules are formed of a primary structure, an amino acid chain, which self assembles into a secondary structure;  $\alpha$ -helices and  $\beta$ -sheets through hydrogen bonds.<sup>40,41</sup> Long amino acid chains can self-assemble into many separate secondary structures which folds into a three-dimensional structure through other non-covalent interactions, such as hydrophobic interactions, ionic interactions and hydrogen bonds, named the tertiary structure.<sup>42–44</sup> Furthermore, multiple tertiary structures can self-assemble to form a quaternary structure (Figure 7).<sup>45</sup> Another inspirational biological system is DNA (deoxyribonucleic acid), the structure of DNA was deduced by Francis Crick and James Watson in 1953, as two strands of polynucleotides that are complementary and interact to form a double helix.<sup>46</sup>

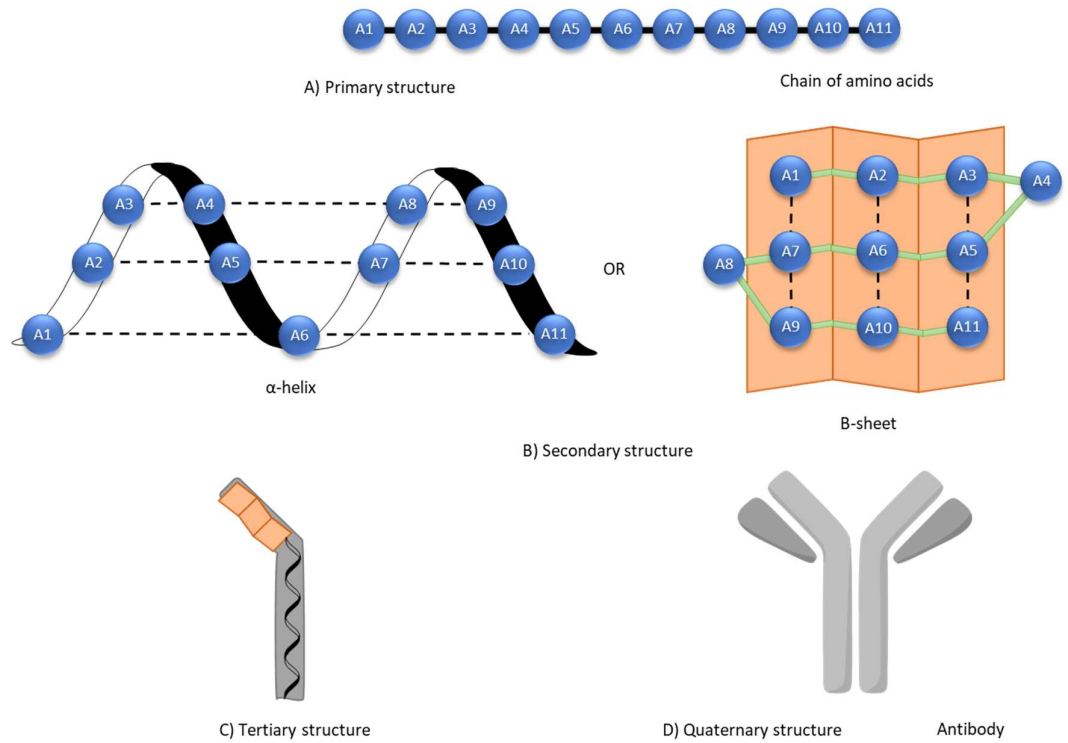


Figure 7 – Illustration of the structures within a protein. A) Primary structure, the amino-acid chain. B) Secondary structure,  $\alpha$ -helix or  $\beta$ -pleated sheet. C) Tertiary structure, folding of secondary structure into a three-dimensional structure. D) Quaternary structure, interactions between two or more tertiary subunits.<sup>47</sup>

### 1.3 DNA

DNA contains all the genetic information for the construction, function and reproduction of all known organisms and viruses.<sup>48</sup> DNA is polymer formed of repeating units of nucleotides,<sup>49</sup> which consists of a nucleobase, sugar and phosphate backbone. A nucleobase bound to a sugar forms a nucleoside, then a nucleoside bound to a phosphate group forms a nucleotide (Figure 8).<sup>50</sup> Two complementary polynucleotide strands interact to form a supra molecule.

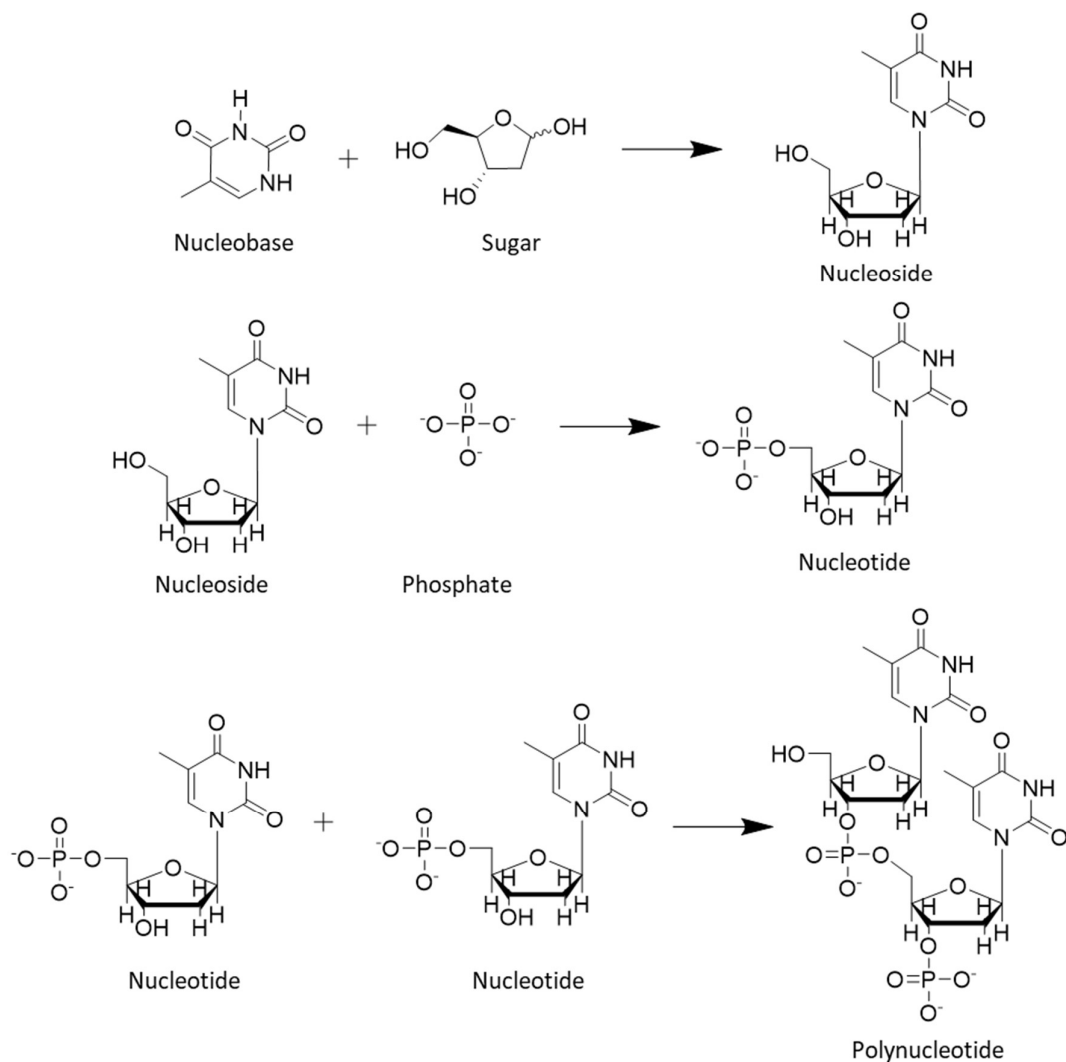


Figure 8 – Illustration of the structure of a nucleic acid.

Non-covalent interactions play a vital role in the formation of DNA, both hydrogen bonding and  $\pi$ - $\pi$  interactions are required for the stabilisation of the double helix.<sup>51</sup> There are four nucleobases in DNA, adenine, cytosine, guanine and thymine. Adenine and guanine are purines, while cytosine and thymine are pyrimidines. These types of molecules complement each other and bind through hydrogen bonding, forming adenine-thymine (A-T) and cytosine-guanine (C-G) bonds. Adenine interacts with thymine through two hydrogen bonds while cytosine interacts with guanine through three hydrogen bonds (Figure 9). Due to the additive effects of non-covalent interactions the C-G interaction is stronger than the A-T interaction.<sup>52</sup>

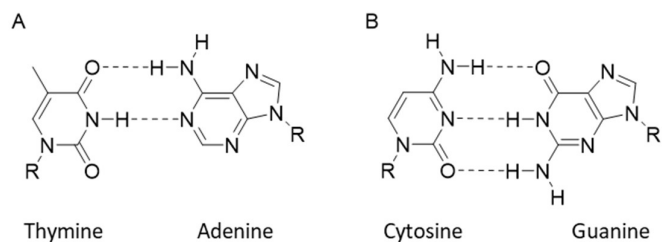


Figure 9 – Hydrogen bonding between the complementary base pairs. A) Adenine and thymine. B) Cytosine and guanine.

The  $\pi$ - $\pi$  interactions occur between the stacked nucleobases, then the stacked nucleobases form a dipole, which attracts another nucleobase through van der Waals forces, which is propagated throughout the entire polynucleotide. Although these forces are weaker than hydrogen bonds individually, recent studies have found that the  $\pi$ - $\pi$  interactions contribute more to the stabilisation of DNA than previously thought.<sup>53</sup> DNA replication requires the two strands to separate, an enzyme named DNA helicase separates the polynucleotide strands between the nucleobases by breaking the hydrogen bonds.<sup>54</sup>

Due to the specific self-associating properties of DNA, the Watson-Crick base pairing, it inspired a new area of supramolecular chemistry termed 'supramolecular DNA assembly'.<sup>55</sup> By combining DNA complementary base pairing with synthetic chemistry, it is possible to design precise assembly of molecules. Oligonucleotides have been used as a supramolecular scaffold for the synthesis of functional molecules in the nanometre scale. Supramolecular DNA assembly evolved from 2D lattices into 3D lattices, starting from a 2D smiley face to lego-like structures which can self-assemble to form larger 3D structures.<sup>56,57</sup> From there, dynamic DNA nanostructures were synthesised by Sherman et al,<sup>58</sup> where it was demonstrated a DNA footpath could be transversed by a DNA bipedal walking device through its oligonucleotide feet.<sup>59</sup> While DNA and the interactions between it were being studied, chemists were simultaneously researching micelles and microemulsions.<sup>60</sup> Micelles and microemulsions consist of amphiphiles aggregating through non-covalent interactions to form extended structures.<sup>61</sup> They play an important role in biology and have a wide range of consumer applications.

## 1.4 Amphiphiles

Amphiphiles are molecules that consist of a hydrophilic and hydrophobic component.<sup>62</sup> Depending on the nature of the hydrophilic group, amphiphiles can be categorised as neutral, anionic, cationic or zwitterionic.<sup>63</sup> Neutral amphiphiles do not carry a charge, their solubility is dependent on the functional groups and how easily they deprotonate (Figure 10A). Anionic amphiphiles carry a negative charge, common head groups are carboxylates, sulphates, sulfonates and phosphates (Figure 10B).<sup>64</sup> Cationic amphiphiles carry a positively charged head group, amines or ammonium ions are common examples (Figure 10C).<sup>65</sup> While a zwitterionic amphiphile carries both a positive and negative charge in the head group (Figure 10D).<sup>66</sup> The hydrophobic component usually consists of a hydrocarbon chain, however, there are exceptions such as aromatic rings and trifluoromethyl functional groups.<sup>67,68</sup>

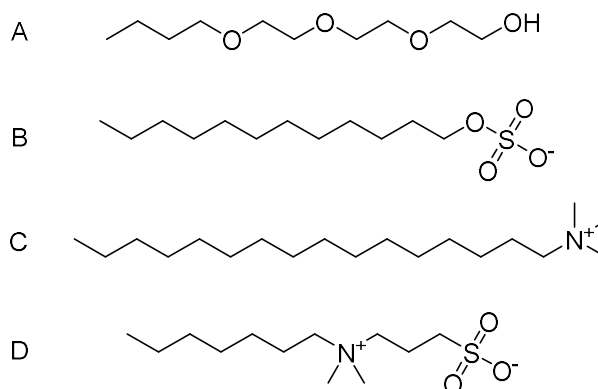


Figure 10 – Examples of amphiphiles: A) Neutral; B) Anionic; C) Cationic; D) Zwitterionic.

Amphiphiles can aggregate to form different structures, this is achieved by maximising the preferred interactions while minimising the non-preferred interactions. Which leads to the following structures: micelles, reverse micelles, lipid bilayers or vesicles. Micelle can form when the amphiphiles are in a polar solution (Figure 11A), whereas in a non-polar solution, the amphiphiles will form a reverse micelle (Figure 11B).<sup>69</sup> The number of hydrophobic moieties of the amphiphile itself can affect the result of the aggregate formation. For example, Phospholipids with a single hydrocarbon chain can aggregate into micelles, while amphiphiles with multiple hydrocarbon chains form bilayer structures as the chains are too large to fit inside a micelle (Figure 11 C, D).<sup>70</sup>

Page | 15

These structures play an important role in biological systems. The lipid bilayers compartmentalise different cells to increase efficiency, while micelles and vesicles transport water insoluble products in and out of the cells.<sup>71</sup>

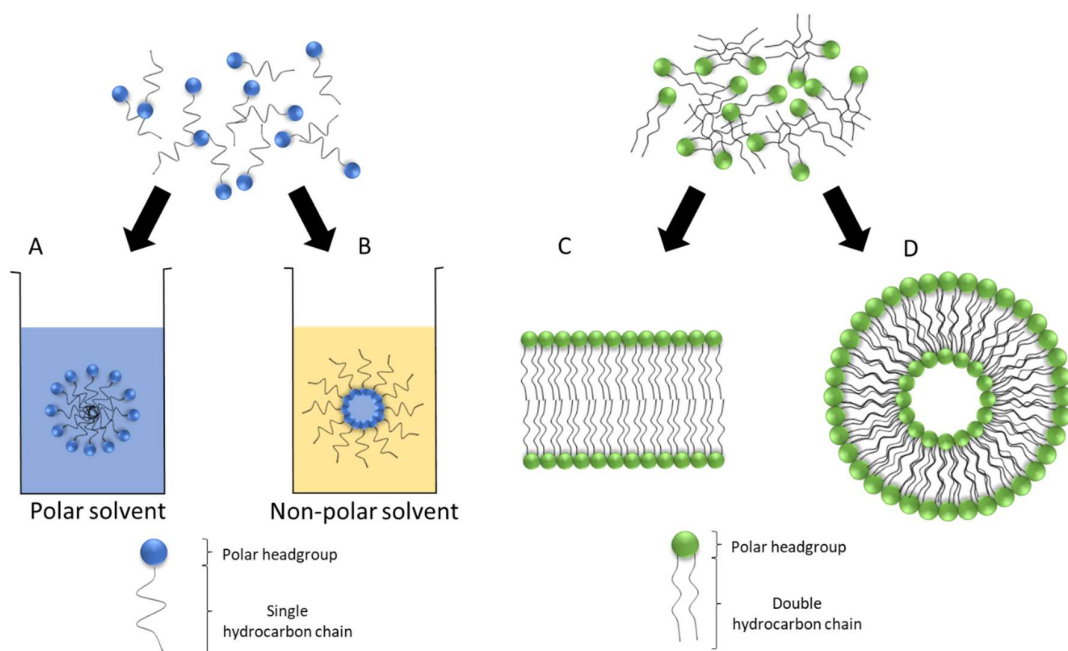


Figure 11 – Examples of amphiphile aggregation. A) Single chain amphiphile in a polar solvent. B) Single chain amphiphile in a non-polar solvent. C) Double chain amphiphile forming a lipid bilayer. D) Double chain amphiphile forming a vesicle.

Peptides are proteins that are produced in all living organisms and have shown pharmacological activity against microbes. The antimicrobial peptides are oligopeptides and most are charged amphiphiles that display minimal toxicity to mammalian cells.<sup>72–74</sup> In contrast to other types antimicrobials, which target DNA or enzymes on the membrane, antimicrobial peptides associate with cell membranes of the microbes, this discovery has consequently led to the development of new amphiphilic drugs. Examples include: tranquilizers,<sup>75</sup> antihistamines,<sup>76</sup> antibiotics,<sup>77</sup> antidepressants,<sup>78,79</sup>  $\beta$ -blockers and more.<sup>80</sup> Over the last decade amphiphiles have been developed into supra-amphiphiles,<sup>81</sup> they interact through non-covalent interactions.<sup>82</sup> A study conducted by Wang et al., stated there are two main ways to create a supra-amphiphile; firstly, through the combination of the hydrophobic and hydrophilic components using non-covalent interactions or dynamic covalent bonds to create the amphiphile.<sup>83</sup> The other method was

to modify a molecule with non-covalent interactions, changing the physical properties of the molecule, such as the amphiphilicity.<sup>84</sup>

Meanwhile, low molecular weight amphiphiles have been found to self-associate through hydrogen bonds,<sup>85</sup> especially those with urea functional groups.<sup>86</sup> Combining these concepts, Faustino et al. developed a series of anionic urea based salts derived from sulphur containing amino acids (Figure 12A, B).<sup>87</sup> The studies show hydrogen bonding occurs at the urea moiety, however it did not affect micelle formation. The amphiphile also showed no antimicrobial activity which was presumed to be due to the short alkyl chains.

Following this, Pittelkow et al. synthesised aromatic, anionic-urea salts derived from sweeteners (Figure 12C).<sup>88-90</sup> However, the main focus of the research was on the complexation of dendrimers, thus the self-association properties of these low molecular anionic-urea compounds were not analysed. Hiscock et al. modified the sulfonate-urea salts and began to look at the self-association properties of the compounds and found some of these amphiphilic salts showed signs of antimicrobial activity (Figure 12D).<sup>91</sup>

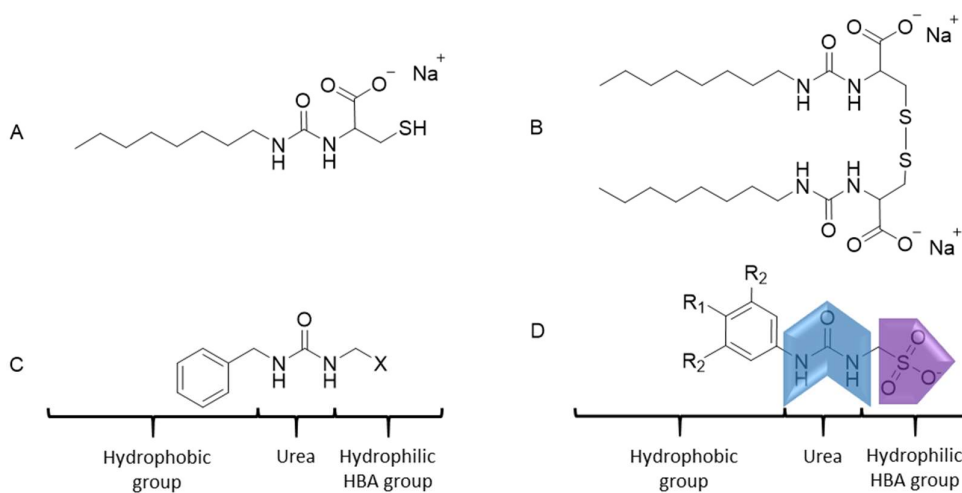


Figure 12 – Illustration of the evolution of anionic urea amphiphile A) anionic monomeric urea amino acid B) anionic dimeric urea amino acid C) anionic aromatic urea D) modified anionic aromatic urea.

The amphiphile consists of an anionic hydrophilic HBA group and a urea groups which can adopt a minimum of four different binding modes. These binding modes cannot exist at the same time making the system 'frustrated'. The amphiphile can self-assemble through the urea-urea or urea-anion through hydrogen bonding. Binding through the urea-urea can form a dimer or tape structure, whereas binding through the urea-anion the compound forms either a syn-stacking or anti-stacking structure (Figure 13). The research concluded the binding mode was dependant on the molecular structure of the amphiphile and the solvent system the aggregate was assembled in.

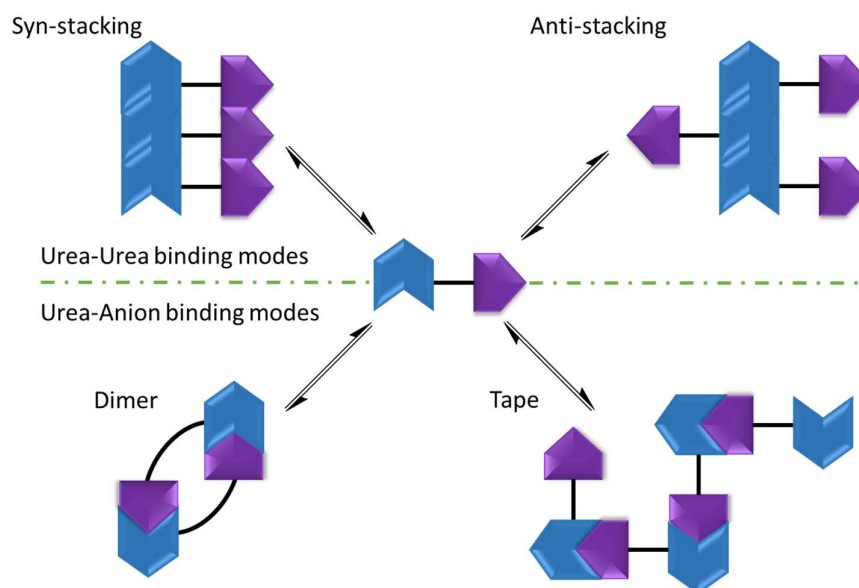


Figure 13 – Possible self-associated hydrogen bonded modes of the modified anionic urea compounds.

Subsequently, Hiscock et al. expanded the collection of amphiphiles while keeping the general structure.<sup>92</sup> The functional groups on the hydrophobic aromatic ring were altered, electron withdrawing groups such as an amide or more electron donating group such as a nitro group were affixed. The urea moiety was swapped to a thiourea moiety and the cation was exchanged. The self-association properties of these compounds were analysed in all three states: solid state, gas phase and solution state.<sup>93</sup>

The research concluded that compounds containing urea-anionic moieties with a weakly coordinating counter cation forms urea-anion complex. These compounds formed dimeric species in the gas phase, additionally, within the solution state, these compounds also tend to form dimeric

species within DMSO. Whereas in H<sub>2</sub>O: EtOH 19:1 solution the compounds formed aggregates with a size of 91-460 nm, 3 of the compounds showed signs of antimicrobial activity when tested against *Staphylococcus aureus* (*S.aureus*) and *Escherichia coli* (*E.coli*).<sup>92,94</sup>

The next step was to investigate the mode of action of the compounds and visualise them using microscopy, intrinsically fluorescent compounds were synthesised.<sup>93</sup> The compounds aggregate and form micellular-like structures (Figure 14A), which coats the surface of the *S.aureus* cell (Figure 14B, C). Finally, the compound penetrates the membrane, internalises within the cell and appears to associate with the nucleoid (Figure 14D, E).<sup>95</sup>

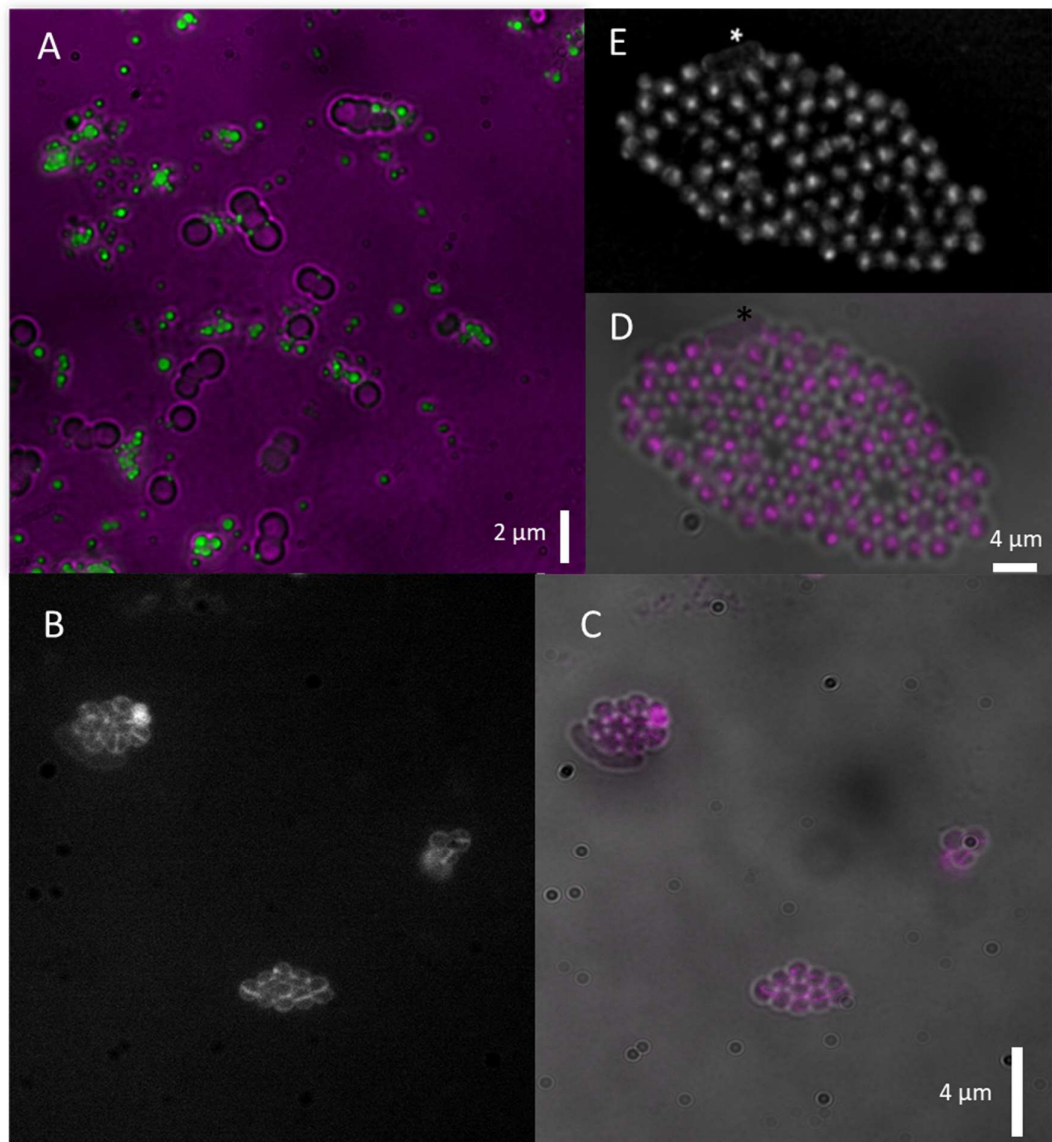


Figure 14 – A) Overlaid fluorescence and transmitted light microscopy image of green micellar aggregates binding to the bacterial membrane of *S.aureus*. B) Fluorescence confocal microscopy image of the aggregates (white) coating the bacterial membrane of *S.aureus*. C) Overlaid fluorescence and transmitted light microscopy image of the aggregates (pink) coating the bacterial membrane of *S.aureus*. D) Overlaid fluorescence and transmitted light microscopy image of the aggregates (pink) interacting with the nucleoid of *S.aureus*. E) Fluorescence confocal microscopy image of the aggregates (white) interacting with the nucleoid of *S.aureus*. Attributed to Jennifer Hiscock, Dan Mulvihill and Laura Blackholly.

Due to the compounds interaction with the nucleoid, Hiscock et al. synthesised a DNA inspired molecule (Thymine) derived from the previous compounds;<sup>96</sup> the study reports the molecule self-associates to form dimers in DMSO and the DOSY NMR studies report the solvation sphere diameter at 1.6-1.8 nm depending on the concentration. The crystal structure of the molecule shows that it

dimerises then the dimers interact to form a tetramer. The tetramers then interact again to form a pseudo porous extended structure. The paper shows the tetramer forms through the amide NH leaving the thymine moiety free to interact (Figure 15).

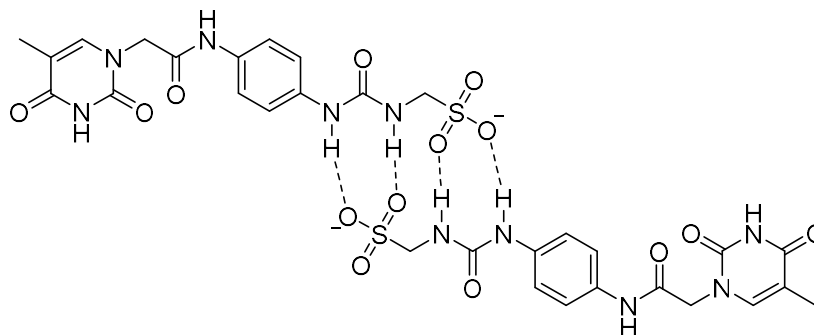


Figure 15 – Illustration of the dimer formation of the thymine inspired molecule.

As the thymine moiety is free to interact and is part of a complementary base pair, an adenine inspired molecule can be synthesised to attempt to form a preorganised extended aggregate through DNA base pairing.

## 1.5 Project Aims

The aims of this project are to synthesise a complementary molecule to the thymine inspired amphiphile.<sup>96</sup> Hence, an adenine inspired amphiphile will be synthesised, characterised and the self-association and complex formation properties will be explored within the solid state, gas phase and solution state using single crystal X-ray diffraction, negative electrospray ionisation mass spectrometry (ESI-MS), NMR spectrometry, dynamic light scattering (DLS), zeta potential, tensiometry and low level computational modelling. Compounds **1** and **2** will be synthesised as the precursor to compounds **3-5**. As compounds **3-5** are complex molecules, compounds **6-10** will be synthesised to break down the complex interactions between the DNA inspired molecules (Figure 16). Previous amphiphiles have shown antimicrobial properties,<sup>94</sup> therefore, compounds **3-5** will be also be tested for antimicrobial properties. It has been shown that the amphiphiles interact with the nucleoid, it is hypothesised that the DNA inspired amphiphiles will interact with any single stranded DNA and further increase efficacy. The amphiphiles will be tested against *S.aureus* and *E.coli*.

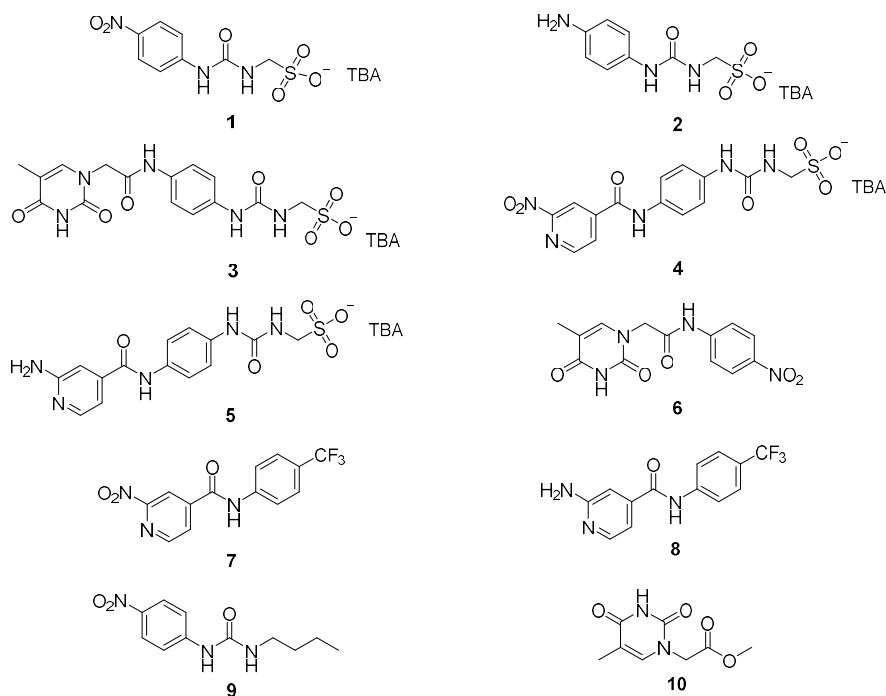


Figure 16 – Structures of compounds **1-10**.

## 2. Results and discussion

### 2.1 Synthesis

The synthesis of compounds **1** and **2** has been previously published,<sup>91,92</sup> they are required for the synthesis of compounds **3-5** (Figure 17). Compound **3** was also previously published and synthesised accordingly, however; it could not be purified according to the method. Compound **4** was synthesised through an amide couple reaction of compound **2**, 2-nitroisonicotinic acid and 1-Ethyl-3-(3-dimethylaminopropyl) carbodiimide (EDC) with a final yield of 51 %. Finally, compound **5** was synthesised through a reduction of compound **4** using hydrazine hydrate and palladium on carbon (Pd/C) with a yield of 84 %.

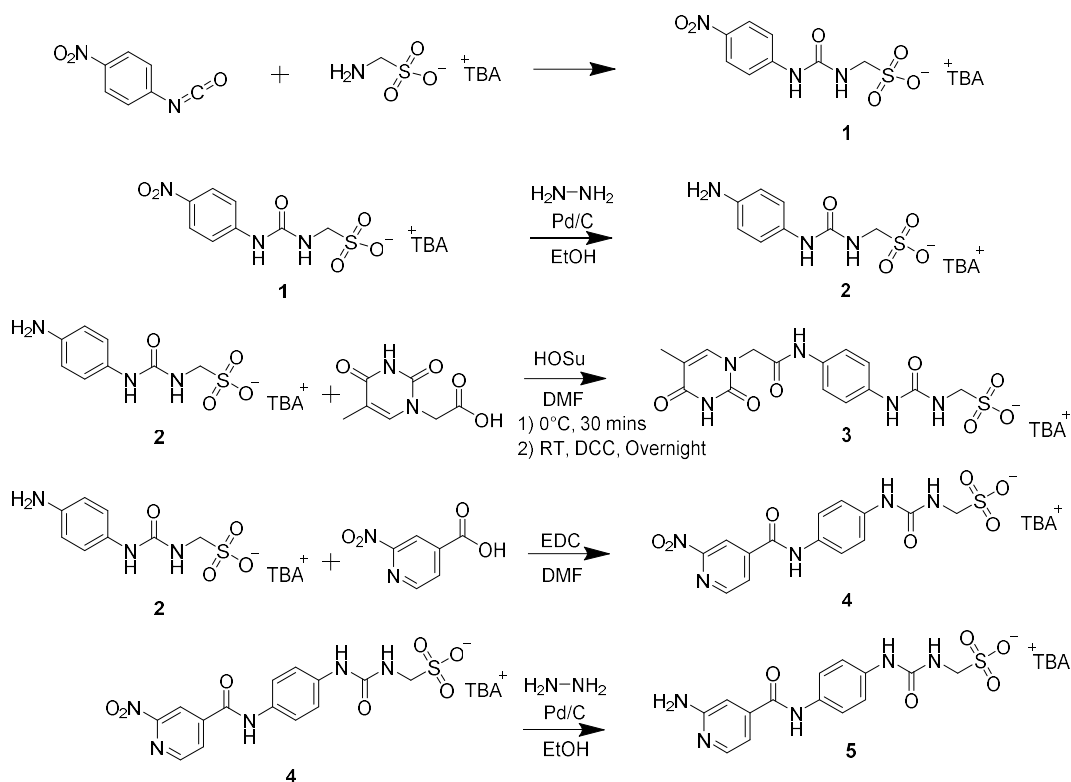


Figure 17 – Synthesis scheme for compounds **1-5**.

Compound **3** was synthesised with each attempt; however, many problems arose. Initially, there was still starting material in the crude product (Figure 18A), this was due to the reactant, N,N'-Carbonyldiimidazole (CDI) decomposing to form imidazole. The amount of CDI was increased to drive the reaction to completion; however, this caused the crude product to contain excess

Page | 23

imidazole, which was challenging to remove (Figure 18B). Hence, other coupling agents, such as N,N'- Dicyclohexylcarbodiimide (DCC) and 1-Ethyl-3-(3-dimethylaminopropyl) carbodiimide (EDC) were used in an attempt to synthesis compound **3**. DCC successfully yielded Compound **3**, but contained excess TBA (Figure 18C). Separations, precipitations and columns were used to remove the excess TBA, however, all methods removed all the TBA instead (Figure 18D). After these attempts, a literature based method was found to use N-Hydroxysuccinimide (HOSu) to stabilize the thymine analogue from the contributing structures before the coupling process, this method was applied to the synthesis process and the yield increased to 54% (Figure 18E).

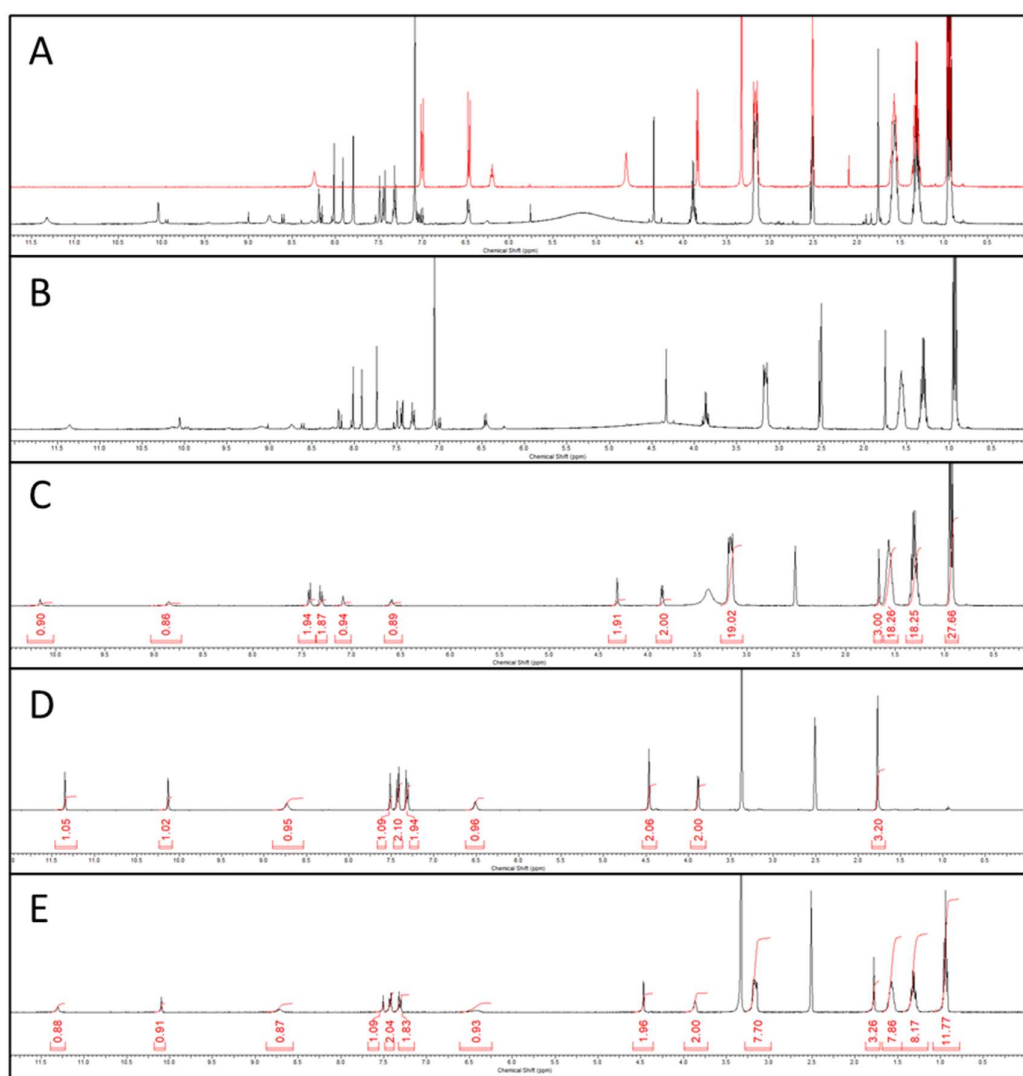


Figure 18 - A) Overlaid  $^1\text{H}$  NMR of Compound **2** and compound **3** using the previously published method. B)  $^1\text{H}$  NMR of Compound **3** synthesised with additional CDI. C)  $^1\text{H}$  NMR of Compound **3** synthesised using DCC showing a higher ratio of TBA. D)  $^1\text{H}$  NMR of Compound **3** with TBA removed. E)  $^1\text{H}$  NMR of compound **3** synthesised using the final method.

## 2.2 Self-association in the solid state

### 2.2.1 Single-crystal X-Ray diffraction

A single crystal is a material in which the crystal lattice of the entire sample is continuous, single crystals can be formed from almost all materials. As the crystals have a repeating pattern, Max von Laue suggested the use of crystals as a grating for the diffraction of X-rays.<sup>97</sup> Due to the non-destructive nature of the technique, it is used to obtain a three-dimensional structure of the material and it can observe both covalent and non-covalent interactions in the solid state.<sup>98</sup> Crystals of compounds **4**, **5**, **7** and **10** were obtained through slow evaporation of a H<sub>2</sub>O: MeOH 19:1 solution, while crystal structures of compounds **1-3** were previously published,<sup>92</sup> compounds **1** and **2** forms dimers through urea-anion interactions, while compound **3** forms a tetramer through urea oxygen-amide NH interactions. A crystal structure of the 1:1 mixture of compounds **3** and **5** was not obtained. Many solvent systems were attempted; however, a crystal was not produced. Crystallography data was obtained and refined by Dr. Jennifer Hiscock.

#### 2.2.1.1 Results and discussion

The crystal structure of compound **4** exhibits a dimerization between the urea-anion through the formation of four hydrogen bonds, like previously published compounds (Figure 19).<sup>92</sup> However, it also shows a water-bridged urea-pyridine and an amide-sulfonate hydrogen bond extending the aggregate species.

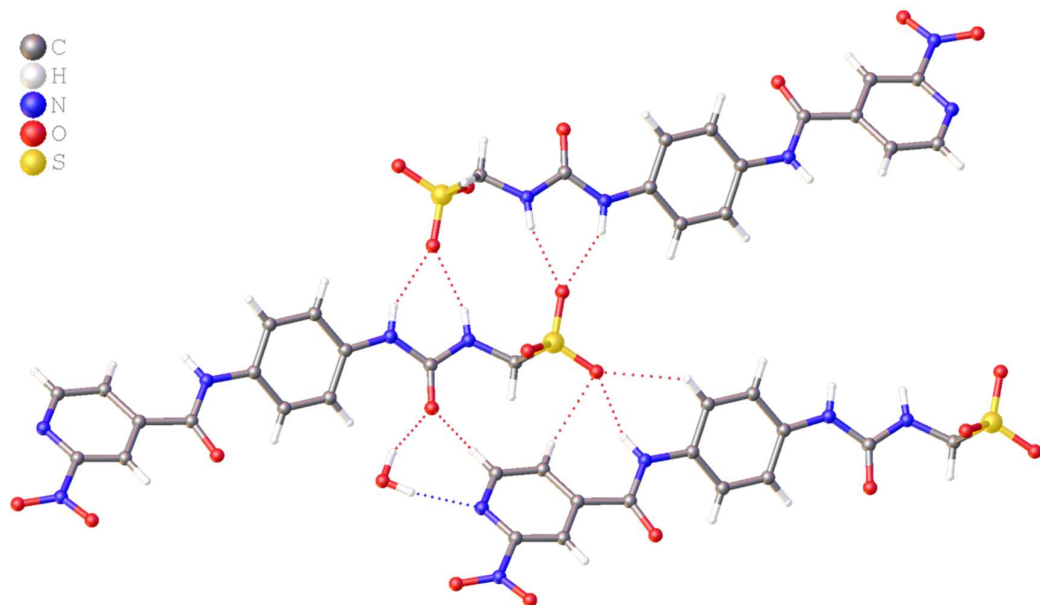


Figure 19 – Single crystal X-ray structure of compound **4**, exhibiting hydrogen bonded extended structures. TBA counter cation has been omitted for clarity.

Compound **5** also forms the dimeric species between the urea-anion with four hydrogen bonds (Figure 20). End-end interactions are also seen in the crystal structure through the HBD nitrogen and HBA amino functional group on the aminopyridine forming two hydrogen bonds. Sulfonate-aminopyridine interactions are also seen within the crystal structure and are either directly bonded or water-bridged.

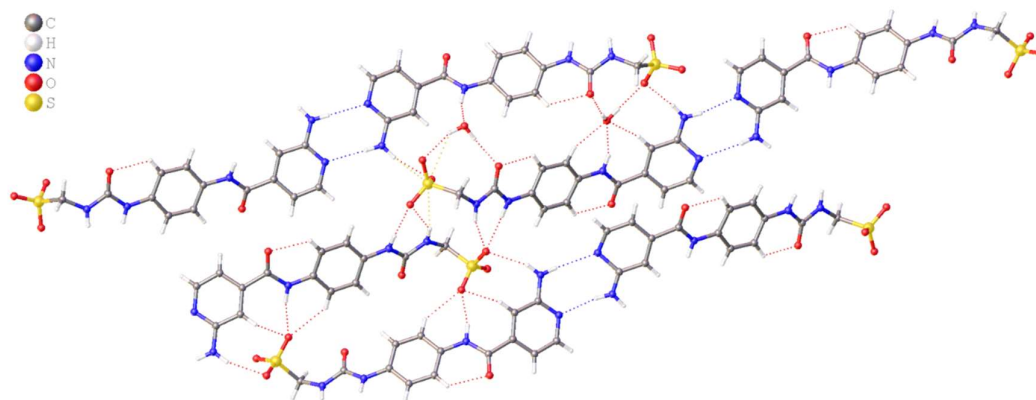


Figure 20 – Single crystal X-ray structure of compound **5**, exhibiting hydrogen bonded extended structures. TBA counter cation has been omitted for clarity.

Compound **7** forms a hydrogen bond between the amide-amide moiety, forming a syn-stacking structure (Figure 21).

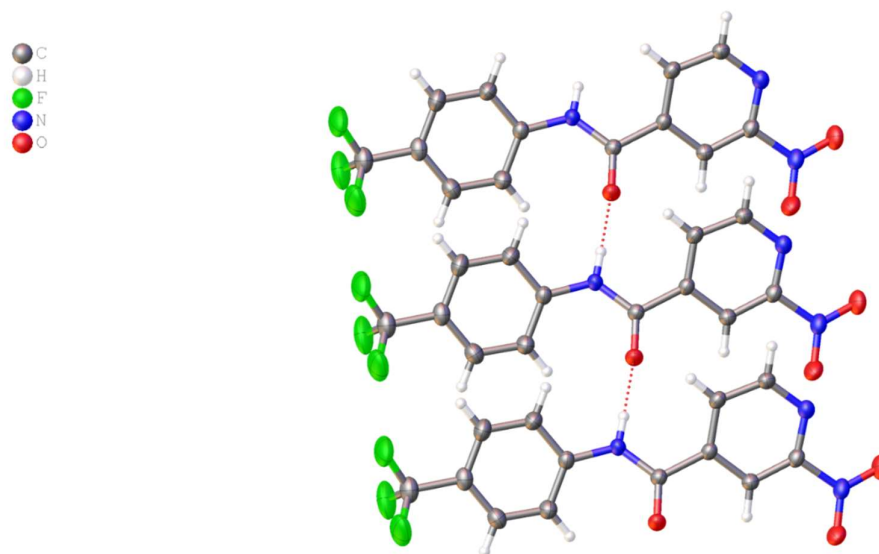


Figure 21 – Single crystal X-ray structure of compound **7**, exhibiting hydrogen bonded syn-stacking through an amide-amide binding mode.

Compound **10** forms a dimer through two hydrogen bonds between the amide on the ring and the oxygen in between two nitrogen atoms (Figure 22). It was hypothesised that it interacts there due to the inductive effect of electron donating nitrogen causing the oxygen to be a stronger HBD.

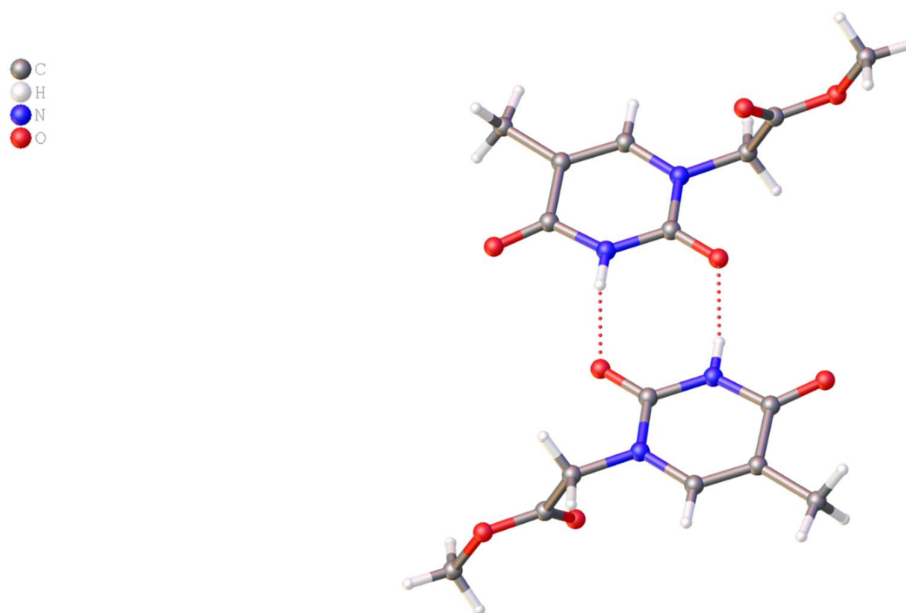


Figure 22 – Single crystal X-ray structure of compound **10**, exhibiting a hydrogen bonded dimer.

To conclude, all crystal structures show the formation of a dimeric species and the sulfonate-urea amphiphiles show the same interaction at the sulfonate-urea as with previously published amphiphiles.<sup>99</sup>

## 2.3 Self-association in the gas phase

### 2.3.1 Electrospray ionisation mass spectrometry

ESI-MS has become an irreplaceable tool in science, it provides qualitative information about the analytes and it can preserve weak non-covalent bonds in the gas phase.<sup>100</sup> However, molecules must be an ionic species or be converted into an ionic species to use this technique, this is achieved through injecting the sample into an ionisation source.<sup>101</sup> Compounds **3-8** were analysed using negative ESI-MS to determine whether low complex formation could be seen in the gas phase.

#### 2.3.1.1 Results and discussion

The data obtained from the ESI-MS show that compounds **3-8** behave the same as the previous compounds, existing as both the monomers and dimers in the gas phase. Compounds **3-5** are salts, therefore shows the monomeric state  $[M]^-$  and dimeric state  $[M + M + H^+]^-$  (Table 1). The dimer is not limited to the hydrogen ion, other ions such as sodium and potassium can be seen,<sup>94</sup> however, were not looked at here. Sample preparation was completed to ensure optimization, resulting in a very low concentration of the analysed sample (1 mg in 1 mL, diluted further by a factor of one hundred giving the concentrations at  $\approx 1.6 \times 10^{-6}$  mol).

Table 1 – High Resolution mass spectrometry theoretical and experimentally derived values for compounds **3-5**.

Compound	$m/z [M]^-$		$m/z [M + M + H^+]^-$		$m/z [M + M + M + 2H^+]^-$	
	Theoretical	Actual	Theoretical	Actual	Theoretical	Actual
<b>3<sup>a</sup></b>	410.0771	410.0755	821.1612	821.1591	1232.2453	N/A
<b>4</b>	394.0458	394.0440	789.0986	789.0951	1184.1514	N/A
<b>5</b>	364.0716	364.0702	729.1502	729.1471	1094.2288	1094.2227

<sup>a</sup> – Previously published data.<sup>96</sup>

The protonated dimeric species for compounds **3-5** were observed. Using compound **4** as an example (Figure 23). The monomeric  $[M]^-$   $m/z$  peak is observed at 364.0702 and the protonated dimeric species  $[M + M + H^+]^-$  is observed at  $(2 \times 410.0755) + 1.007 = 729.1471$ , this indicates that a dimerised species is present in the gaseous phase. This trend is apparent for compounds **3** and **5**, moreover, compound **5** also indicates that a trimeric species  $[M + M + M + 2H^+]^-$  is present at  $(3 \times 364.0702) + (2 \times 1.007) = 1094.2227$ . The appearance of the trimeric species in the gas phase has not yet been seen in any previously published compounds, further investigation of the trimer will be required to determine the reason for its presence.

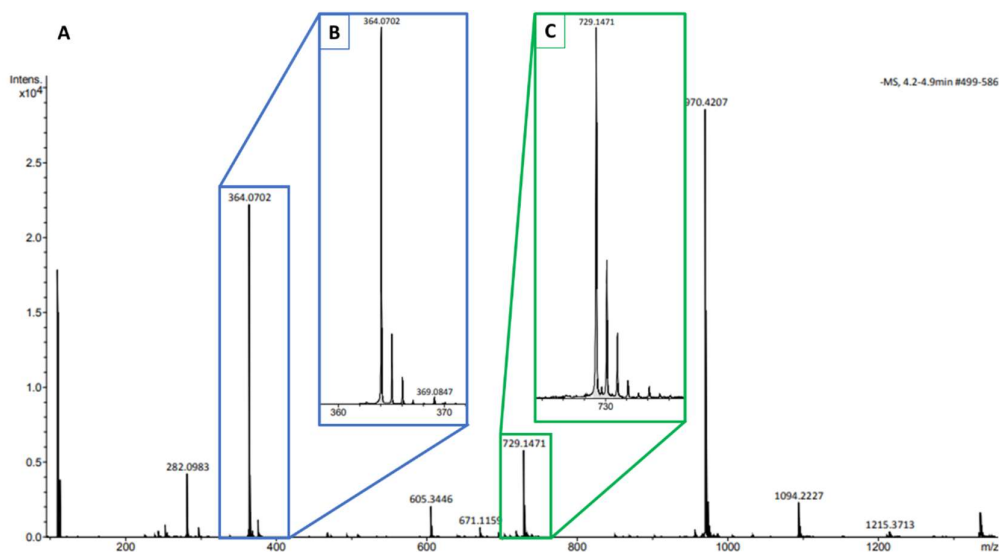


Figure 23 – Electrospray mass spectrometry spectrum of compound **5**, showing both the monomeric, dimeric and trimeric species (A), monomeric species (B) and protonated species (C).

Alternatively, compounds **6-8** are neutral species, therefore requires ionisation to show the monomeric state  $[M - H^+]^-$  (Table 2).

Table 2 – High Resolution mass spectrometry theoretical and experimentally derived values for compounds **6-8**.

Compound	m/z [M - H] <sup>-</sup>		m/z [M + M - H] <sup>-</sup>	
	Theoretical	Actual	Theoretical	Actual
<b>6</b>	303.0738	303.0863	607.1546	607.1776
<b>7</b>	310.0448	310.0433	621.0966	621.0916
<b>8</b>	280.0706	280.0820	561.1482	561.1680

The deprotonated dimeric species were observed for compounds **6-8**. Using compound **6** as an example (Figure 24, 25). The monomeric [M - H]<sup>-</sup> m/z peak is observed at 304.2620 - 1.007 = 303.0863 and the deprotonated dimeric [M + M - H]<sup>-</sup> m/z peak is observed at (2 x 304.2620) - 1.007 = 607.1776. This trend is also apparent for compounds **7** and **8**.

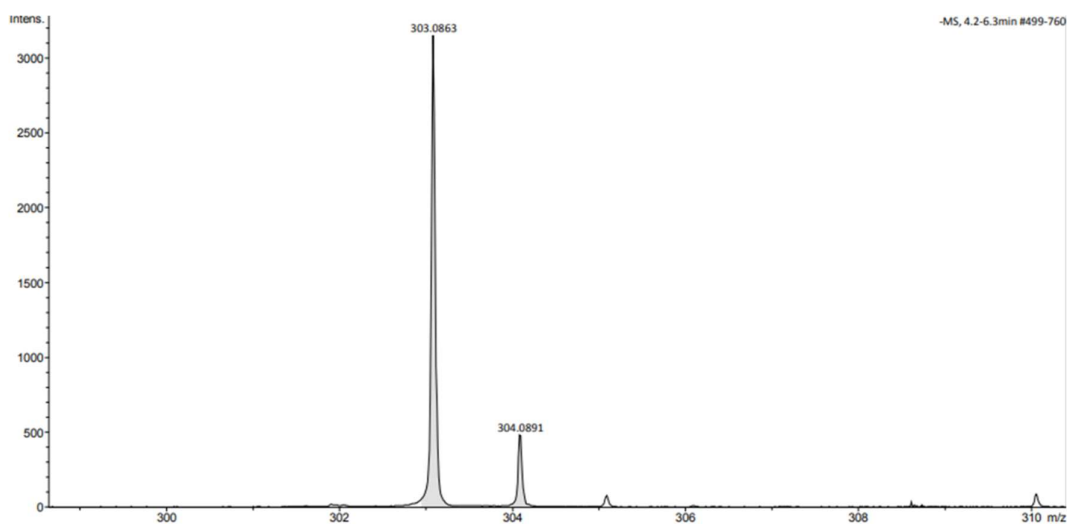


Figure 24 – Electrospray mass spectrometry spectrum of compound **6** showing the monomeric species.

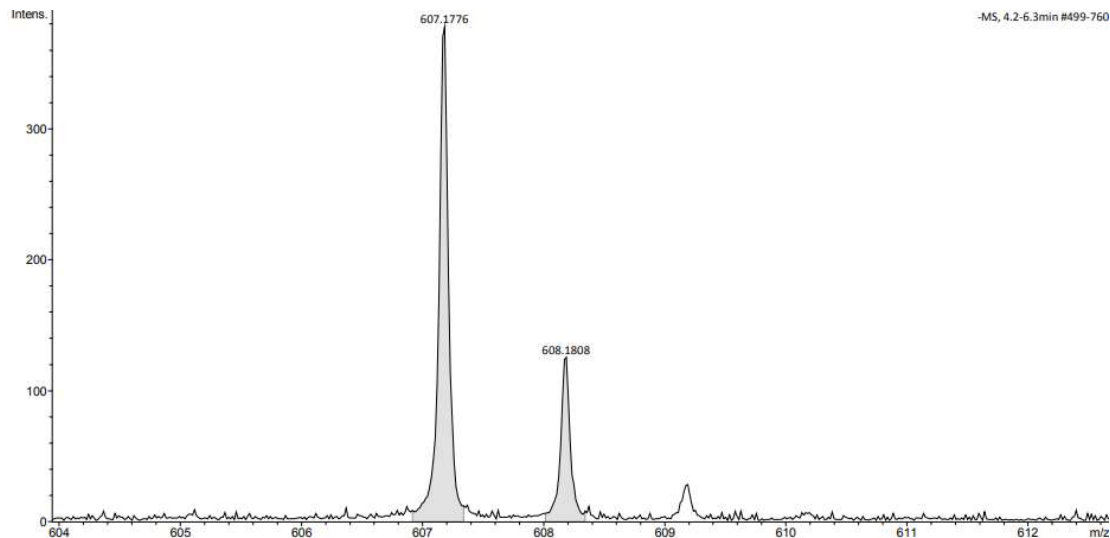


Figure 25 – Electrospray mass spectrometry spectrum of compound **6** showing the dimeric species.

The ESI-MS data reveals that the non-covalent bonds of compounds **3-8** do not dissociate under these conditions, indicating the strength of the interactions of these low complex formations are quite strong. The strength of the interactions cannot be determined within the gas phase; therefore, the self-association properties of the compounds will be explored in the solution state. All ESI-MS for compounds **3-8** can be found in the appendix (Figures 89-100).

#### 2.4 Association in the solution state

The solid state and gas phase complex formations occur in the absence of solvent-solute interactions. This allows us to observe the interactions between the compounds, however, in the solution state, solvent-solute interactions can alter the complex formation when self-associating. The solvent molecules can act as HBA or HBD which plays a role in the self-association of molecules. For example, water is a polar protic solvent, which interacts through the proton when hydrogen bonding, acting as a HBA. Whereas DMSO is a polar aprotic solvent, it interacts with solutes through the oxygen atom acting as a HBD.<sup>102</sup> Previous studies by Hiscock et al. conclude that this class of novel amphiphiles tend to form dimers in DMSO, while in an aqueous H<sub>2</sub>O: EtOH 19:1 solution they form aggregates with an approximate size of 100-500 nm.<sup>92</sup> Compounds **3-5** consists of the same hydrophilic sulfonate anion and urea moieties; these compounds will be analysed with the same techniques to investigate their self-association properties.

#### 2.4.1 $^1\text{H}$ NMR quantification studies

Quantitative  $^1\text{H}$  NMR (qNMR) is a technique which compares the compound with an internal standard to calculate the proportion of molecules in solution. This technique utilises an inherent property of NMR; the magnitude of each NMR signal is proportional to the number of nuclei responsible for the peak.<sup>103</sup> Therefore, using a known standard and a known concentration of the compound, it is possible to calculate the percentage of molecules in the solvent. If the percentage is lower than 100% in the solvent, they are classified as being 'NMR silent' as it is outside the limitations of this technique. The limitations to solution state NMR spectroscopy are as followed, sensitivity, natural abundance of the isotope and solubility of the molecule. It is possible to restrict the limitations of sensitivity and natural abundance of the isotope by using a concentrated sample and a nucleus with a high natural abundance, in this case,  $^1\text{H}$  NMR.<sup>104</sup> Therefore, if the compound is 'NMR silent' it will be due to the compound self-associating into an aggregate that adopts solid-like characteristics and can no longer be seen by solution state NMR.

Herein, compounds **3-5** and a 1:1 mixture of compounds **3** and **5** will be compared using previously used solvents, DMSO- $d_6$  and water. The DMSO will be spiked with 1% DCM as the internal standard due to the peak appearing at 5.76 ppm, which appears away from the compound signals. The D<sub>2</sub>O will be spiked with 5% EtOH as the internal standard due to the peak appearing at 3.65 ppm, away from the aromatic signals and can, therefore, be referenced.

##### 2.4.1.1 Results and discussion

The data obtained from the qNMR studies show that there is no loss of compound in DMSO for compounds **4** and **5**, whereas there is a loss of compound **3** and the mixture (Table 3). Compound **3** shows no loss in the H<sub>2</sub>O: EtOH solution, while compounds **4,5** and the mixture shows a loss in the H<sub>2</sub>O: EtOH solution.

Table 3: Overview of the calculated % loss of compound at a total concentration of 111.12 mM in DMSO-*d*<sub>6</sub> and a total concentration of 6.00 mM in H<sub>2</sub>O: EtOH 19:1 solution for compounds **3-5** and the 1:1 mixture of compounds **3** and **5**.

Compound	% Loss	
	DMSO- <i>d</i> <sub>6</sub> w/ 1% DCM	D <sub>2</sub> O w/ 5% EtOH
<b>3*</b>	6	0
<b>4</b>	0	29
<b>5</b>	0	32
<b>3 and 5*</b>	7	58

\* = repeated three times.

The results show a small percentage of compound **3** and the mixture form aggregates with solid-like characteristic. This is unusual as most previously published compounds show no loss in DMSO-*d*<sub>6</sub>, similar to compounds **4** and **5**. Therefore, this experiment was repeated three times to check the validity of the results, showing an average loss of 6 % and 7 % of compound **5** and the 1:1 mixture, respectively. On the other hand, in D<sub>2</sub>O compound **3** shows no loss, while compounds **4**, **5** and the mixture shows a loss of 29, 32 and 58 %, respectively. Which indicates approximately a third of compounds **4** and **5** forms extended aggregates which cannot be seen by this technique and a combination of compounds **3** and **5** causes more molecules to be aggregated in D<sub>2</sub>O, indicating a greater interaction when the compounds are combined. Using compound **3** in DMSO as an example, the DCM peak is calculated to be 2.87. The CH<sub>2</sub> peak at 3.65 ppm should integrate to be 2, however, it only shows 1.88 (Figure 26). Therefore, it is possible to see 94 % of the compound, while 6 % is lost to solid-like characteristics. Compound **3** is different from the previously published compounds, the results for the qNMR the opposite to what was found. It is hypothesised that as the functional group on compound **3** is not aromatic, it is less hydrophobic than compounds **4** and **5**, hence, is more soluble in the H<sub>2</sub>O: EtOH solution. Further research will be carried out to find the cause of this anomaly. All qNMR spectra can be found in the appendix (Figures 101-108).

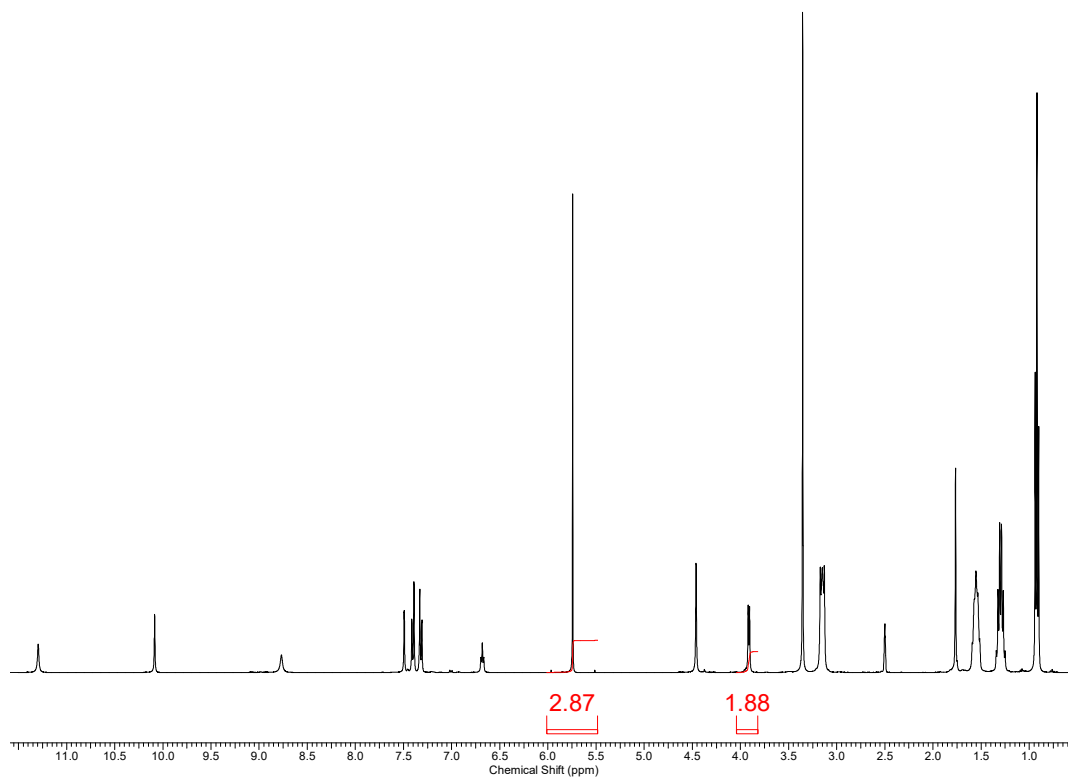


Figure 26 –  $^1\text{H}$  NMR spectrum ( $d_1 = 60$  s) of compound **3** (0.0364 g, 111.12 mM) and DCM (5  $\mu\text{l}$ , 0.08 mM) in  $\text{DMSO-}d_6$ . 6% loss of compound observed upon comparative signal integration.

#### 2.4.2 $^1\text{H}$ NMR DOSY studies

$^1\text{H}$  NMR DOSY studies is used to calculate the hydrodynamic radius of the complex in solution. The  $^1\text{H}$  NMR DOSY experiment reports the diffusion coefficients for the individual resonances in a  $^1\text{H}$  NMR spectrum, then using the Stokes-Einstein equation (Equation 1), the solvation sphere diameter can be calculated.

Equation 1 – The Stokes-Einstein equation used to calculate the hydrodynamic diameter from the diffusion coefficient.

$$d_H = \frac{kT}{3\pi\eta D}$$

$d_H$  = Hydrodynamic diameter (m)  
 $k$  = Boltzmann constant  
 $T$  = Temperature (K)  
 $\eta$  = solvent viscosity (kg/ms)  
 $D$  = diffusion coefficient ( $\text{m}^2/\text{s}$ )

To calculate the solvation sphere diameter of a compound, the calculation assumes that the particle is spherical, however, in practice the particle shapes are not spherical (Figure 27). Therefore, the size of particles obtained from this experiment will be treated as an estimate.

Additionally, the hydrodynamic diameter can only be determined if the compounds are fully observable in the solution with this technique. Herein, the  $^1\text{H}$  NMR DOSY will be carried out in  $\text{DMSO-}d_6$ , compound **3** and the 1:1 mixture will be done in the future as due to synthetic troubles leading to time constraints.

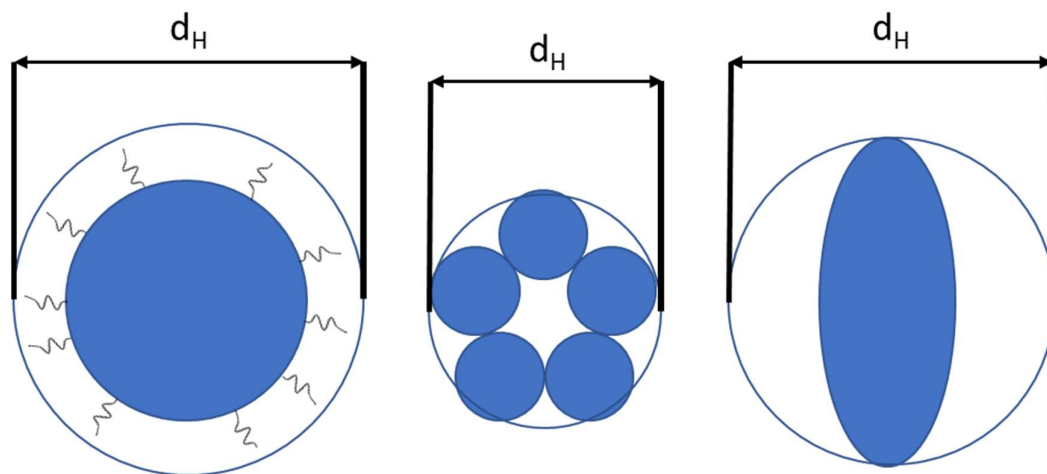


Figure 27 – Examples of non-spherical particles and how the hydrodynamic diameter would be calculated.

#### 2.4.2.1 Results and discussion

The  $^1\text{H}$  NMR DOSY results calculate that compounds **4** and **5** have a diameter of 1.78 and 1.94 nm, respectively (Table 4). Which represents low complex formation, such as monomers, dimers or trimers.

Table 4 – Calculated hydrodynamic radius of compounds **4** and **5** (nm) in  $\text{DMSO-}d_6$  (111.12 mM).

Compound	Hydrodynamic diameter (nm)	
	Anion	Cation
<b>4</b>	1.78	1.28
<b>5</b>	1.94	1.37

The results calculate the cation and anion have different diffusion constants, hence the compound and its counter cation, TBA, does not coordinate strongly in  $\text{DMSO-}d_6$ . The  $^1\text{H}$  NMR DOSY spectra and the table of diffusion coefficients can be found below (Figure 28, 29).

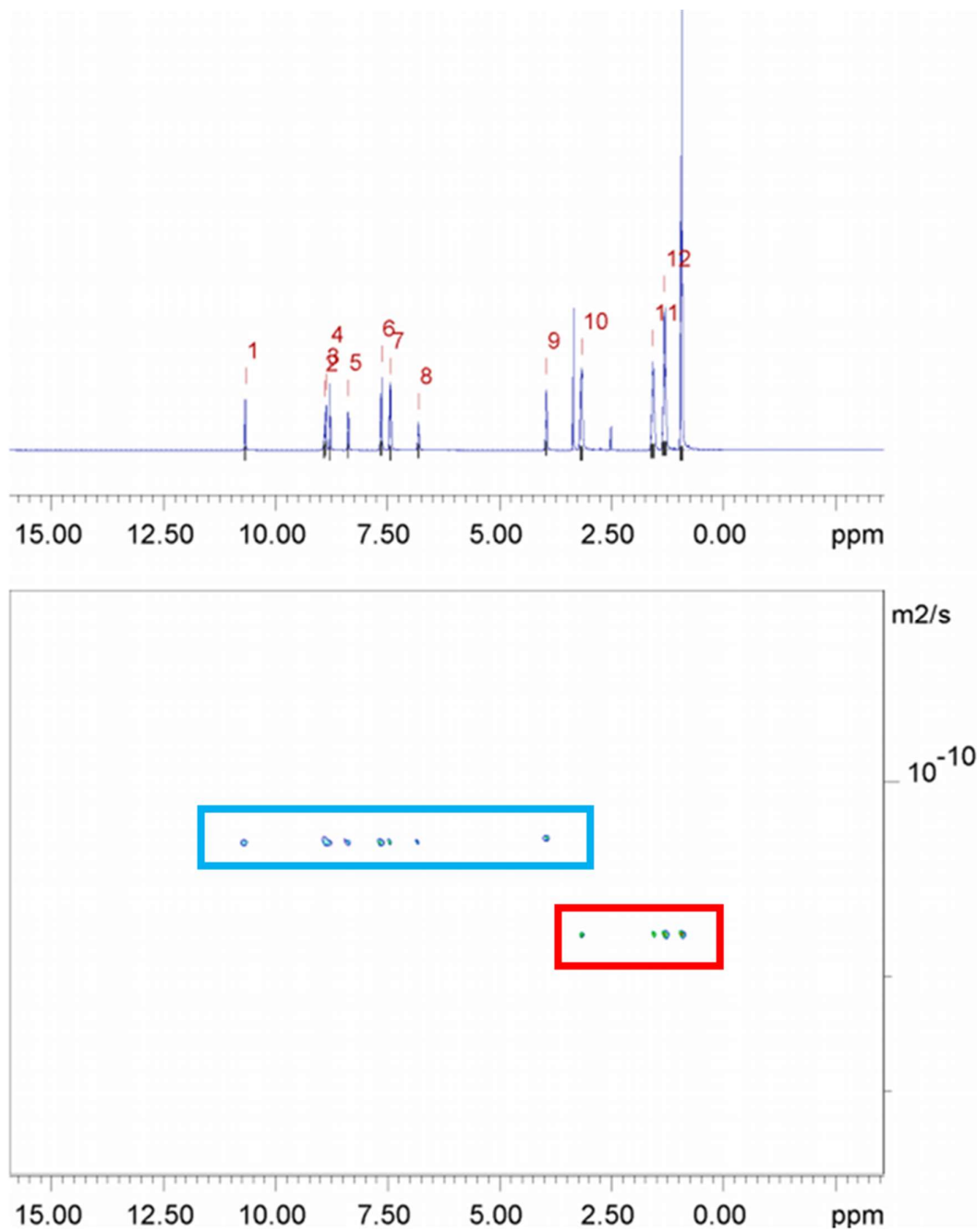


Figure 28 – <sup>1</sup>H DOSY NMR of compound **4** (111.12 mM) in DMSO-*d*<sub>6</sub> conducted at 298.15 K. Anionic component highlighted in blue, TBA counter cation highlighted in red. Including the table representing the values for the diffusion constant for each peak used to calculate the hydrodynamic diameter (*d*<sub>H</sub>). Peaks 1-9 correspond to the anionic component of compound **4**, while peaks 10-13 correspond to the cationic component of compound **4**.

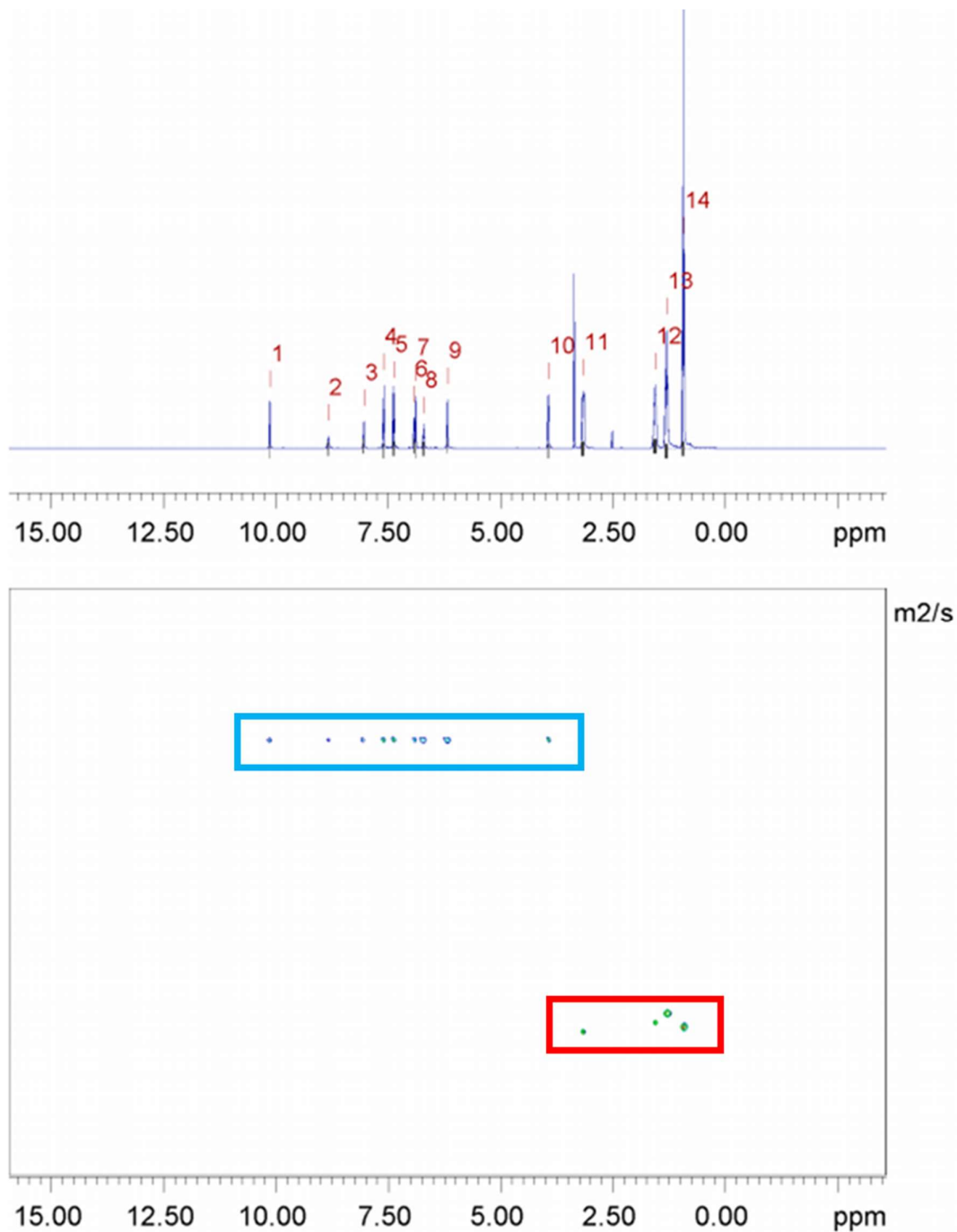
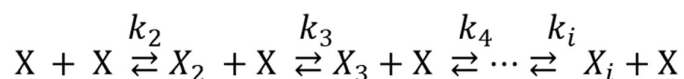


Figure 29 – <sup>1</sup>H DOSY NMR of compound **5** (111.12 mM) in DMSO-*d*<sub>6</sub> conducted at 298.15 K. Anionic component highlighted in blue, TBA counter cation highlighted in red. Including the table representing the values for the diffusion constant for each peak used to calculate the hydrodynamic diameter ( $d_H$ ). Peaks 1-10 correspond to the anionic component of compound **5**, while peaks 11-14 correspond to the cationic component of compound **5**.

### 2.4.3 <sup>1</sup>H NMR self-association studies

A series of <sup>1</sup>H NMR dilution studies were performed to explore the strength of the molecular interactions. The dilution studies were conducted for compounds **4** and **5** in DMSO-*d*<sub>6</sub> with 0.5 % H<sub>2</sub>O at a constant temperature of 298.15 K. This solvent system allowed the binding mechanism of the HBD urea NH groups to be studied. The data was processed under the assumption of the compounds forming low complex species from the DOSY results, the data obtained from <sup>1</sup>H NMR dilution studies was used to calculate self-association constants using a program called Bindfit v0.5,<sup>105</sup> showing the strength of the self-association within the molecule. The data was fitted to both dimerization/ equal K (EK) and cooperative equal K (CoEK) models. Both of these models assume one component, one-dimensional homogenous aggregation.<sup>106</sup> The EK model assumes all self-association constants are identical (Equation 2A), whereas, the CoEK model assumes the first association event has a different energy compared to all of the subsequent events (Equation 2B).<sup>107</sup> If  $\rho < 1$  there is positive cooperativity, if  $\rho > 1$  then there is negative cooperativity and if  $\rho = 1$  then it is non-cooperative.

Equation 2 – One component general linear aggregation system and the EK (A) and CoEK binding model (B).



$$\text{A.} \quad k_E = k_2 = k_3 = k_4 = k_i$$

$$\text{B.} \quad k_E = k_2/\rho = k_3 = k_4 = k_i$$

Where  $\rho = k_2/k_E$

#### 2.4.3.1 Results and discussion

The results of the self-association studies for compound **4** show that for the urea NH's the chemical shift increases downfield as the concentration increases (Figure 30). This indicates the protons becomes more deshielded, suggesting the formation of a self-associating hydrogen bonded molecule at the urea NH. The amide NH (grey) has a negative change in chemical shift becoming more shielded, showing a hydrogen bond breaking. There are several hypothesises for this result;

inductive effects could cause the amide NH to be more shielded or it could already be a complexed molecule and the upfield change in chemical shift shows the complex breaking at the amide.

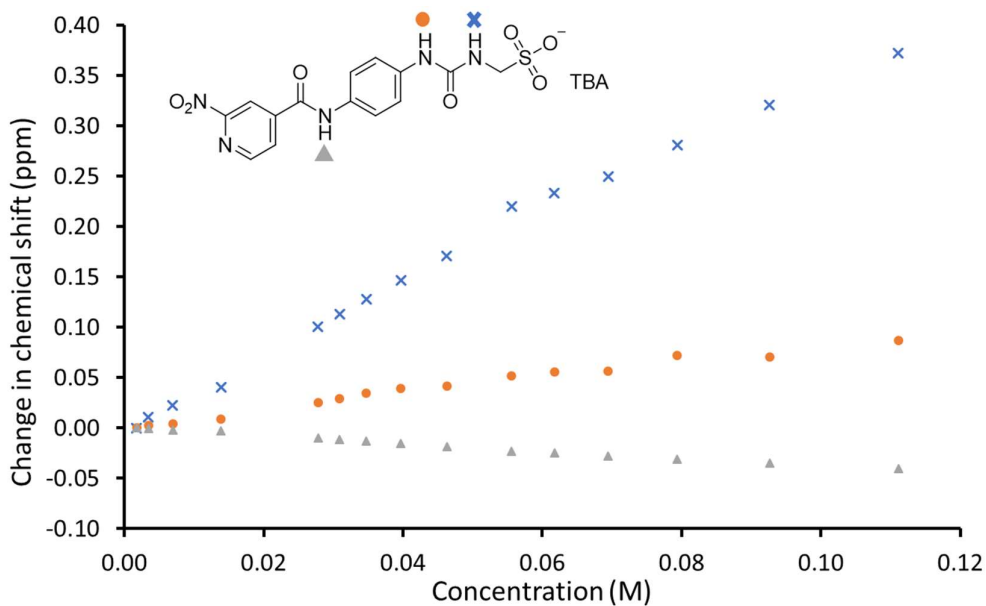


Figure 30 – Graph illustrating the <sup>1</sup>H NMR down-field change in chemical shift of NH resonances with increasing concentration of compound **4** in DMSO- *d*<sub>6</sub> - 0.5 % H<sub>2</sub>O (298.15 K).

Compound **5** shows a similar trend to compound **4** where the urea NH's show a downfield change in chemical shift (Figure 31), while the amide NH also shows an upfield shift (grey). There is no change in chemical shift for the amine NH<sub>2</sub> which shows there are no interactions at that point (yellow), which leaves it free to interact.

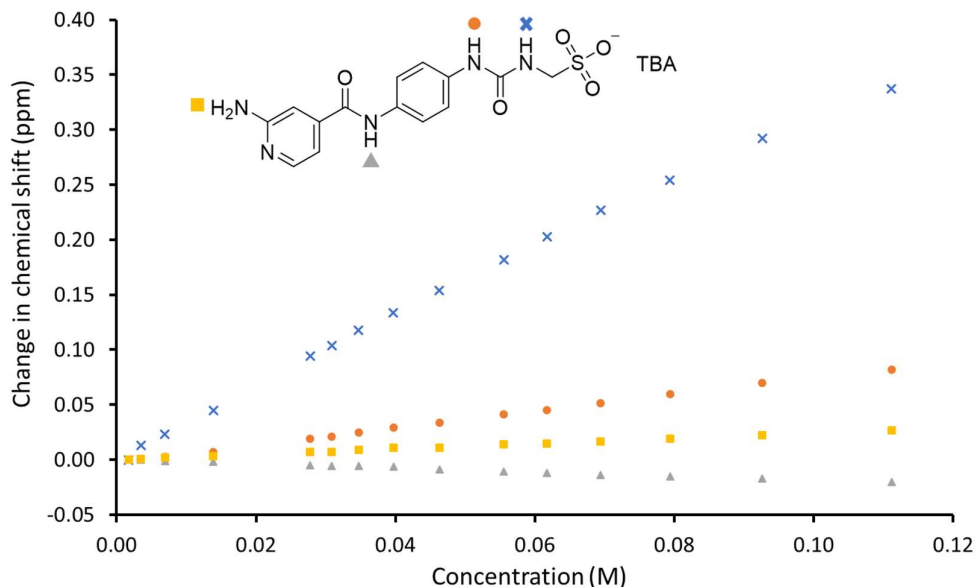


Figure 31 – Graph illustrating the  $^1\text{H}$  NMR down-field change in chemical shift of NH resonances with increasing concentration of compound **5** in  $\text{DMSO-}d_6$  - 0.5 %  $\text{H}_2\text{O}$  (298.15 K).

Both compounds were successfully fitted to both the dimerisation EK and CoEK model. Comparatively, the CoEK model shows a self-association constant approximately four times stronger than the EK model, however, considering the associated errors calculated for both models, the data supports the EK model. It is possible to conclude that the compounds dimerise with equal energies and the interactions are weak.

Table 5 – Self-association constants ( $\text{M}^{-1}$ ) calculated for compounds **4** and **5** in a  $\text{DMSO-}d_6$  – 0.5%  $\text{H}_2\text{O}$  solution at 298 K. These constants were obtained from the fitting of  $^1\text{H}$  NMR dilution data and refined to EK and CoEK models using Bindfit v0.5.<sup>105</sup> The links for the Bindfit data are provided within the appendix.

Compound	EK Model ( $\text{M}^{-1}$ )		CoEK Model ( $\text{M}^{-1}$ )		
	$K_e$	$K_{\text{dim}}$	$K_e$	$K_{\text{dim}}$	$\rho$
<b>4</b>	1.41 ( $\pm 1.5\%$ )	0.71 ( $\pm 0.7\%$ )	10.91 ( $\pm 3.4\%$ )	5.45 ( $\pm 1.7\%$ )	0.30 ( $\pm 10.0\%$ )
<b>5</b>	1.78 ( $\pm 0.6\%$ )	0.89 ( $\pm 0.3\%$ )	8.32 ( $\pm 3.1\%$ )	4.16 ( $\pm 1.6\%$ )	0.50 ( $\pm 5.2\%$ )

$^1\text{H}$  NMR dilution studies will be performed on compounds **7** and **8** in the future to model the interactions at the nitro/aminopyridine.

#### 2.4.4 $^1\text{H}$ NMR titration studies

A series of  $^1\text{H}$  NMR titration studies were carried out for compounds **4**, **5**, **7-9** as hosts molecules with compounds **10** and TBA  $\text{HSO}_4^-$  as guest molecules to mimic the thymine functional group and the sulfonate anion, respectively. This would allow us to calculate the strength of the interaction between the molecules. The titration results for compound **9** and TBA  $\text{HSO}_4^-$  are previously published,<sup>96</sup> it models the urea-sulfonate interaction and it is shown to interact with a weak association constant of  $27 \text{ M}^{-1}$ . Association constants were calculated using Bindfit v0.5,<sup>105</sup> refining it to three binding isotherms, these models assume one component, one-dimensional homogenous aggregation. Each NH resonance was separately refined to distinguish whether the interaction formed on a 1:1, 1:2 and 2:1 relationship. These studies were performed in collaboration with Milan Dimitrovski.

##### 2.4.4.1 Results and discussion

The titration results of compound **4** with compound **10** show no correlation between the two compounds (Figure 32). The change in chemical shift between the compounds is negligible ( $< 0.01$  ppm), concluding that compound **4** does not interact with compound **10**.

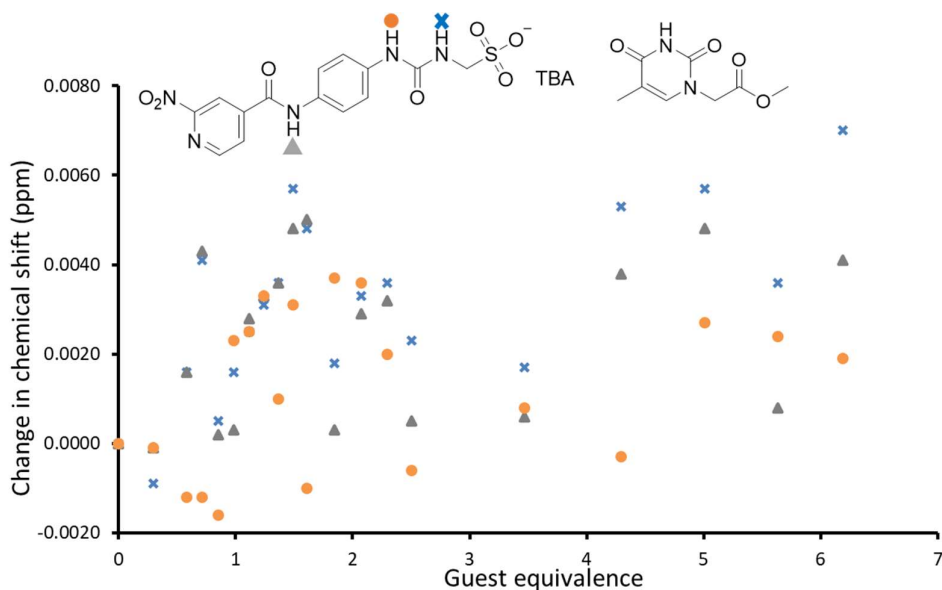


Figure 32 – A graph showing the downfield  $^1\text{H}$  NMR change in chemical shift for each NH in compound **4** (host) with increasing the concentration of compound **10** (guest) in a  $\text{DMSO}-d_6 - 0.5\% \text{ H}_2\text{O}$  solution (298 K).

Titration results of compound **4** with TBA  $\text{HSO}_4^-$  show an interaction between the molecules (Figure 33). However, it is not possible to fit these data to a binding model as multiple interactions are occurring within this system and is therefore no longer a one component system.

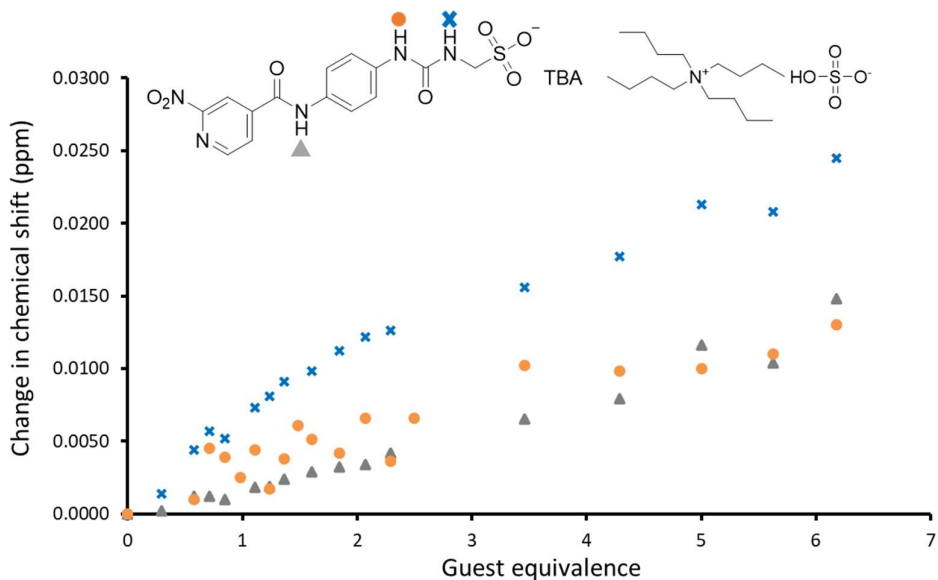


Figure 33 – A graph showing the downfield  $^1\text{H}$  NMR change in chemical shift for each NH in compound **4** (host) with increasing the concentration of TBA  $\text{HSO}_4^-$  (guest) in a  $\text{DMSO}-d_6 - 0.5\% \text{H}_2\text{O}$  solution (298 K).

The titration results for compound **5** with compound **10** show no correlation, as the change in chemical shift is negligible (Figure 34). The two compounds were theorised to interact; however, it is hypothesised that the compound **5** interacts with the solvent, preventing the interaction between the compounds.

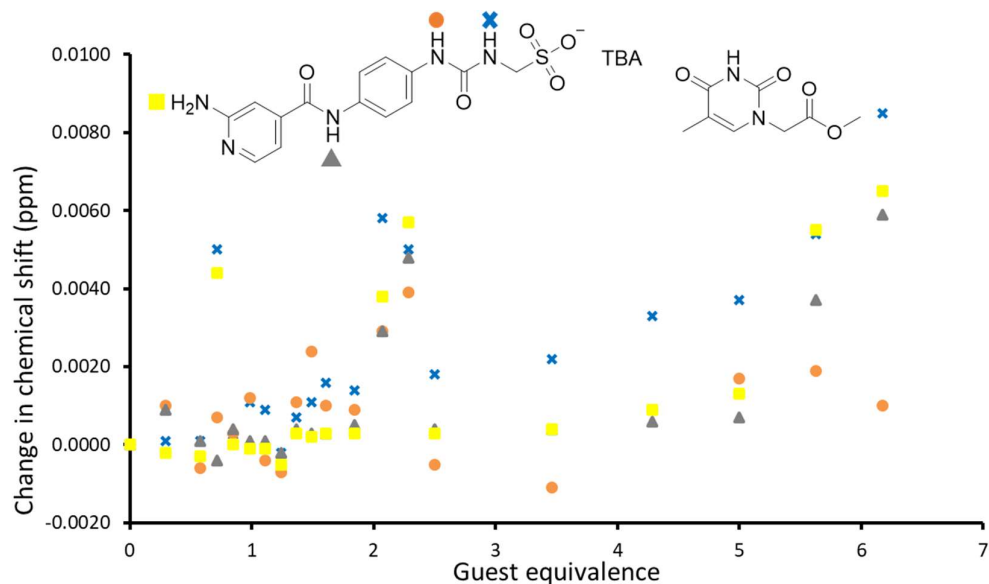


Figure 34 – A graph showing the downfield  $^1\text{H}$  NMR change in chemical shift for the NHs of compound **5** (host) with increasing the concentration of compound **10** (guest) in a  $\text{DMSO-}d_6$  – 0.5%  $\text{H}_2\text{O}$  solution (298 K).

The titration results of compound **5** with TBA  $\text{HSO}_4^-$  show correlation with the urea NH and the amino group (Figure 35). The results correspond to the crystal structure showing an interaction between the sulfonate-urea (Figure 20). The graph also shows an interaction between the amino functional group and the sulfonate, which is also seen in the crystal structure. These data were unable to be fitted to the Bindfit model as multiple interactions are occurring in this system.

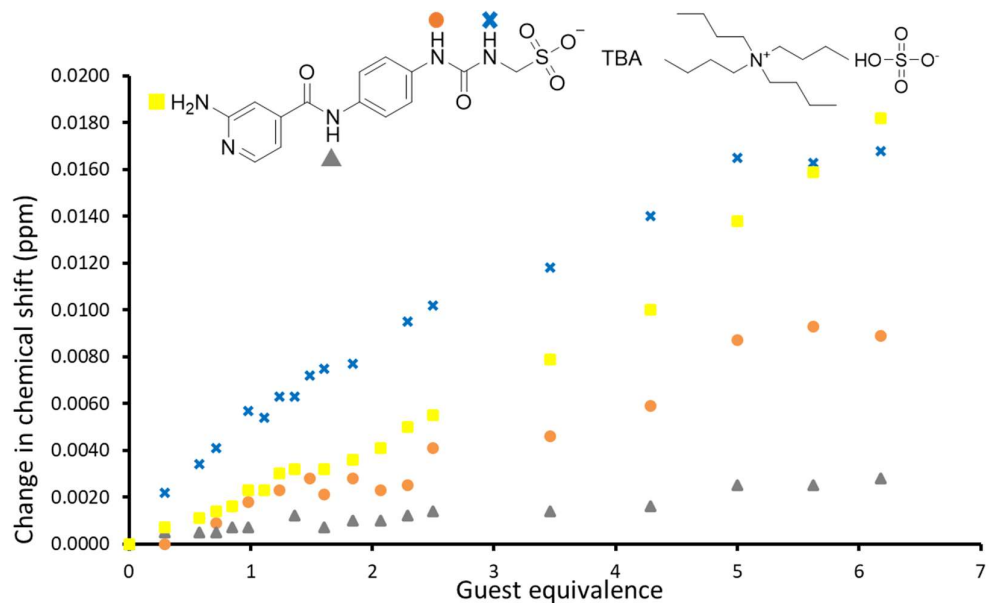


Figure 35 – A graph showing the downfield  $^1\text{H}$  NMR change in chemical shift for the NHs of compound **5** (host) with increasing the concentration of TBA  $\text{HSO}_4^-$  (guest) in a  $\text{DMSO}-d_6 - 0.5\% \text{H}_2\text{O}$  solution (298 K).

The titration results for compound **7** with compound **10** shows that there is no interaction between them as the change in chemical shift is negligible ( $< 0.01$  ppm) (Figure 36). Using the results from this experiment and the titration between compound **4** and **10**, there is no complex formation between compounds **7** and **10**, this was expected as nitropyridine is not an analogue of adenine.

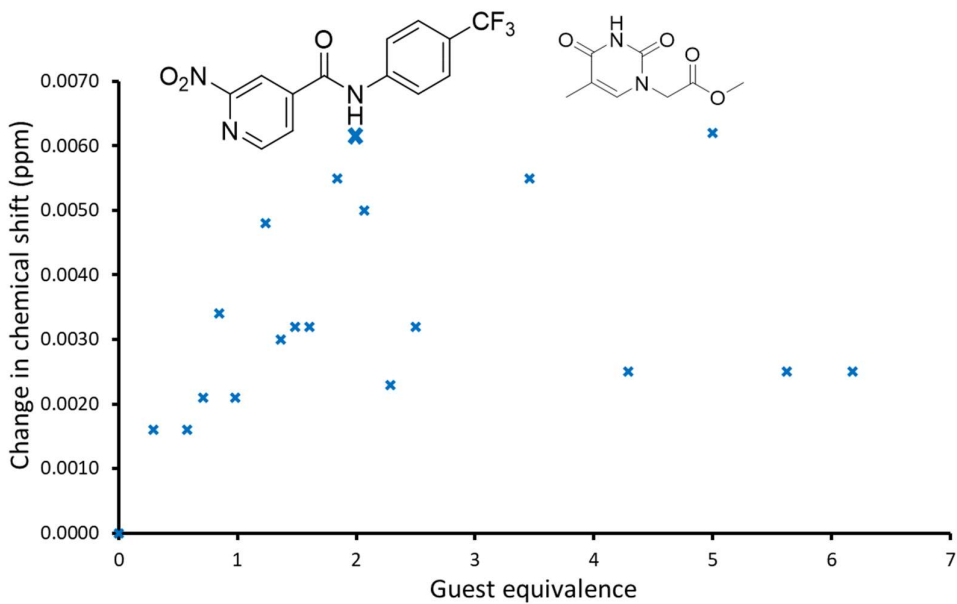


Figure 36 – A graph showing the downfield  $^1\text{H}$  NMR change in chemical shift for the NHs of compound **7** (host) with increasing the concentration of compound **10** (guest) in a  $\text{DMSO}-d_6 - 0.5\% \text{H}_2\text{O}$  solution (298 K).

The titration results for compound **7** with TBA HSO<sub>4</sub><sup>-</sup> show a weak association between them (Figure 37), it can be concluded that the compounds interact with a 1:1 ratio due to the numbers calculated for the 1:2 and 2:1 host: guest ratio either being too large or negative. However, the interaction between the sulfonate and the amide is weak.

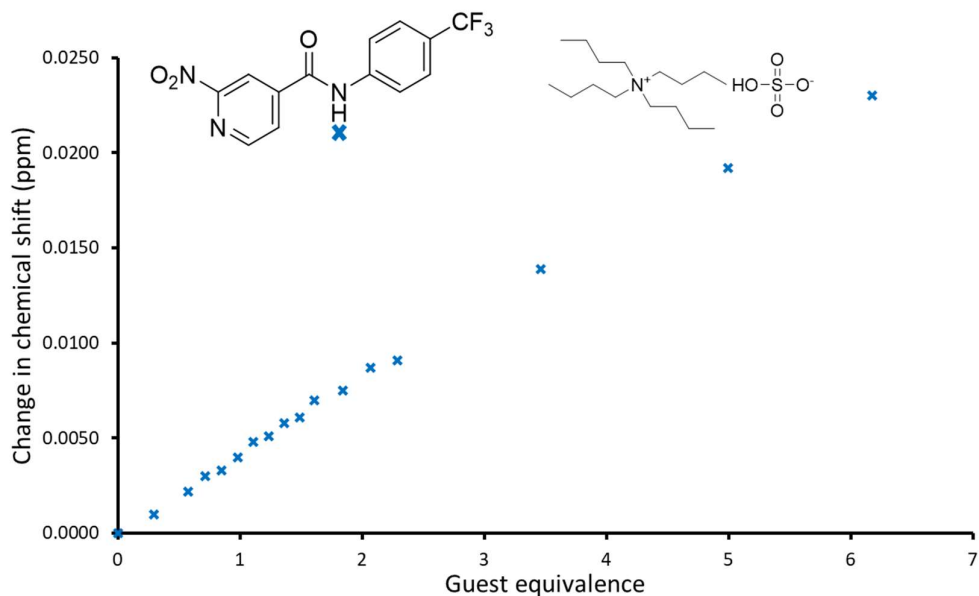


Figure 37 – A graph showing the downfield <sup>1</sup>H NMR change in chemical shift for the NHs of compound **7** (host) with increasing the concentration of TBA<sup>+</sup> HSO<sub>4</sub><sup>-</sup> (guest) in a DMSO-*d*<sub>6</sub> – 0.5% H<sub>2</sub>O solution (298 K).

Table 6 – Association constants (M<sup>-1</sup>) calculated for each NH in compound **7** (host) titrated against TBA<sup>+</sup> HSO<sub>4</sub><sup>-</sup> (guest) in a DMSO-*d*<sub>6</sub> – 0.5% H<sub>2</sub>O solution (298 K). The links for the Bindfit data is provided within the appendix.

Host: Guest	1: 1	1: 2		2: 1	
NH	K	K <sub>11</sub>	K <sub>12</sub>	K <sub>11</sub>	K <sub>21</sub>
<b>Circle</b>	3.35 (± 1.1 %)	436846684486 (± 8309238 %)	3.49 (± 1.8 %)	-48.36 (± -9.0 %)	-24.69 (± - 8.1 %)

The titration results for compound **8** with compound **10** show a negative change in chemical shift, which here represents an upfield shift (Figure 38). However, these data could not be fitted to the Bindfit models as self-association is suspected, therefore, has multiple interactions occurring in this system. The dilution study of this compound is will be carried out in the future to figure out this complex system.

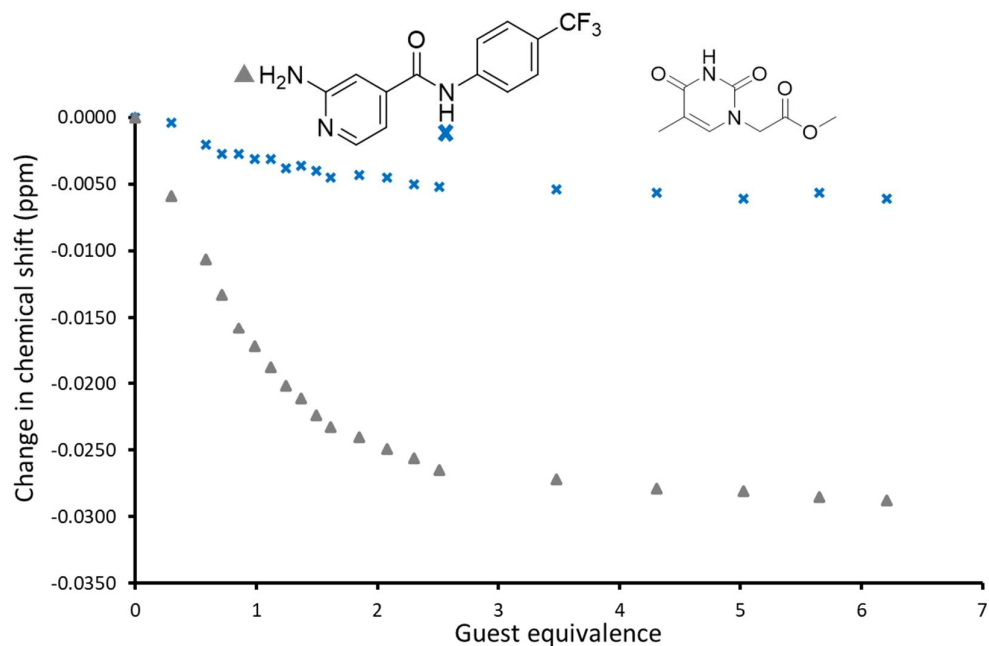


Figure 38 – A graph showing the downfield  $^1\text{H}$  NMR change in chemical shift for the NHs of compound **8** (host) with increasing the concentration of compound **10** (guest) in a  $\text{DMSO-}d_6$  – 0.5%  $\text{H}_2\text{O}$  solution (298 K).

The titration results for compounds **8** and  $\text{TBA}^+ \text{HSO}_4^-$  shows an interaction between the aminopyridine and the sulfonate (Figure 39). The initial upfield change in chemical shift suggests a hydrogen bond breaking, which is hypothesised to be the interruption of the self-associated species. Then the downfield change in chemical shift is hypothesised to be a complex formation between compounds **8** and **10** as the crystal structure of compound **5** shows an interaction between the aminopyridine-sulfonate (Figure 20).

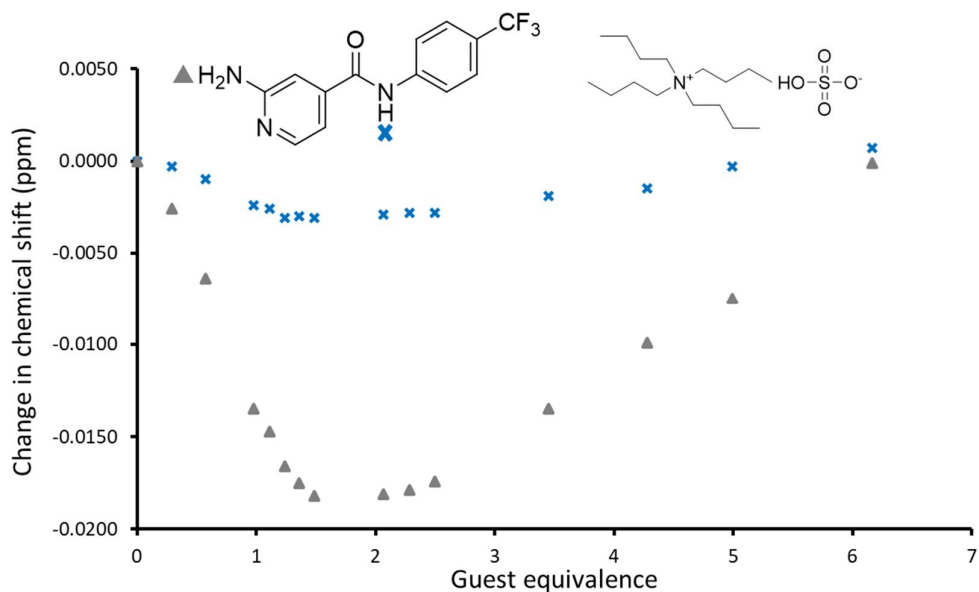


Figure 39 – A graph showing the downfield  $^1\text{H}$  NMR change in chemical shift for the NHs of compound **8** (host) with increasing the concentration of  $\text{TBA}^+ \text{HSO}_4^-$  (guest) in a  $\text{DMSO}-d_6 - 0.5\% \text{H}_2\text{O}$  solution (298 K).

The titration results for compound **9** and compound **10** shows that there is an interaction between them (Figure 40), there is a weak 1:1 association constant of  $26 \text{ M}^{-1}$  and  $17 \text{ M}^{-1}$  between the two NHs. The 1:2 and 2:1 binding models were not accepted as the errors are too large or the association constant is negative.

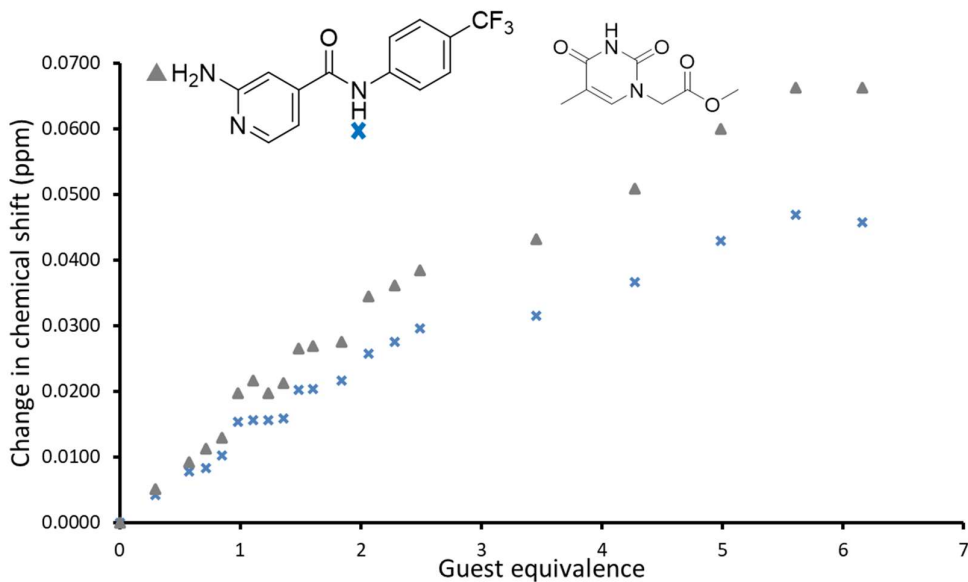


Figure 40 – A graph showing the downfield  $^1\text{H}$  NMR change in chemical shift for the NHs of compound **9** (host) with increasing the concentration of compound **10** (guest) in a  $\text{DMSO}-d_6 - 0.5\% \text{H}_2\text{O}$  solution (298 K).

Table 7 – Association constants ( $M^{-1}$ ) calculated for each NH in compound **9** (host) titrated against compound **10** - (guest) in a  $DMSO-d_6 - 0.5\% H_2O$  solution (298 K). The links for the Bindfit data is provided within the appendix.

Host: Guest	1: 1	1: 2		2: 1	
NH	K	$K_{11}$	$K_{12}$	$K_{11}$	$K_{21}$
<b>Circle</b>	25.92 ( $\pm 5.7\%$ )	2010437381651813 ( $\pm 169434405\%$ )	20.46 ( $\pm 9.7\%$ )	56.18 ( $\pm 97.5\%$ )	639.76 ( $\pm 112.9\%$ )
<b>Triangle</b>	17.33 ( $\pm 4.8\%$ )	38.31 ( $\pm 9.3\%$ )	-5.25 ( $\pm -24.1\%$ )	0.00881 ( $\pm 104.1\%$ )	5400616 ( $\pm 115.3\%$ )

From the titration results, we can conclude that thymine does not interact with the nitropyridine amide functional group. However, the sulfonate shows interaction with the amide, hence, it is possible to form amide-sulfonate interactions, this is observed in the solid state (Figure 19). As hypothesised, the thymine shows an interaction with the aminopyridine, but the aminopyridine also shows an interaction with the sulfonate and the thymine interacts with the urea. Therefore, it is hypothesised that with compound **5**, there are competitive interactions between the sulfonate-aminopyridine, thymine-urea and thymine-aminopyridine weakening the thymine-aminopyridine interaction.

#### 2.4.5 Dynamic light scattering (DLS) and zeta potential

DLS is a non-destructive technique used to determine the state of motion of particles and the spherical size of the particles which have been dissolved in a solvent system.<sup>108</sup> Moreover, the lower limit of particle size in DLS is approximately 1 nm,<sup>109</sup> therefore, low ordered complex species will be visible but the data will not be reliable. From the qNMR studies, the data shows over a quarter of the molecules in compounds **4**, **5** and the mixture of compounds **3** and **5** forms an aggregate with solid-like characteristics in  $H_2O: EtOH$  19:1 solution, compound **3** was also tested in this study to compare with the mixture. It is assumed they form large aggregates that precipitate out of solution, DLS will be used to measure the size of these aggregates. DLS studies were not conducted for compound **3** as it did not show any loss of compound from the qNMR studies. These studies were

conducted at 3.00 mM due to solubility issues, then diluted to 0.30 mM to check whether the aggregates still form in a diluted sample. The sample was annealed to allow the aggregate to obtain a thermodynamic minimum. Zeta potential was also measured in the same solution to determine the stability of the aggregates formed in solution at 3.00 mM. Literature states that a zeta potential in between -30 mV and 30 mV is considered unstable.<sup>110</sup>

#### 2.4.5.1 Results and discussion

The results show that compounds **4**, **5** and the 1:1 mixture forms stable extended aggregates (> 50 nm and zeta potential < -30 mV) in a H<sub>2</sub>O: EtOH 19:1 solution (Table 11). The aggregates formed from compound **4** are larger than **5** and the mixture of compounds **3** and **5**, however, the polydispersity index (PDI) increases from 26 % to 96 % which signifies it goes from a uniform distribution to a non-uniform distribution. Therefore, it is possible to conclude that this compound is relatively unstable in comparison to compound **5** and the mixture. This hypothesis is supported by the zeta potential, although it is considered stable at < -30 mV it is at the boundary of what is considered stable. Hence, it can be concluded that as the concentration decreases, the stability of the compound decreases too. Compound **5** forms aggregates with a size of 189 nm which decreases when the concentration decreases. However, as the concentration decreases, the PDI of the compound also decreases from 23 % to 14 %, which shows the aggregates become more uniform. The mixture of compounds **3** and **5** forms the smallest aggregates in comparison, with a size of 94 nm down to 88 nm with decreasing concentration. As the PDI change is negligible as concentration decrease, it indicates that the aggregates remain stable. The addition of compound **3** to compound **5** shows that it decreases the stability and size of the aggregates. This could be due to compound **3** being more hydrophilic hence decreasing the stability of compound **5** in a H<sub>2</sub>O solution. Compound **3** appears to form extended aggregates in a H<sub>2</sub>O: EtOH 19:1 solution, however, the zeta potential shows that the aggregates that are formed are unstable within this solution. This is hypothesised to be due to the hydrophilic properties of the compound.

Table 8 – Average intensity particle size distribution for compounds **3-5** and a 1:1 mixture of compounds **3** and **5** calculated from 10 DLS runs at a total concentration of 3.00 mM and 0.3 mM. Zeta potential for compounds **3-5** and a 1:1 mixture of compounds **3** and **5**, calculated from 10 runs at a total concentration of 3.00 mM. Samples were prepared in series, with an aliquot of the most concentrated solution undergoing serial dilution and measured after heating to 40 °C and cooling to 25 °C. Error = standard error of the mean.

Compound	Peak maxima (nm)		PDI (%)		Zeta potential (mV)
	3 mM	0.3 mM	3 mM	0.3 mM	
<b>3</b>	147.23 (± 7.4)	126.23 (± 2.85)	25.02 (± 0.7)	21.79 (± 0.3)	-14.40
<b>4</b>	230.97 (± 12.8)	222.45 (± 9.7)	26.13 (± 0.8)	96.25 (± 3.2)	- 32.05
<b>5</b>	189.30 (± 3.0)	128.41 (± 2.7)	23.56 (± 0.4)	14.20 (± 2.5)	- 53.75
<b>3 and 5</b>	94.47 (± 2.0)	88.61 (± 3.9)	24.69 (± 0.4)	25.68 (± 0.8)	- 43.00

All DLS graphs, DLS correlation functions and zeta potential graphs can be found in the appendix (Figures 126-145).

#### 2.4.6 Surface tension and critical micelle concentration (CMC)

The CMC is the concentration at which the addition of any extra amphiphile will result in the formation of aggregates in solution,<sup>111</sup> however, the aggregates can be present before the CMC is reached. The CMC will be determined as the concentration at which any addition of compound will no longer decrease the surface tension and has been found that a low CMC forms stable micelles.<sup>112</sup> The surfactant properties of the amphiphiles was tested using a pendant drop method in a H<sub>2</sub>O: EtOH 19:1 solution, corresponding to the DLS and zeta potential studies. Due to time constraints, the CMC for the mixture of compound **3** and **5** is not available, however, it will be done in the future.

##### 2.4.6.1 Results and discussion

The CMC values were calculated for compounds **3-5** and the mixture (Table 12), it shows the following trend **3 > 4 > 5**. Comparing the CMC to the zeta potential as the trend for zeta potential is as followed, **3 > 4 > 5**, this shows the CMC and zeta potential have a positive correlation. The surface tension at CMC for compound **3** is the lowest, indicating that compound **3** is the best surfactant.

Table 9 – Overview of CMC and surface tension (obtained at CMC) measurements for compounds **3-5** at 25°C.

Compound	CMC (mM)	Surface tension at CMC (mN/ m)
<b>3</b>	24.98	53.70
<b>4</b>	6.00	56.87
<b>5</b>	4.24	57.70

The 1:1 mixture was not studied with this technique due to time constraints, the CMC for the mixture will be done in the future. All CMC graphs can be found in the appendix (Figures 146-148).

## 2.5 Low level in-silico modelling

Computational chemistry is often combined with chemistry to help form hypothesis for problems that arise. An example of computational chemistry supporting chemistry is within synthetic chemistry, the electrostatic potential map can be calculated to help visualise the electronegative and electropositive areas of a compound and help support the hypothesis of the molecular interactions.<sup>113</sup> Herein, computational chemistry will be used to calculate the electrostatic potential maps for compounds **3-10** using Spartan 16" with energy minimised semi-empirical PM6 modelling methods to derive comparative  $E_{\max}$  and  $E_{\min}$  values.<sup>114</sup>

### 2.5.1 Results and discussion

The electrostatic potential maps show that for compound **3** the most negative point on the surface ( $E_{\min}$ ) of the molecules is predominately at the sulfonate (Figure 41), which is expected as the negative charge is carried there, however, there is also a negative point on the surface around the urea oxygen. Hence, the sulfonate and urea oxygen are the areas which are likely to be HBA groups. The most positive points on the surface ( $E_{\max}$ ) are compound **3** is at the urea NHs, amide NH and around the DNA moiety, therefore, these areas are likely to be HBD groups. This trend also occurs within compounds **4** and **5** (Figures 150-151). These electrostatic potential maps correlate with the crystal structures of compounds **4** and **5** as we see interactions between the sulfonate-urea, the sulfonate-DNA moiety and the sulfonate-amide group (Figures 19-20).

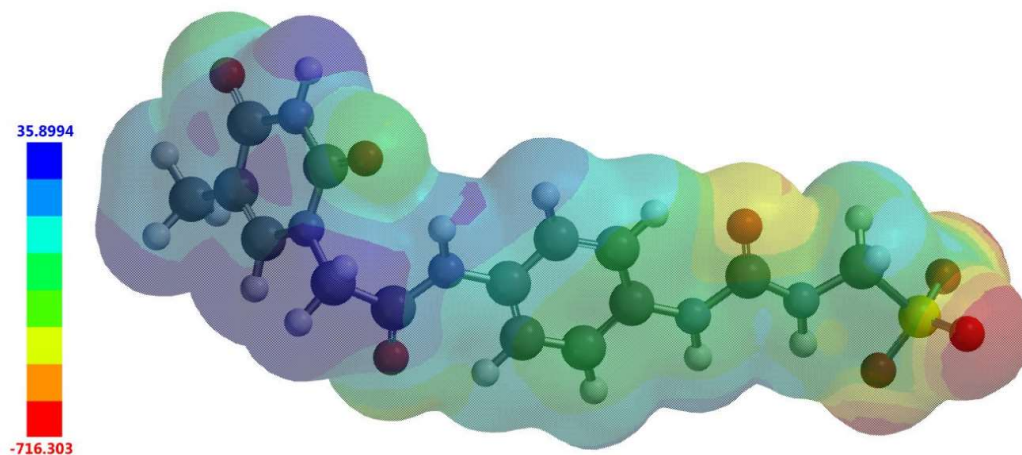


Figure 41 – Electrostatic potential map calculated for the anionic component of **3**.  $E_{\max}$  and  $E_{\min}$  values depicted in the Figure legends are given in kJ/mol.

The electrostatic potential map for compound **7** shows that the  $E_{\min}$  occurs around nitro functionality and amide oxygen (Figure 42), while the  $E_{\max}$  occurs around the amide NH and nitrogen on the nitropyridine. However, when comparing to the crystal structure, it self-associates through the amide functionality showing that the  $E_{\min}$  and  $E_{\max}$  lies more towards the amide as opposed to the nitropyridine moiety. This trend is also apparent for compound **8** (Figure 154), however, a crystal structure was not obtained for compound **8**, therefore, it is hypothesised that it would self-associate through a similar motif.

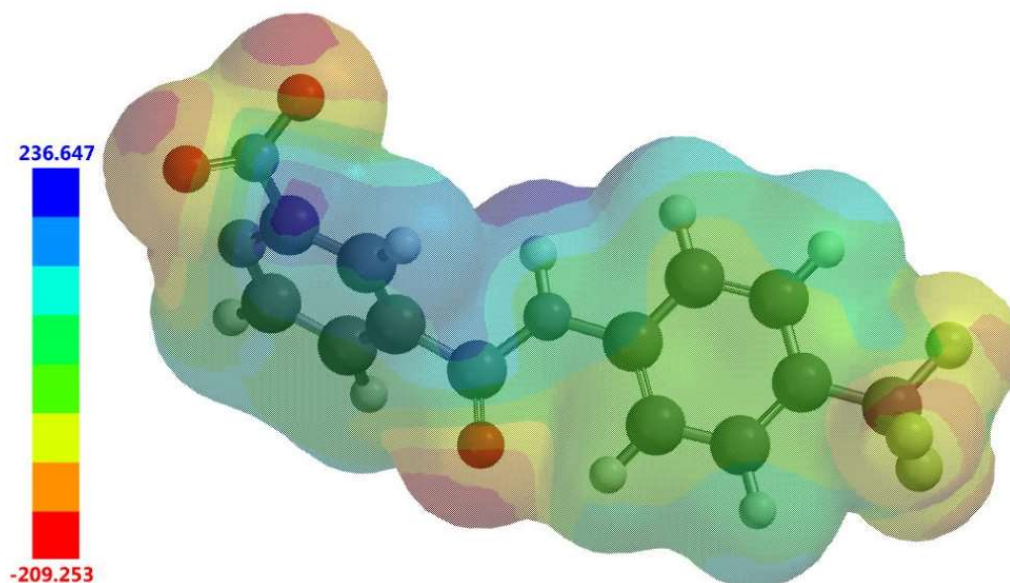


Figure 42 – Electrostatic potential map calculated for compound **7**.  $E_{\max}$  and  $E_{\min}$  values depicted in the Figure legends are given in kJ/mol.

To conclude, the  $E_{\min}$  areas are likely to be HBA groups while the  $E_{\max}$  areas are likely to be HBD groups. It is hypothesised that low-level computational chemistry can be used to help predict where the hydrogen bonding will occur within the solid state.

## 2.6 Antimicrobial properties

Antimicrobial resistance is an ongoing problem and it is predicted to overtake cancer in the number of deaths by 2050,<sup>115</sup> therefore, new antimicrobials must be discovered or the current antimicrobials must be improved to combat this problem. Antibiotics are often overused and misused, leading to a greater increase in antibiotic resistance.<sup>116</sup> Bacteria can be classified into two types; Gram positive which have a single cell membrane and a thick cell wall, and Gram negative which have two cell membranes and a thin cell wall between the membranes. The amphiphiles will be tested on both types of bacteria, *S.aureus* for Gram positive and *E.coli* for Gram negative bacteria. The compounds will be screened at 3.33 mM, using a micro broth dilution method.<sup>117</sup> Compounds **3-5** and the 1:1 mixture were screened against *S.aureus* and *E.coli*, if a compound inhibits more than 10% of growth, the compound would be considered to show antimicrobial activity and will be taken further to calculate the MIC<sub>50</sub>. This study was conducted by Jess Boles.

## 2.6.1 Results and discussion

The screening results for the compounds shows that for both *S.aureus* and *E.coli*, only compound **3** inhibits more than 10 % of growth for both types of bacteria (Figures 43-44), therefore only compound **3** will be taken further to calculate the MIC<sub>50</sub>.

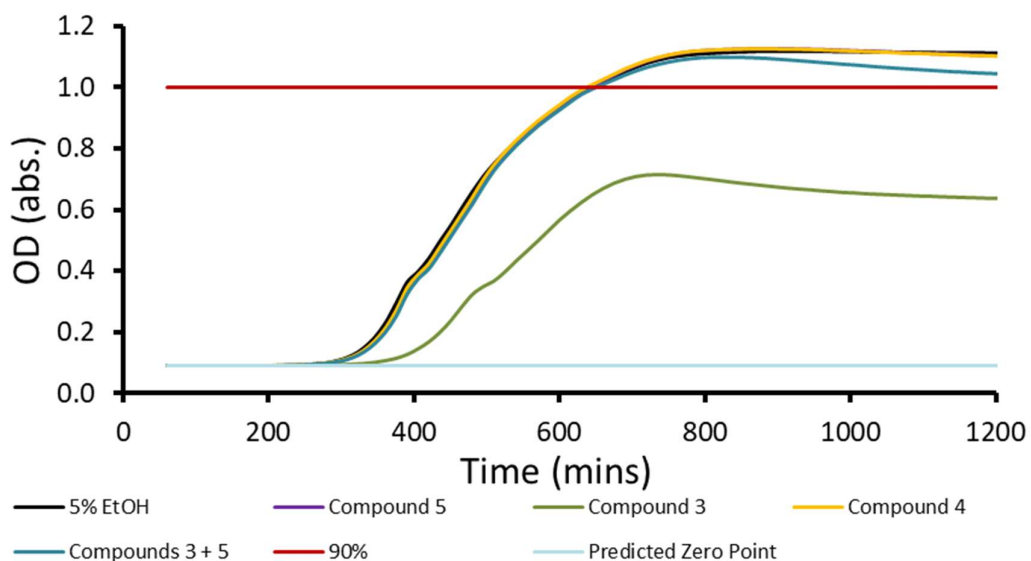


Figure 43 – Averaged growth curves created from absorbance readings of MRSA in the presence of compounds **3**, **4**, **5** and **3 + 5** in combination at a total concentration of 3.3 mM.

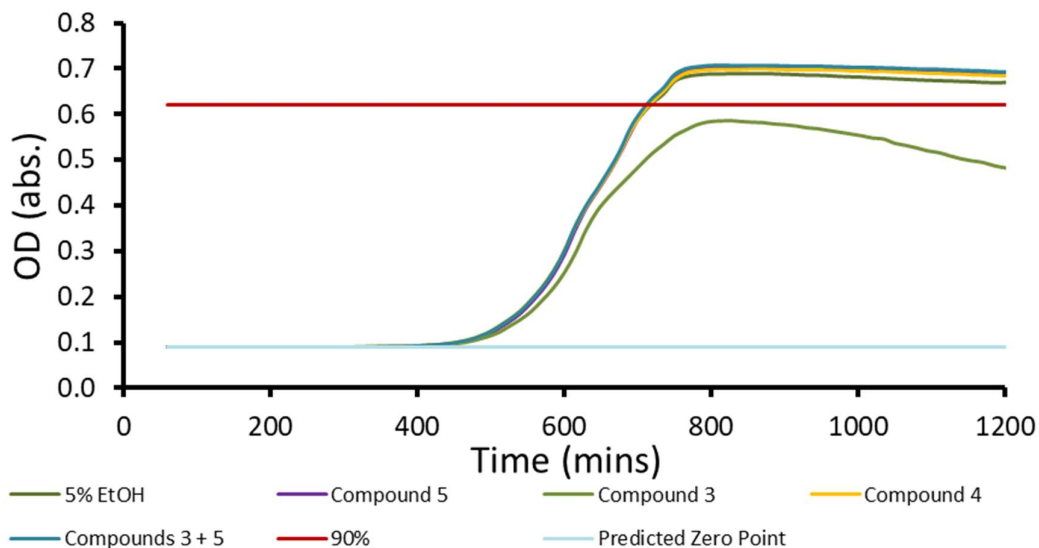


Figure 44 – Averaged growth curves created from absorbance readings of *E. coli* DH10B in the presence of compounds **3**, **4**, **5** and **3 + 5** in combination at a total concentration of 3.3 mM.

## 2.7 Conclusion

In conclusion, two novel DNA inspired amphiphiles were synthesised, characterised and self-association properties were studied and shown to be in line with previously published methods. Novel comparative DNA inspired compounds were also synthesised to break down the complex interactions within the amphiphiles. Solid state, gas phase and solution state experiments showed the amphiphiles can self-associate and form low complex species in DMSO or aggregate into stable micelles in aqueous solutions. Only the thymine inspired amphiphile showed signs of antimicrobial activity against both *S.aureus* and *E.coli*. The titration results conclude that the adenine analogue amphiphile shows no interaction between the thymine comparative compound, this is hypothesised to be due to the competitive interactions of the functional groups between the compounds negating any changes.

## 3. Future works

The self-association and association properties of these novel amphiphiles were studied, they showed the formation of aggregates. They shared similar properties to previously published results from Hiscock et al. Hence, the future works that will be carried out are as followed:

- As Compound **3** passed the antimicrobial screening, it will be taken further and the MIC<sub>50</sub> will be calculated for Gram positive (*S.aureus*) and Gram negative (*E.coli*) bacteria.
- DLS and DOSY studies will be carried out for compound **3** in DMSO. The CMC for the 1:1 mixture of compounds **3** and **5** will be completed and self-association studies for compounds **6** and **7** will be carried out. A crystal structure of compound **8** will be obtained.
- Synthesising the adenine inspired amphiphile and test the association properties with the thymine inspired amphiphile (Figure 45A).

- Synthesising a guanine and cytosine inspired amphiphiles and testing association properties between them (Figure 45 B, C).

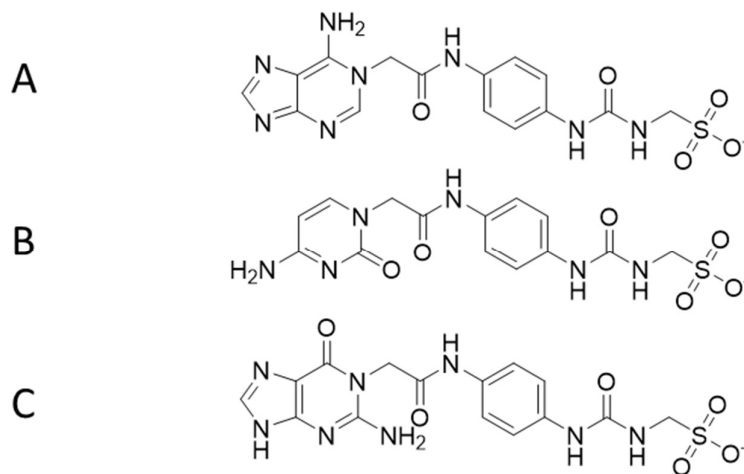


Figure 45 – Theoretical structures of DNA inspired amphiphiles A) adenine B) cytosine C) guanine.

## 4. Experimental techniques

### 4.1 General remarks

All reactions were performed under a slight positive pressure of nitrogen using oven-dried glassware. NMR spectra were determined using a Bruker AV2 400 MHz or Bruker AVNEO 400 MHz spectrometer with the chemical shifts reported in parts per million (ppm), calibrated to the centre of the solvent peak set. The data was processed using ACD Labs, all solvents and starting materials were purchased from commercial sources where available. High-resolution mass spectra were collected using a Bruker micrOTOF-Q mass spectrometer. Melting points were recorded in open capillaries using a Stuart SMP10 melting point apparatus. Infrared (IR) spectra were recorded using a Shimadzu IR-Affinity 1, the data was analysed in wavenumbers ( $\text{cm}^{-1}$ ) using IRsolution software. DLS and Zeta Potential studies were carried out using Anton Paar Litesizer™ 500 and processed using Kalliope™ Professional.

### 4.2 DLS studies

Studies conducted with compounds **4** and **5** were prepared in series with an aliquot of the most concentrated solution undergoing serial dilution. Sample sizes were kept to 1 mL. All solvents used for DLS studies were filtered to remove particulates from the solvents. Samples were heated to the appropriate temperature and allowed to equilibrate for 1 hour and then a series of 10 'runs' were performed with each sample to give enough data to derive an appropriate average. In some instances, the raw correlation data indicated that a greater amount of time may be needed for the samples to reach a stable state. For this reason, only the last 9 'runs' were included in the average size distribution calculations.

### 4.3 Zeta potential studies

All solvents used for Zeta potential studies were filtered to remove particulates from the solvents. Samples were heated to the appropriate temperature and allowed to equilibrate for 1 hour and then a series of 10 'runs' at 25 °C were performed with each sample to give enough data

to derive an appropriate average. In some instances, the raw correlation data indicated that a greater amount of time may be needed for the samples to reach a stable state. For this reason, only the last 9 'runs' were included in the average size distribution calculations.

#### 4.4 High-resolution mass spectra studies

Samples were dissolved in HPLC-grade methanol at a concentration of 1 mg/mL before being diluted 1 in 100 in methanol. 10  $\mu$ L of the sample was injected into a flowing stream of 10 mM ammonium acetate in 95% methanol in water (flow rate: 0.02 mL/min) and the flow directed into the electrospray source of the mass spectrometer. Mass spectra were acquired in the negative ion mode and data processed in Bruker's Compass Data Analysis software.

#### 4.5 Self-association and association constant calculation

All association constants were calculated using the freely available bindfit programme (<http://app.supramolecular.org/bindfit/>). All the data relating to the calculation of the association constants can be accessed online, through the links given for each complexation event.

#### 4.6 Single-crystal X-ray studies

A suitable crystal of each amphiphile was selected and mounted on a Rigaku Oxford Diffraction Supernova diffractometer. Data were collected using Cu K $\alpha$  radiation at 293 K. Structures were solved with the ShelXT<sup>118</sup> or ShelXS structure solution programs via Direct Methods and refined with ShelXL<sup>119</sup> by Least Squares minimisation. Olex2<sup>120</sup> was used as an interface to all ShelX programs (CCDC 1866274-1866275)

## 4. Synthesis

**Compound 1:** This compound was synthesised in line with our previously published methods. Proton NMR were found to match our previously published values.<sup>91</sup> <sup>1</sup>H NMR (400 MHz, DMSO-*d*<sub>6</sub>): 0.93 (t, J = 7.34 Hz, 12H), 1.31 (s, J = 7.36 Hz, 8H), 1.56 (m, 8H), 3.16 (m, 8H), 3.92 (d, J = 6.00 Hz, 2H), 6.99 (br s, NH), 7.58 (d, J = 9.20 Hz, 2H), 8.09 (d, J = 9.28 Hz, 2H), 9.56 (br s, NH).

**Compound 2:** This compound was synthesised in line with our previously published methods.

Proton NMR were found to match our previously published values.<sup>92</sup> <sup>1</sup>H NMR (400 MHz, DMSO-*d*<sub>6</sub>): 0.93 (t, J = 7.24 Hz, 12H), 1.30 (m, 8H), 1.56 (m, 8H), 3.16 (m, 8H), 3.84 (d, J = 5.85 Hz, 2H), 4.62 (br s, 2H, NH<sub>2</sub>), 6.23 (m, NH), 6.45 (d, J = 8.68 Hz, 2H), 7.00 (d, J = 8.72 Hz, 2H), 8.26 (br s, NH).

**Compound 3:** HOSu (0.118 g, 1.027 mM) was added to a stirring solution of thymine-1-acetic acid (0.190 g, 1.027 mM) and compound **2** (0.50 g, 1.027 mM) in DMF (2 mL) in an ice-bath for 30 mins. After the 30 mins DCC (0.254 g, 1.233 mM) in DMF (2 mL) was added to the solution and taken out of the ice bath and left stirring overnight. Water (10 mL) was added, the precipitate was filtered and removed. The water was taken to dryness and the solid was dissolved DCM (20 mL). The precipitate was filtered, collected and dissolved in ethanol (20 mL). The precipitate was filtered, removed and the ethanol was taken to dryness. Pure product was obtained by precipitation with acetone yielding a white solid. Yield: 54% (0.36 g, 0.55 mM); <sup>1</sup>H NMR (400 MHz, DMSO-*d*<sub>6</sub>): 0.93 (t, J = 14.60 Hz, 12H), 1.30 (m, 8H), 1.54 (m, 8H), 1.76 (s, 3H), 3.16 (m, 8H), 3.84 (d, J = 5.88 Hz, 2H), 4.46 (s, 2H), 6.40 (br s, NH), 7.30 (d, J = 8.88 Hz, 2H), 7.41 (d, J = 9.08 Hz, 2H), 7.51 (s, 1H), 8.70 (s, NH), 10.12 (s, NH), 11.34(s, NH);

**Compound 4:** EDC (0.087 g, 0.452 mM) was added to a stirring solution 2-nitroisonicotinic acid (0.07 g, 0.411 mM) and Compound **2** (0.20 g, 0.411 mM) in DMF (2 mL) in an ice-bath overnight. Water (10 mL) was added and separated with ethyl acetate (2 x 20 mL). The organic layer was taken to dryness, and the pure product was obtained by precipitation with water yielding a bright yellow solid. Yield: 51% (0.133 g, 0.209 mM); Melting point: 200°C; <sup>1</sup>H NMR (400 MHz, DMSO-*d*<sub>6</sub>): 0.93 (t, J = 14.68 Hz, 12H), 1.30 (m, 8H), 1.56 (m, 8H), 3.16 (m, 8H), 3.87 (d, J = 5.76 Hz, 2H), 6.47 (m, NH), 7.40 (d, J = 8.80 Hz, 2H), 7.63 (d, J = 8.92 Hz, 2H), 8.36 (d, J = 4.88 Hz, 1H), 8.78 (s, 1H), 8.81 (br s, NH), 8.87 (d, J = 4.96 Hz, 1H), 10.67 (br s, NH); <sup>13</sup>C{<sup>1</sup>H} NMR (100 MHz, DMSO-*d*<sub>6</sub>): δ: 13.5 (CH<sub>3</sub>), 19.2 (CH<sub>2</sub>), 23.1 (CH<sub>2</sub>), 56.1 (CH<sub>2</sub>), 57.5 (CH<sub>3</sub>), 116.2 (CH), 117.6 (CH), 121.2 (CH), 127.8 (CH), 131.6 (C), 137.4 (C), 146.4 (C), 149.7 (CH), 154.6 (C), 157.0 (C), 161.2 (C); IR (film): ν = 3333 (NH stretch), 1693 (C=O stretch), 1520 & 1312 (NO<sub>2</sub> stretch) ; HRMS for the sulfonate-urea ion (C<sub>14</sub>H<sub>12</sub>N<sub>5</sub>O<sub>7</sub>S) (ESI<sup>-</sup>): m/z: act: 394.0440 [M]<sup>-</sup> cal: 394.3385 [M]<sup>-</sup>.

**Compound 5:** Compound **4** (3.50 g, 0.55 mM), hydrazine hydrate (1.00 mL, 28.75 mM) and Pd/C 10 % (0.10 g) were heated at reflux overnight in ethanol (20 mL). The Pd/C 10 % was removed by filtration and the remaining solution taken to dryness. Pure product was obtained by precipitation with acetone. Yield: 84% (2.80 g, 0.46 mM); Melting point: >200°C; <sup>1</sup>H NMR (400 MHz, DMSO-*d*<sub>6</sub>): 0.93 (t, J = 7.24 Hz, 12H), 1.30 (m, 8H), 1.56 (m, 8H), 3.16 (m, 8H), 3.85 (d, J = 5.60 Hz, 2H), 6.20 (s, NH<sub>2</sub>), 6.42 (m, NH), 6.85 (s, 1H), 6.91 (d, J = 4.96 Hz, 1H), 7.33 (d, J = 8.68 Hz, 2H), 7.58 (d, J = 8.64 Hz, 2H), 8.02 (d, J = 5.16 Hz, 1H), 8.74 (br s, NH), 10.15 (s, NH); <sup>13</sup>C{<sup>1</sup>H} NMR (100 MHz, DMSO-*d*<sub>6</sub>): δ: 13.6 (CH<sub>3</sub>), 19.2 (CH<sub>2</sub>), 23.1 (CH<sub>2</sub>), 56.1 (CH<sub>2</sub>), 57.5 (CH<sub>3</sub>), 106.2 (CH), 109.4 (CH), 117.6 (CH), 121.0 (CH), 132.3 (C), 136.8 (C), 143.5 (C), 148.4 (CH), 154.6 (C), 160.3 (C), 164.4 (C); IR (film): ν = 3329 (NH stretch), 1676 (C=O stretch); HRMS for the sulfonate-urea ion (C<sub>14</sub>H<sub>14</sub>N<sub>5</sub>O<sub>5</sub>S) (ESI<sup>-</sup>): m/z: act: 364.0702 [M]<sup>-</sup> cal: 364.3565 [M]<sup>-</sup>.

**Compound 6:** This compound was synthesised in line with our previously published methods. Proton NMR were found to match our previously published values.<sup>96</sup> <sup>1</sup>H NMR (400 MHz, DMSO-*d*<sub>6</sub>): 1.77 (s, 3H), 4.57 (s, 2H), 7.53 (s, 1H), 7.81 (d, J = 9.28 Hz, 2H), 8.24 (d, J = 9.28 Hz, 2H), 10.92 (s, NH), 11.41 (s, NH).

**Compound 7:** 2-nitroisonicotinic acid (0.37 g, 2.17 mmol) was added to a stirred solution of CDI (0.387 g, 2.38 mmol) in chloroform (15 mL) and heated at reflux at 70°C under nitrogen for 4 hours. 4-(trifluoromethyl) aniline (0.45 mL, 2.17 mmol) was added to the mixture and left overnight. Crude product was diluted in chloroform (20 mL) and water (3 x 20 mL). The organic layer was reduced in volume and pure product was obtained by precipitation with hexane. Yield: 54% (0.366 g, 1.18 mM); Melting point: 195°C; <sup>1</sup>H NMR (400 MHz, DMSO-*d*<sub>6</sub>): 7.77 (d, J = 8.60 Hz, 2H), 8.01 (d, J = 8.52 Hz, 2H), 8.37 (dd, J = 1.36, 4.94 Hz, 1H), 8.80 (s, 1H), 8.90 (d, J = 4.88 Hz, 1H), 11.09 (s, NH); <sup>13</sup>C{<sup>1</sup>H} NMR (100 MHz, DMSO-*d*<sub>6</sub>): δ: 116.3 (ArCH), 120.5 (ArCH), 124.5 (CF<sub>3</sub>, J = 31.69 Hz), 126.1 (ArCH, J = 269.99 Hz), 128.0 (ArCH, J = 3.79 Hz), 141.9 (ArC), 145.8 (ArC), 149.9 (ArCH), 156.9 (ArC), 162.4 (C=O); IR (film): ν = 3333 (NH stretch), 1662 (C=O stretch), 1535 & 1327 (N-O stretch); HRMS for the sulfonate-urea ion (C<sub>13</sub>H<sub>8</sub>F<sub>3</sub>N<sub>3</sub>O<sub>3</sub>) (ESI<sup>-</sup>): m/z: act: 310.0433 [M]<sup>-</sup> cal: 311.2202 [M]<sup>-</sup>.

**Compound 8:** Hydrazine hydrate (0.5 mL, 10 mM) was added to a stirring solution of Compound 7 (0.200 g, 0.64 mM) and Pd/C (0.05 g, mM) in ethanol (20 mL) and was heated to 80° C. The solution was filtered and taken to dryness. Yield: 75% (0.136g, 0.48 mM); Melting point: >200°C; <sup>1</sup>H NMR (400 MHz, DMSO-*d*<sub>6</sub>): 6.27 (br s, NH<sub>2</sub>), 6.88 (s, 1H), 6.93 (m, 1H), 7.72 (d, J = 8.52 Hz, 2H), 7.98 (d, J = 8.60 Hz, 2H), 8.07 (d, J = 5.24 Hz, 1H) 10.62 (br s, NH); <sup>13</sup>C{<sup>1</sup>H} NMR (100 MHz, DMSO-*d*<sub>6</sub>): δ: 106.3 (ArCH), 109.4 (ArCH), 120.2 (ArCH), 123.0 (q, J = 31.87 Hz, ArC), 123.9 (q, J = 270.00 Hz, CF<sub>3</sub>), 126.0 (q, J = 3.79 Hz, ArCH), 142.5 (ArC), 143.0 (ArC), 148.4 (ArCH), 160.2 (C=O), 165.5 (ArC); IR (film): ν = 3304 (NH stretch), 1676 (C=O stretch); HRMS for the sulfonate-urea ion (C<sub>13</sub>H<sub>10</sub>F<sub>3</sub>N<sub>3</sub>O) (ESI<sup>-</sup>): m/z: act: 280.0820 [M]<sup>-</sup> cal: 281.2382 [M]<sup>-</sup>.

**Compound 9:** This compound was synthesised in line with our previously published methods. Proton NMR were found to match our previously published values.<sup>96</sup> <sup>1</sup>H NMR (400 MHz, DMSO-*d*<sub>6</sub>): 0.89 (t, J = 7.24 Hz, 3H), 1.30 (m, 2H), 1.41 (m, 2H), 3.10 (q, J = 5.76 Hz, 2H), 6.41 (m, NH), 7.61 (d, J = 9.36 Hz, 2H), 8.12 (d, J = 9.36 Hz, 2H), 9.19 (br s, NH).

**Compound 10:** This compound was synthesised in line with previously published methods. Proton NMR were found to match previously published values.<sup>121</sup> <sup>1</sup>H NMR (400 MHz, DMSO-*d*<sub>6</sub>): 1.75 (d, J = 1.10 Hz, 3H), 3.68 (s, 3H), 4.48 (s, 2H), 7.50 (d, J = 1.2 Hz, 1H), 11.43 (br s, NH).

## 5. References

- 1 J. -M Lehn, *Angew. Chemie Int. Ed.*, 1988, **27**, 89–112.
- 2 J. M. Lehn, *Acc. Chem. Res.*, 1978, **11**, 49–57.
- 3 F. Wöhler, *Ann. Phys.*, 1828, **88**, 253–256.
- 4 E. Kinne-Saffran and R. K. H. Kinne, *Am. J. Nephrol.*, 1999, **19**, 290–294.
- 5 A. S. Travis, *Technol. Cult.*, 1990, **31**, 51.
- 6 G. N. Lewis, *J. Am. Chem. Soc.*, 1916, **38**, 762–785.
- 7 G. N. Lewis, *J. Am. Chem. Soc.*, 1913, **35**, 1448–1455.
- 8 J. J. Thomson, *London, Edinburgh, Dublin Philos. Mag. J. Sci.*, 1914, **27**, 757–789.
- 9 J. D. van der Waals, *On the Continuity of the Gaseous and Liquid States*, edited with an introduction by J. S. Rowlinson, Elsevier Science Ltd, Amsterdam; Oxford, 1988.
- 10 J. D. van der Waals, *Nature*, 1874, **10**, 477–480.
- 11 H. Margenau, *Rev. Mod. Phys.*, 1939, **11**, 1–35.

- 12 E. Fischer, *Berichte der Dtsch. Chem. Gesellschaft*, 1894, **27**, 3479–3483.
- 13 T. S. Moore and T. F. Winmill, *J. Chem. Soc. Trans.*, 1912, **101**, 1635–1676.
- 14 W. M. Latimer and W. H. Rodebush, *J. Am. Chem. Soc.*, 1920, **42**, 1419–1433.
- 15 C. J. Pedersen, *J. Am. Chem. Soc.*, 1967, **89**, 7017–7036.
- 16 D. J. Cram and R. H. Bauer, *J. Am. Chem. Soc.*, 1959, **81**, 5971–5977.
- 17 B. Dietrich, J. M. Lehn and J. P. Sauvage, *Tetrahedron Lett.*, 1969, **10**, 2889–2892.
- 18 K. E. Drexler, *Engines of creation: The Coming Era of Nanotechnology*, Anchor Press/Doubleday, New York, NY, 1986.
- 19 J. F. Stoddart, *Angew. Chemie Int. Ed.*, 2017, **56**, 11094–11125.
- 20 J. B. Wittenberg and L. Isaacs, in *Supramolecular Chemistry*, John Wiley & Sons, Ltd, Chichester, UK, 2012.
- 21 G. M. Whitesides and M. Boncheva, *Proc. Natl. Acad. Sci. U. S. A.*, 2002, **99**, 4769–4774.
- 22 X. Lin and M. W. Grinstaff, *Isr. J. Chem.*, 2013, **53**, 498–510.
- 23 J. W. Steed and J. L. Atwood, *Supramolecular Chemistry: Second Edition*, John Wiley & Sons, Ltd, Chichester, UK, 2009.
- 24 B. W. Ninham and V. A. Parsegian, *Biophys. J.*, 1970, **10**, 646–663.
- 25 M. L. Waters, *Curr. Opin. Chem. Biol.*, 2002, **6**, 736–741.
- 26 W. R. Zhuang, Y. Wang, P. F. Cui, L. Xing, J. Lee, D. Kim, H. L. Jiang and Y. K. Oh, *J. Control. Release*, 2019, **294**, 311–326.
- 27 B. Davarcioglu, *Int. J. Mod. Eng. Res.*, 2011, **1**, 443–454.
- 28 D. A. Dougherty, *Acc. Chem. Res.*, 2013, **46**, 885–893.
- 29 B. L. Schottel, H. T. Chifotides and K. R. Dunbar, *Chem. Soc. Rev.*, 2008, **37**, 68–83.
- 30 M. M. Conn and J. Rebek, *Chem. Rev.*, 1997, **97**, 1647–1668.
- 31 P. Dapporto, P. Paoli and S. Roelens, *J. Org. Chem.*, 2001, **66**, 4930–4933.
- 32 G. Ono, A. Izuoka, T. Sugawara and Y. Sugawara, *J. Mater. Chem.*, 1998, **8**, 1703–1709.
- 33 J. W. Larson and T. B. McMahon, *Inorg. Chem.*, 1984, **23**, 2029–2033.
- 34 J. Emsley, *Chem. Soc. Rev.*, 1980, **9**, 91–124.
- 35 J. J. Dannenberg, L. Haskamp and A. Masunov, *J. Phys. Chem. A*, 1999, **103**, 7083–7086.
- 36 T. Steiner, *Angew. Chemie Int. Ed.*, 2002, **41**, 48–76.
- 37 R. Taylor and O. Kennard, *Acc. Chem. Res.*, 1984, **17**, 320–326.
- 38 C. F. Baxter, *Q. Rev. Biol.*, 1957, **32**, 197–197.
- 39 E. Kaneko and R. Niwa, *BioDrugs*, 2011, **25**, 1–11.
- 40 J. M. Berg, J. L. Tymoczko and L. Stryer, *Biochemistry*, W.H. Freeman, New York, NY, 5th edn., 2002.
- 41 H. Lodish, A. Berk and C. A. Kaiser, *Molecular Cell Biology*, W.H. Freeman, New York, NY, 6th edn., 2007.
- 42 K. P. Murphy, *Methods Mol. Biol.*, 1995, **40**, 1–34.

- 43 B. A. Shirley, *Protein Stability and Folding*, Humana Press, Totowa, NJ, 1st edn., 1995.
- 44 N. Darby and T. E. Creighton, *Methods Mol. Biol.*, 1995, **40**, 219–252.
- 45 J. Janin, R. P. Bahadur and P. Chakrabarti, *Q. Rev. Biophys.*, 2008, **41**, 133–180.
- 46 J. D. Watson and Crick. F. H. C., *Nature*, 1953, **171**, 737–738.
- 47 R. J. Heyden, P. DeSaix, J. G. Betts, E. Johnson, J. E. Johnson, O. Korol, D. H. Kruse, B. Poe, J. A. Wise and K. A. Young, *Anatomy & Physiology*, Rice University, Houston, TX, 2013.
- 48 S. Payne, *Viruses: From understanding to investigation*, Academic Press, Cambridge, MA, 1st edn., 2017.
- 49 S. Neidle, *Principles of Nucleic Acid Structure*, Springer New York, New York, NY, 1st edn., 2008.
- 50 IUPAC-IUB-Commission, *Biochemistry*, 1970, **9**, 4022–4027.
- 51 C. F. Matta, N. Castillo and R. J. Boyd, *J. Phys. Chem. B*, 2006, **110**, 563–578.
- 52 E. N. Nikolova, H. Zhou, F. L. Gottardo, H. S. Alvey, I. J. Kimsey and H. M. Al-Hashimi, *Biopolymers*, 2013, **99**, 955–968.
- 53 P. Yakovchuk, E. Protozanova and M. D. Frank-Kamenetskii, *Nucleic Acids Res.*, 2006, **34**, 564–574.
- 54 S. S. Patel and I. Donmez, *J. Biol. Chem.*, 2006, **281**, 18265–18268.
- 55 F. A. Aldaye, A. L. Palmer and H. F. Sleiman, *Science*, 2008, **321**, 1795–1799.
- 56 Y. Ke, J. Sharma, M. Liu, K. Jahn, Y. Liu and H. Yan, *Nano Lett.*, 2009, **9**, 2445–2447.
- 57 Y. Ke, L. L. Ong, W. M. Shih and P. Yin, *Science*, 2012, **338**, 1177–1183.
- 58 W. B. Sherman and N. C. Seeman, *Nano Lett.*, 2004, **4**, 1203–1207.
- 59 T. Omabegho, R. Sha and N. C. Seeman, *Science*, 2009, **324**, 67–71.
- 60 H. Berry and H. S. Bean, *J. Pharm. Pharmacol.*, 1950, **2**, 473–483.
- 61 P. Fromherz, *Chem. Phys. Lett.*, 1981, **77**, 460–466.
- 62 P. A. Hassan, G. Verma and R. Ganguly, in *Functional Materials*, Elsevier, Waltham, MA, 2012, pp. 1–59.
- 63 D. Lombardo, M. A. Kiselev, S. Magazù and P. Calandra, *Adv. Condens. Matter Phys.*, 2015, 1–22.
- 64 R. Azarmi and A. Ashjarian, *J. Chem. Pharm. Res.*, 2015, **7**, 632–640.
- 65 V. S. Kulkarni and C. Shaw, in *Essential Chemistry for Formulators of Semisolid and Liquid Dosages*, Academic Press, Cambridge, MA, 2016, pp. 5–19.
- 66 A. Wu, Y. Gao and L. Zheng, *Green Chem.*, 2019, **21**, 4290–4312.
- 67 G. Graziano, *Biophys. Chem.*, 1999, **82**, 69–79.
- 68 R. Godawat, S. N. Jamadagni and S. Garde, *Proc. Natl. Acad. Sci. U. S. A.*, 2009, **106**, 15119–15124.
- 69 D. Bradburn and T. Bittinger, *Micelles: Structural Biochemistry, Formation and Functions & Usage*, Nova Science, Hauppauge, NY, 2013.
- 70 B. Alberts, A. Johnson, J. Lewis, M. Raff, K. Roberts and P. Walter, *Molecular biology of the*

cell, Garland Science, New York, NY, 1st edn., 2002.

- 71 J. A. Shaeiwitz, *Chem. Eng. Commun.*, 1987, **55**, 225–234.
- 72 P. M. Hwang and H. J. Vogel, *Biochem. Cell Biol.*, 1998, **76**, 235–246.
- 73 A. Markey, V. L. Workman, I. A. Bruce, T. J. Woolford, B. Derby, A. F. Miller, S. H. Cartmell and A. Saiani, *J. Pept. Sci.*, 2017, **23**, 148–154.
- 74 A. A. Bahar and D. Ren, *Pharmaceuticals*, 2013, **6**, 1543–75.
- 75 D. Attwood and J. A. Tolley, *J. Pharm. Pharmacol.*, 1980, **32**, 761–765.
- 76 D. Causon, J. Gettins, J. Gormally, R. Greenwood, N. Natarajan and E. Wyn-Jones, *J. Chem. Soc. Faraday Trans. 2 Mol. Chem. Phys.*, 1981, **77**, 143–151.
- 77 A. D. Atherton and B. W. Barry, *J. Pharm. Pharmacol.*, 1985, **37**, 854–862.
- 78 F. Sarmiento, J. L. López-Fontán, G. Prieto, D. Attwood and V. Mosquera, *Colloid Polym. Sci.*, 1997, **275**, 1144–1147.
- 79 D. Attwood, V. Mosquera, M. Garcia, M. J. Suarez and F. Sarmiento, *J. Colloid Interface Sci.*, 1995, **175**, 201–206.
- 80 D. Attwood and S. P. Agarwal, *J. Pharm. Pharmacol.*, 1979, **31**, 392–395.
- 81 B. Y. Wang, H. Xu and X. Zhang, *Adv. Mater.*, 2009, **21**, 2849–2864.
- 82 X. Zhang and C. Wang, *Chem. Soc. Rev.*, 2011, **40**, 94–101.
- 83 C. Wang, Z. Wang and X. Zhang, *Acc. Chem. Res.*, 2012, **45**, 608–618.
- 84 Y. Kang, K. Liu and X. Zhang, *Langmuir*, 2014, **30**, 5989–6001.
- 85 P. Foley, A. Kermanshahi Pour, E. S. Beach and J. B. Zimmerman, *Chem. Soc. Rev.*, 2012, **41**, 1499–1518.
- 86 F. Lortie, S. Boileau and L. Bouteiller, *Chem. Eur. J.*, 2003, **9**, 3008–3014.
- 87 C. M. C. Faustino, A. R. T. Calado and L. Garcia-Rio, *J. Colloid Interface Sci.*, 2010, **351**, 472–477.
- 88 M. Pittelkow, C. B. Nielsen, A. Kadziola and J. B. Christensen, *J. Incl. Phenom. Macrocycl. Chem.*, 2009, **63**, 257–266.
- 89 M. Pittelkow, J. B. Christensen and E. W. Meijer, *J. Polym. Sci. Part A Polym. Chem.*, 2004, **42**, 3792–3799.
- 90 M. Pittelkow, C. B. Nielsen, M. A. C. Broeren, J. L. J. Van Dongen, M. H. P. Van Genderen, E. W. Meijer and J. B. Christensen, *Chem. Eur. J.*, 2005, **11**, 5126–5135.
- 91 J. R. Hiscock, G. P. Bustone, B. Wilson, K. E. Belsey and L. R. Blackholly, *Soft Matter*, 2016, **12**, 4221–4228.
- 92 L. J. White, S. N. Tyuleva, B. Wilson, H. J. Shepherd, K. K. L. Ng, S. J. Holder, E. R. Clark and J. R. Hiscock, *Chem. Eur. J.*, 2018, **24**, 7761–7773.
- 93 L. J. White, N. J. Wells, L. R. Blackholly, H. J. Shepherd, B. Wilson, G. P. Bustone, T. J. Runacres and J. R. Hiscock, *Chem. Sci.*, 2017, **8**, 7620–7630.
- 94 S. N. Tyuleva, N. Allen, L. J. White, A. Pépés, H. J. Shepherd, P. J. Saines, R. J. Ellaby, D. P. Mulvihill and J. R. Hiscock, *Chem. Commun.*, 2019, **55**, 95–98.
- 95 L. R. Blackholly, MRes Thesis, University of Kent, 2017.

- 96 T. L. Gumbs, L. J. White, N. J. Wells, H. J. Shepherd and J. R. Hiscock, *Supramol. Chem.*, 2018, **30**, 42–51.
- 97 M. Eckert, *Ann. Phys.*, 2012, **524**, A83–A85.
- 98 J. P. Zhang, P. Q. Liao, H. L. Zhou, R. B. Lin and X. M. Chen, *Chem. Soc. Rev.*, 2014, **43**, 5789–5814.
- 99 L. R. Blackholly, H. J. Shepherd and J. R. Hiscock, *CrystEngComm*, 2016, **18**, 7021–7028.
- 100 M. Przybylski and M. O. Glocker, *Angew. Chemie Int. Ed.*, 1996, **35**, 807–826.
- 101 C. S. Ho, C. W. K. Lam, M. H. M. Chan, R. C. K. Cheung, L. K. Law, L. C. W. Lit, K. F. Ng, M. W. M. Suen and H. L. Tai, *Clin. Biochem. Rev.*, 2003, **24**, 3–12.
- 102 V. M. Wallace, N. R. Dhumal, F. M. Zehentbauer, H. J. Kim and J. Kiefer, *J. Phys. Chem. B*, 2015, **119**, 14780–14789.
- 103 R. F. Evilia, *Anal. Lett.*, 2001, **34**, 2227–2236.
- 104 M. C. Malet-Martino and R. Martino, *Clin. Pharmacokinet.*, 1991, **20**, 337–349.
- 105 P. Thordarson, K. Sewell and V. Efremova, Bindfit v0.5, <http://supramolecular.org>.
- 106 L. K. S. Von Krbek, C. A. Schalley and P. Thordarson, *Chem. Soc. Rev.*, 2017, **46**, 2622–2637.
- 107 R. B. Martin, *Chem. Rev.*, 1996, **96**, 3043–3064.
- 108 W. I. Goldberg, *Am. J. Phys.*, 1999, **67**, 1152–1160.
- 109 E. Tomaszewska, K. Soliwoda, K. Kadziola, B. Tkacz-Szczesna, G. Celichowski, M. Cichomski, W. Szmaja and J. Grobelny, *J. Nanomater.*, 2013, **2013**, 1–10.
- 110 T. Tadros, *Colloids and Surfaces*, 1982, **5**, 79–80.
- 111 T. Tadros, in *Encyclopedia of Colloid and Interface Science*, Springer Berlin Heidelberg, Berlin, Heidelberg, 2013, pp. 209–210.
- 112 Y. H. A. Hussein and M. Youssry, *Materials (Basel)*, 2018, **11**, 688.
- 113 M. Schaefer and C. Froemmel, *J. Mol. Biol.*, 1990, **216**, 1045–1066.
- 114 J. J. P. Stewart, *J. Mol. Model.*, 2007, **13**, 1173–1213.
- 115 J. O'Neill, *Rev. Antimicrob. Resist.*, 2016, **1**, 1–16.
- 116 C. L. Ventola, *P T*, 2015, **40**, 277–83.
- 117 I. Wiegand, K. Hilpert and R. E. W. Hancock, *Nat. Protoc.*, 2008, **3**, 163–175.
- 118 G. M. Sheldrick, *Acta Crystallogr. Sect. A Found. Crystallogr.*, 2015, **71**, 3–8.
- 119 G. M. Sheldrick, *Acta Crystallogr. Sect. C Struct. Chem.*, 2015, **71**, 3–8.
- 120 O. V. Dolomanov, L. J. Bourhis, R. J. Gildea, J. A. K. Howard and H. Puschmann, *J. Appl. Crystallogr.*, 2009, **42**, 339–341.
- 121 V. Vendrell-Criado, V. Lhiaubet-Vallet, M. Yamaji, M. C. Cuquerella and M. A. Miranda, *Org. Biomol. Chem.*, 2016, **14**, 4110–4115.

## 6. Appendix

### 6.1 Characterisation NMR

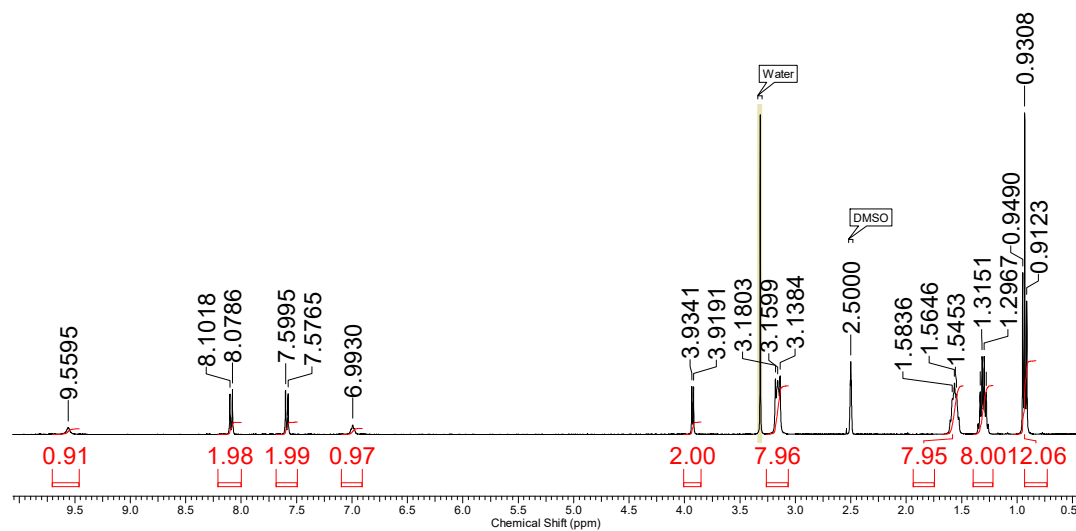


Figure 46 –  $^1\text{H}$  NMR of Compound **1** in  $\text{DMSO} - d_6$ .

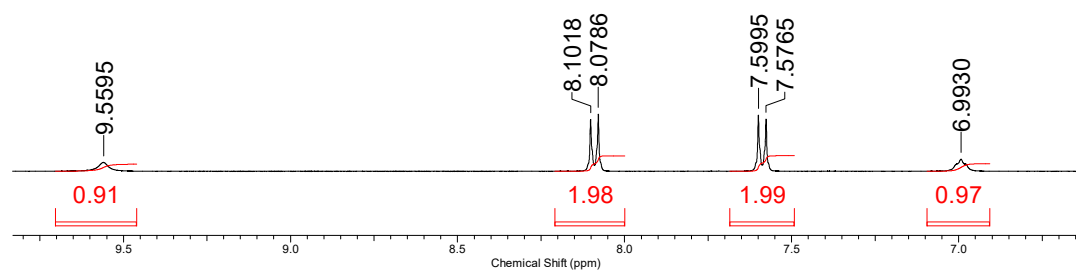


Figure 47 – Enlarged  $^1\text{H}$  NMR of Compound **1** in  $\text{DMSO} - d_6$ .

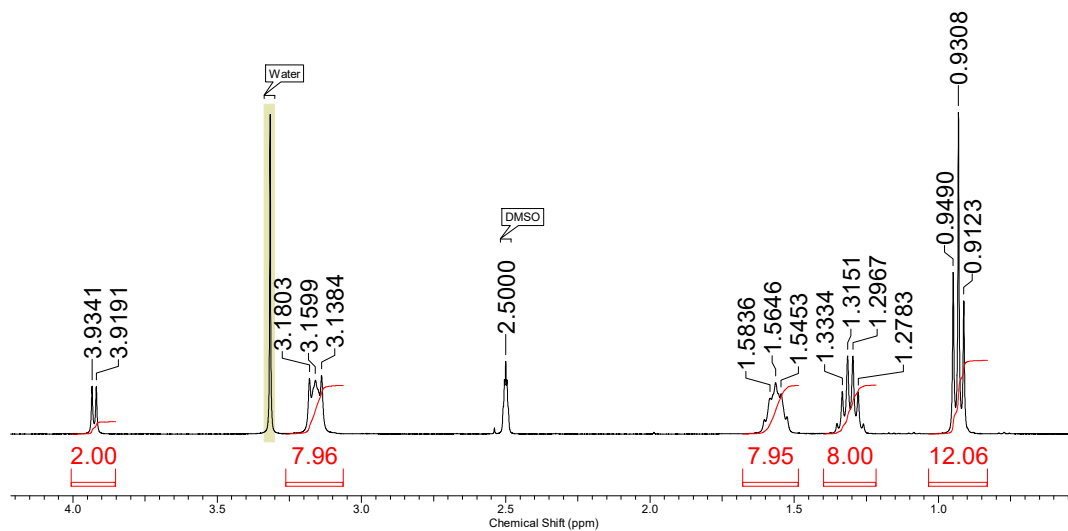


Figure 48 – Enlarged  $^1\text{H}$  NMR of Compound 1 in  $\text{DMSO}-d_6$ .

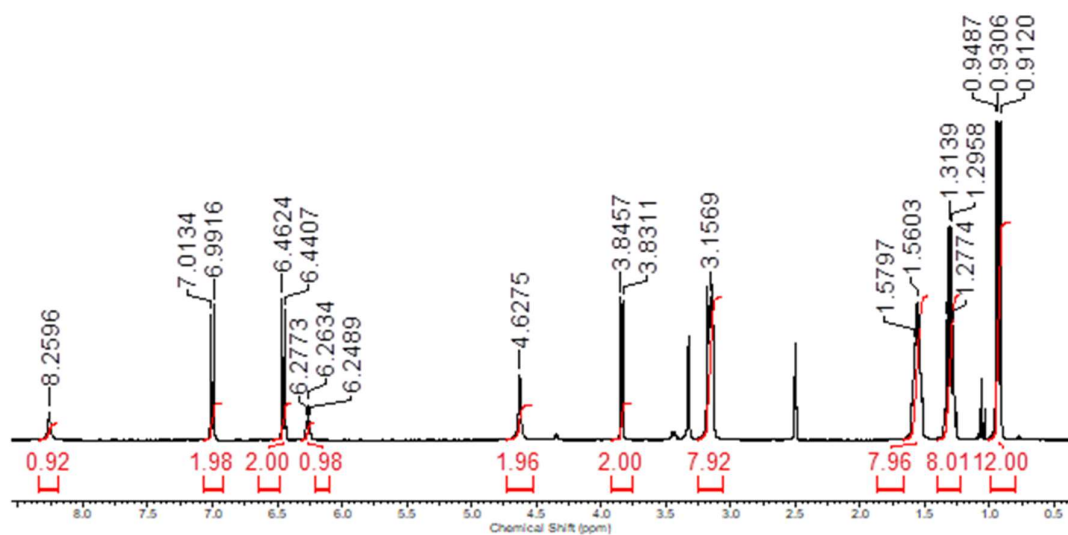


Figure 49 –  $^1\text{H}$  NMR of Compound 2 in  $\text{DMSO}-d_6$ .

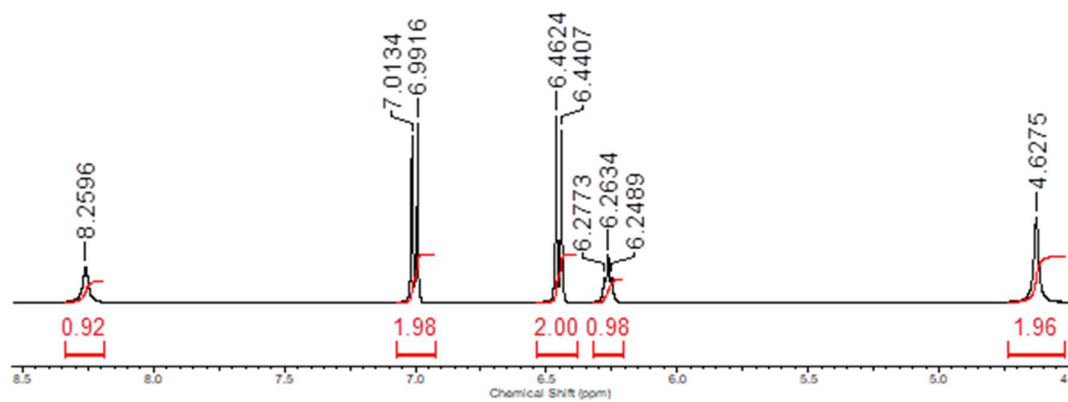


Figure 50 – Enlarged  $^1\text{H}$  NMR of Compound 2 in  $\text{DMSO}-d_6$ .

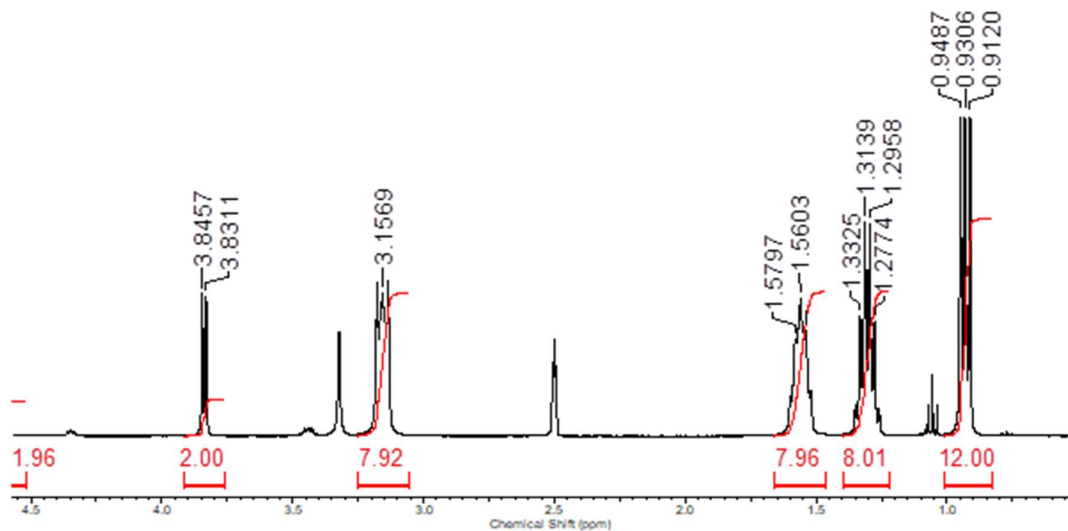


Figure 51 – Enlarged  $^1\text{H}$  NMR of Compound **2** in  $\text{DMSO} - d_6$ .

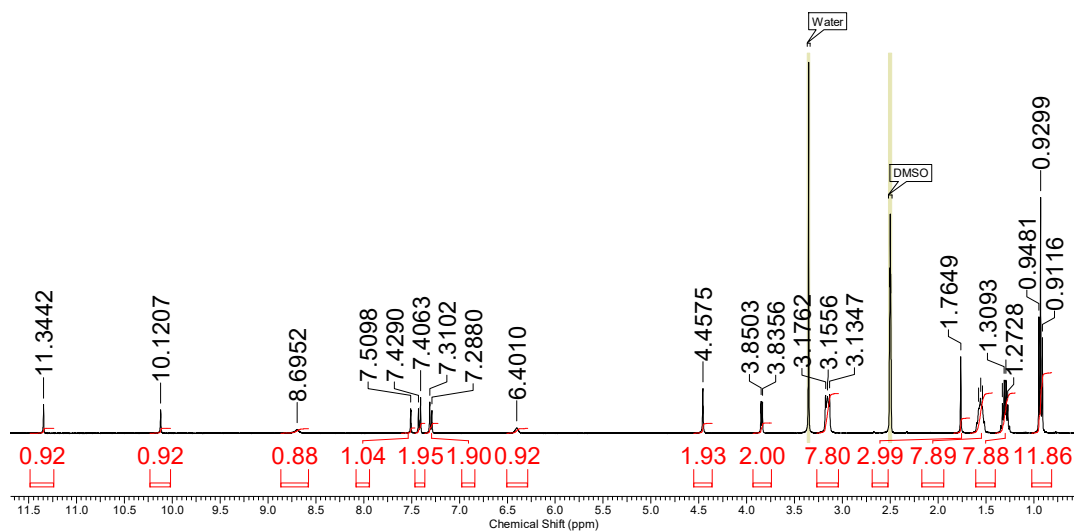


Figure 52 –  $^1\text{H}$  NMR of Compound **3** in  $\text{DMSO} - d_6$ .

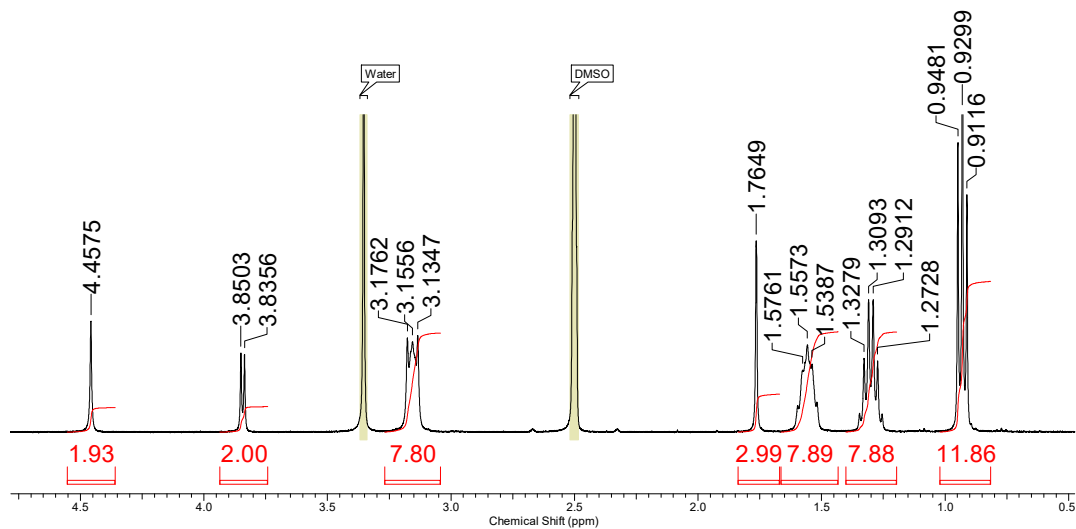


Figure 53 – Enlarged <sup>1</sup>H NMR of Compound 3 in DMSO - *d*<sub>6</sub>.

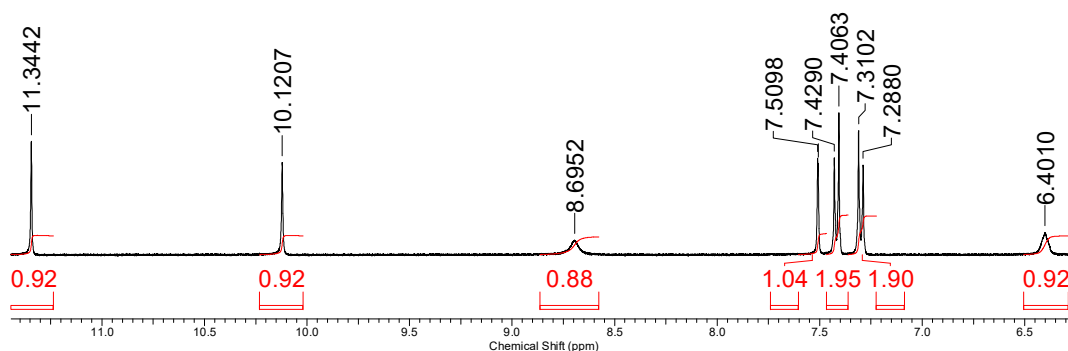


Figure 54 – Enlarged <sup>1</sup>H NMR of Compound 3 in DMSO - *d*<sub>6</sub>.

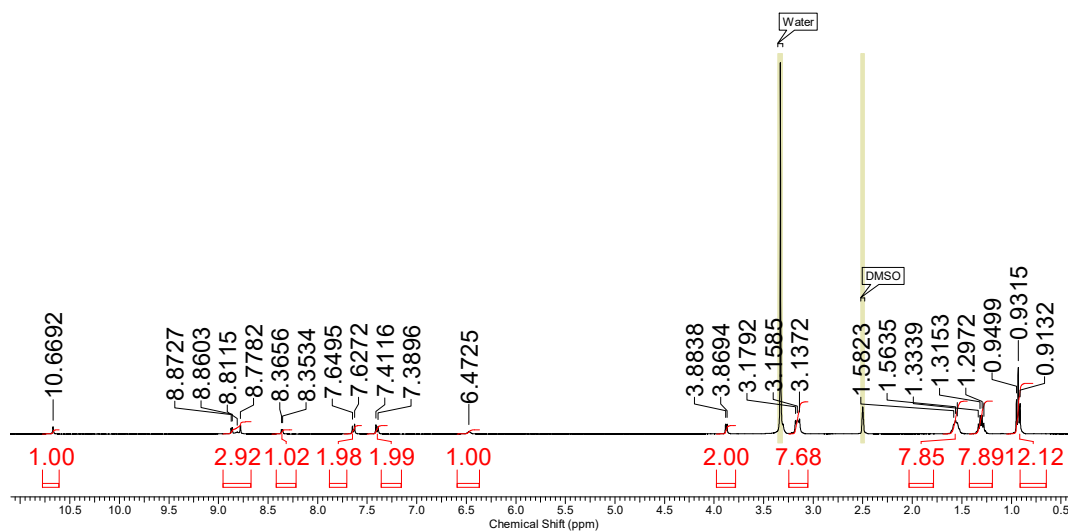


Figure 55 – <sup>1</sup>H NMR of Compound 4 in DMSO - *d*<sub>6</sub>.

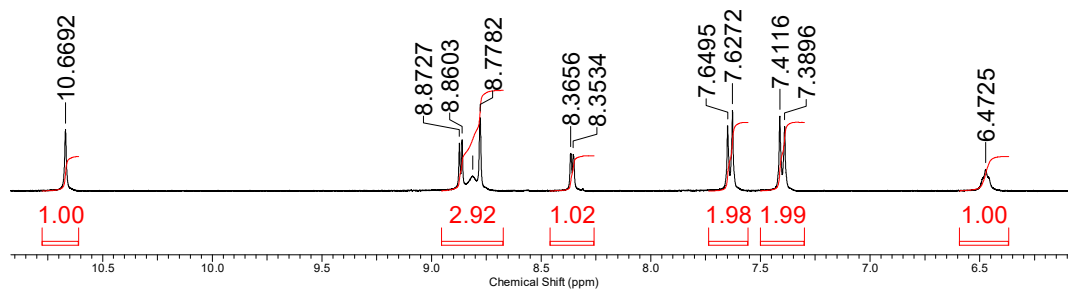


Figure 56 – Enlarged  $^1\text{H}$  NMR of Compound **4** in  $\text{DMSO}-d_6$ .

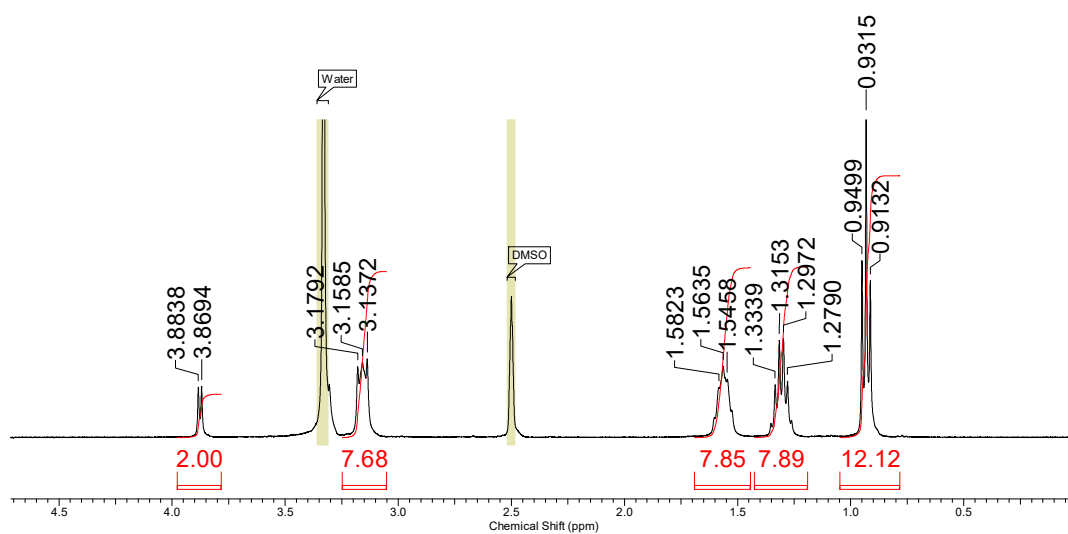


Figure 57 – Enlarged  $^1\text{H}$  NMR of Compound **4** in  $\text{DMSO}-d_6$ .

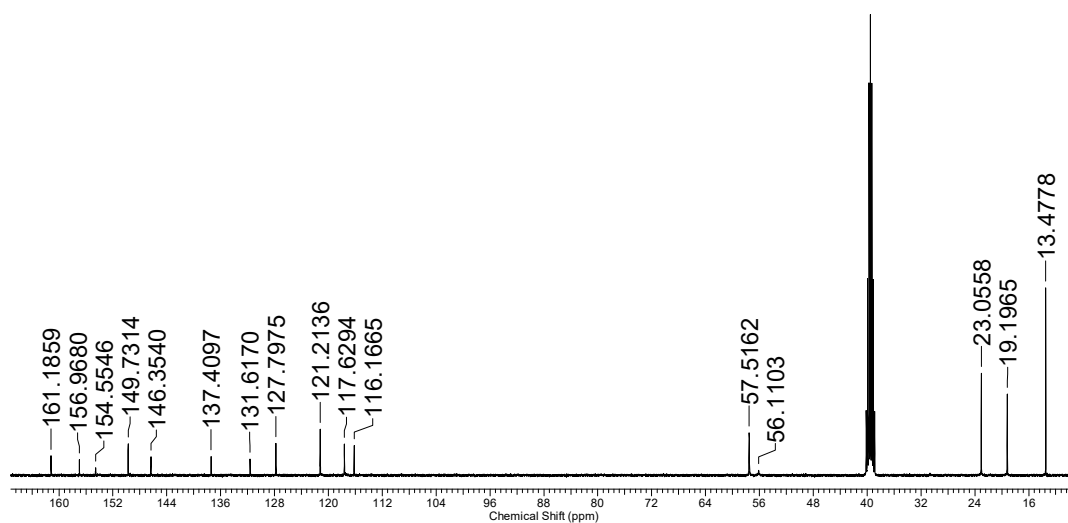


Figure 58 –  $^{13}\text{C}$  NMR of Compound **4** in  $\text{DMSO}-d_6$ .

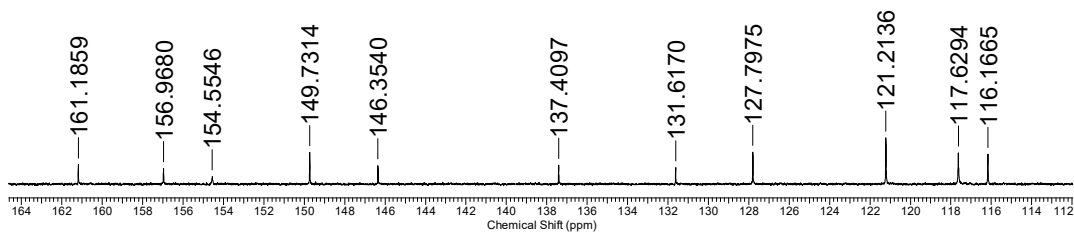


Figure 59 – Enlarged  $^{13}\text{C}$  NMR of Compound 4 in  $\text{DMSO} - d_6$ .

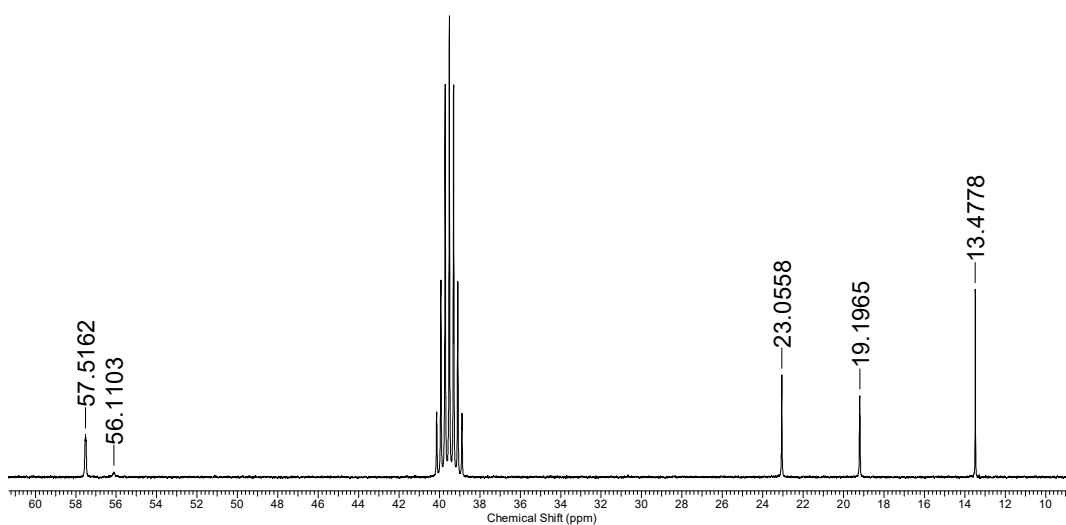


Figure 60 – Enlarged  $^{13}\text{C}$  NMR of Compound 4 in  $\text{DMSO} - d_6$ .

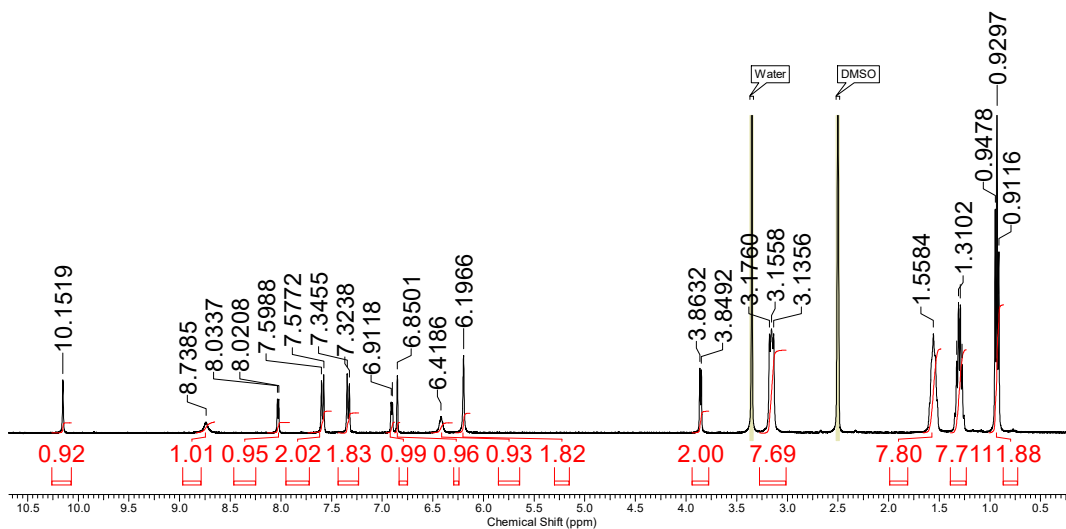


Figure 61 –  $^1\text{H}$  NMR of Compound 5 in  $\text{DMSO} - d_6$ .

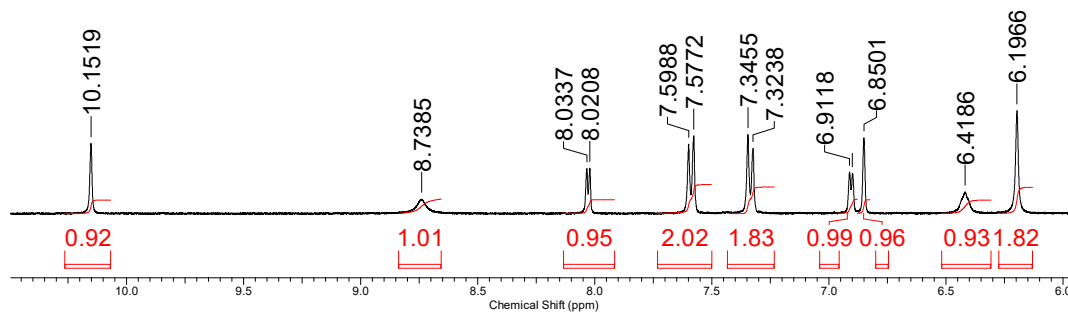


Figure 62 – Enlarged  $^1\text{H}$  NMR of Compound 5 in  $\text{DMSO}-d_6$ .

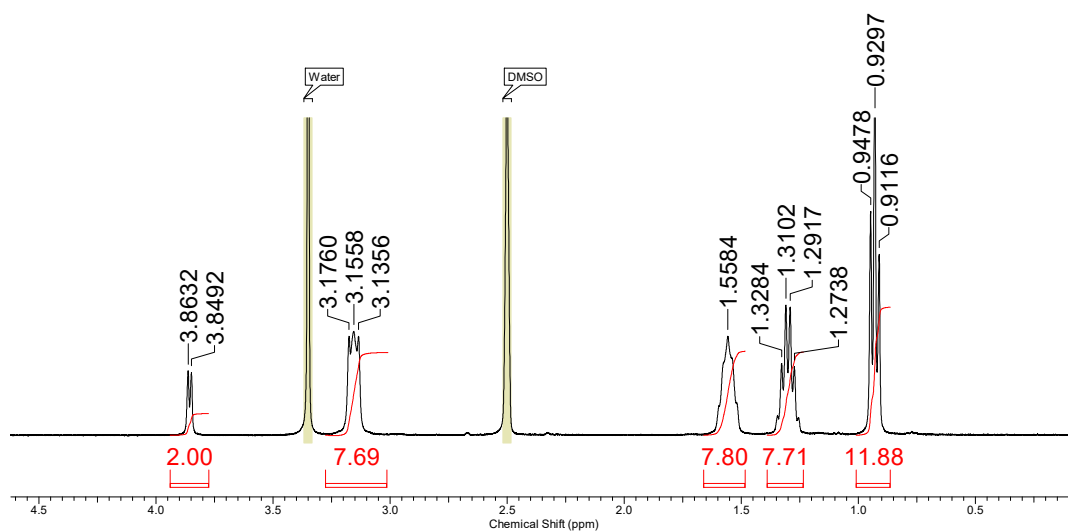


Figure 63 – Enlarged  $^1\text{H}$  NMR of Compound 5 in  $\text{DMSO}-d_6$ .

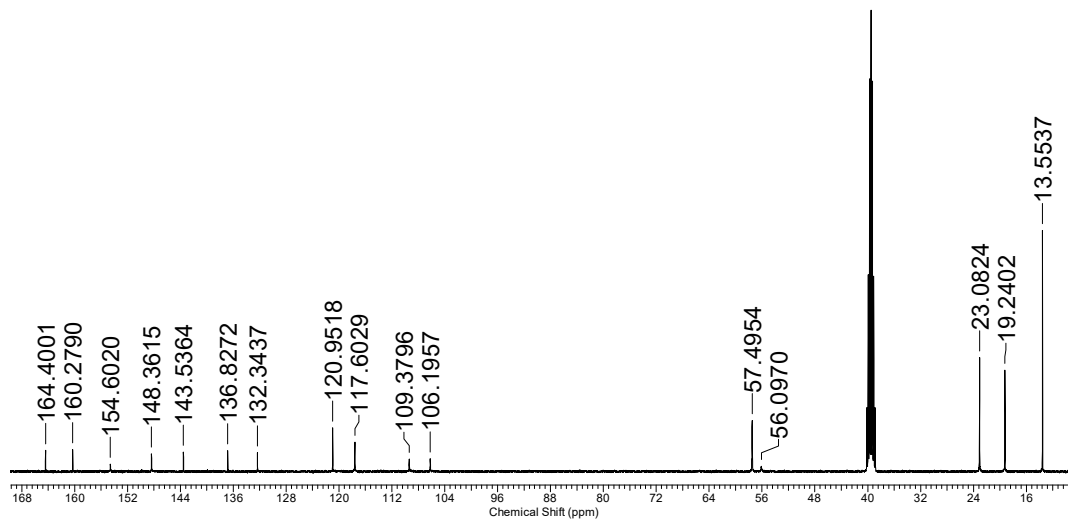


Figure 64 –  $^{13}\text{C}$  NMR of Compound 5 in  $\text{DMSO}-d_6$ .

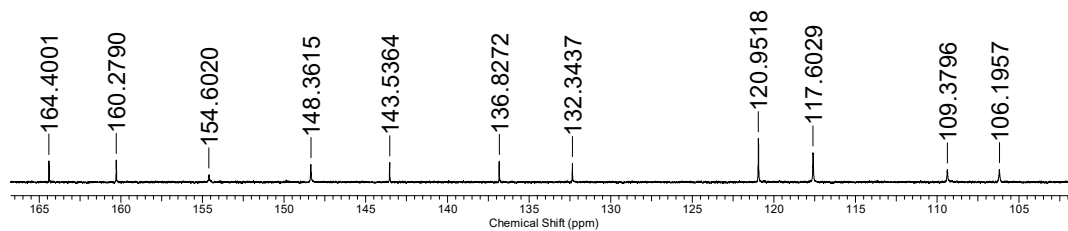


Figure 65 – Enlarged  $^{13}\text{C}$  NMR of Compound 5 in  $\text{DMSO} - d_6$ .

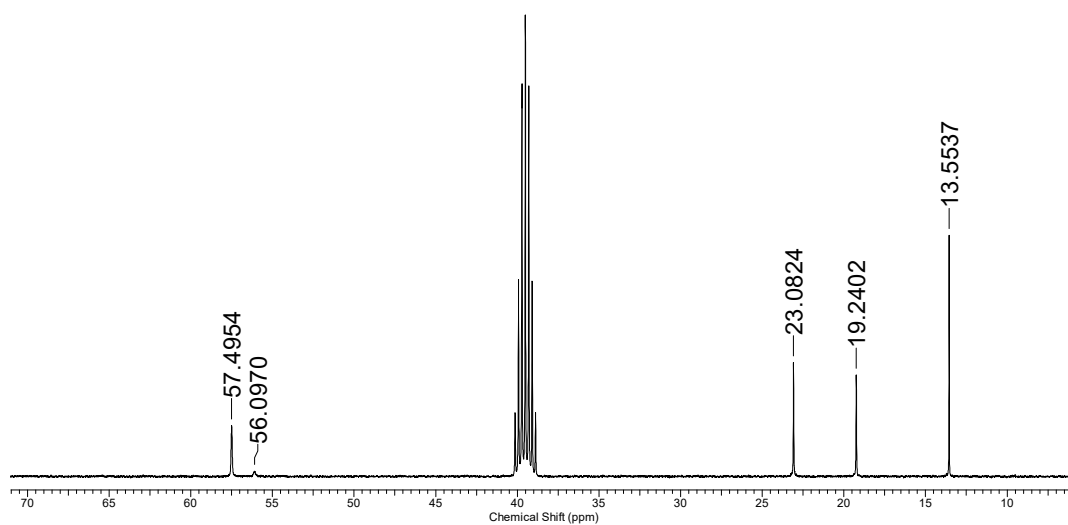


Figure 66 – Enlarged  $^{13}\text{C}$  NMR of Compound 5 in  $\text{DMSO} - d_6$ .

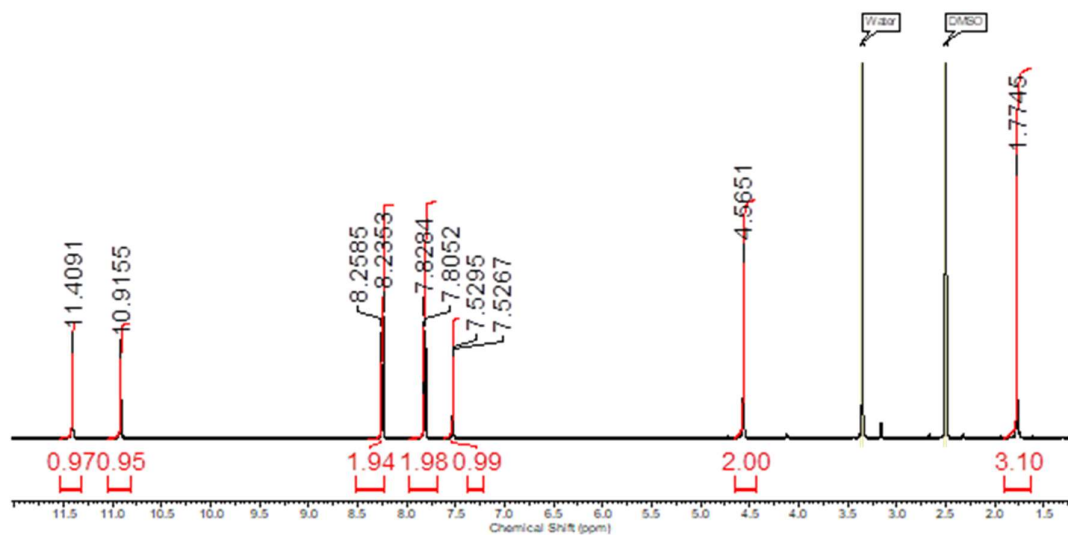


Figure 67 –  $^1\text{H}$  NMR of Compound 6 in  $\text{DMSO} - d_6$ .

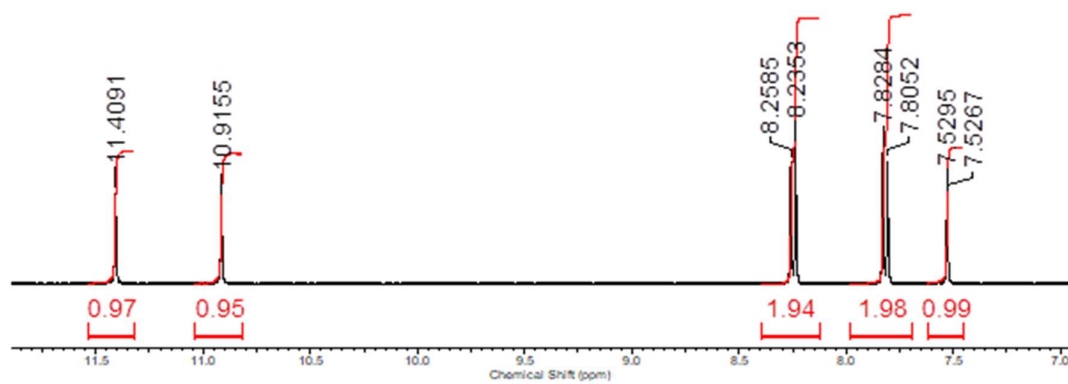


Figure 68 – Enlarged  $^1\text{H}$  NMR of Compound 6 in  $\text{DMSO}-d_6$ .

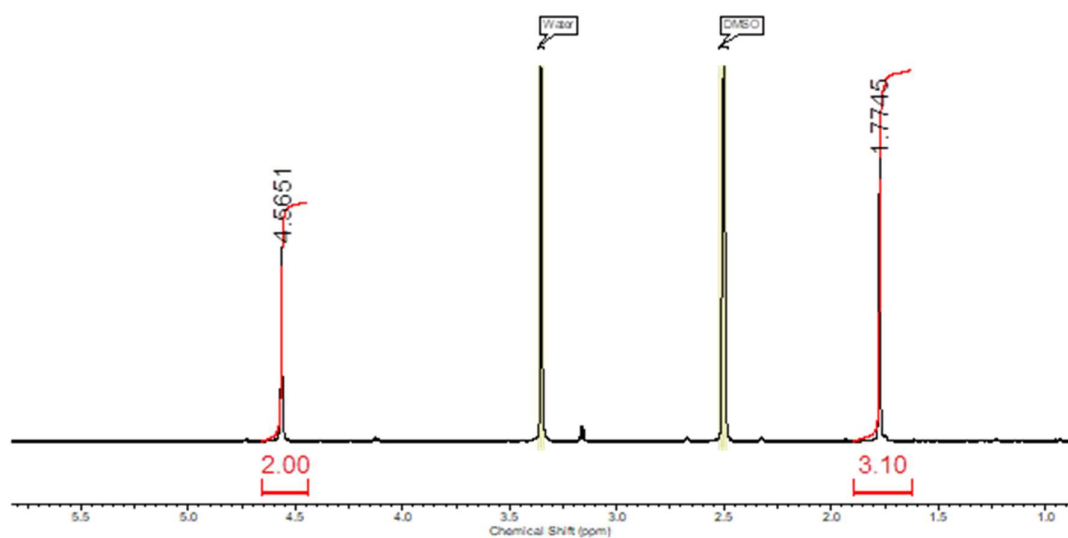


Figure 69 – Enlarged  $^1\text{H}$  NMR of Compound 6 in  $\text{DMSO}-d_6$ .

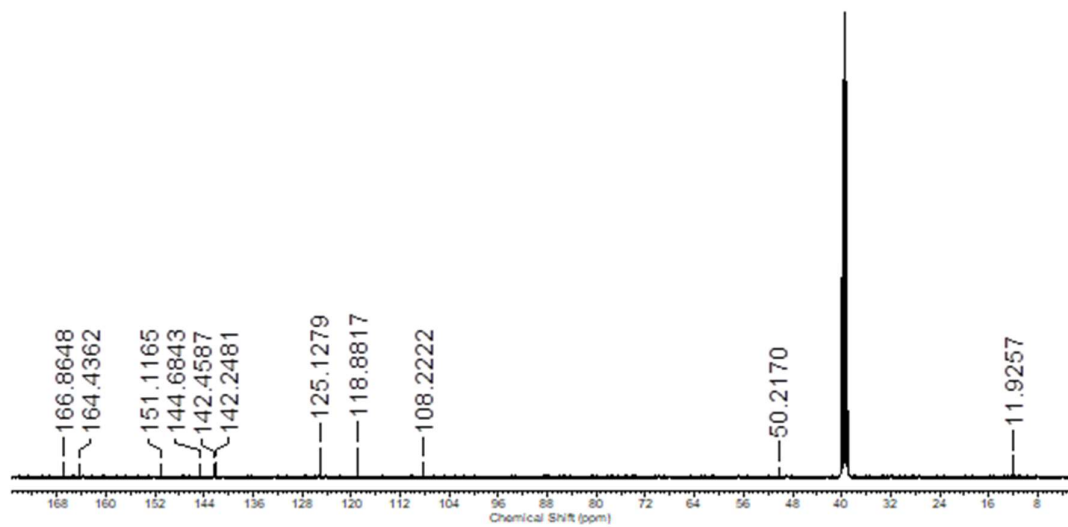


Figure 70 –  $^{13}\text{C}$  NMR of Compound **6** in  $\text{DMSO} - d_6$ .

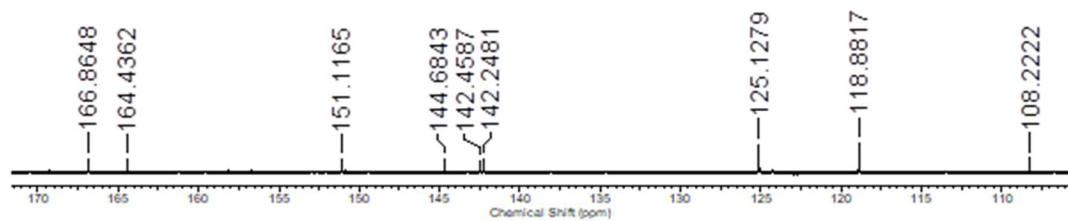


Figure 71 – Enlarged  $^{13}\text{C}$  NMR of Compound **6** in  $\text{DMSO} - d_6$ .

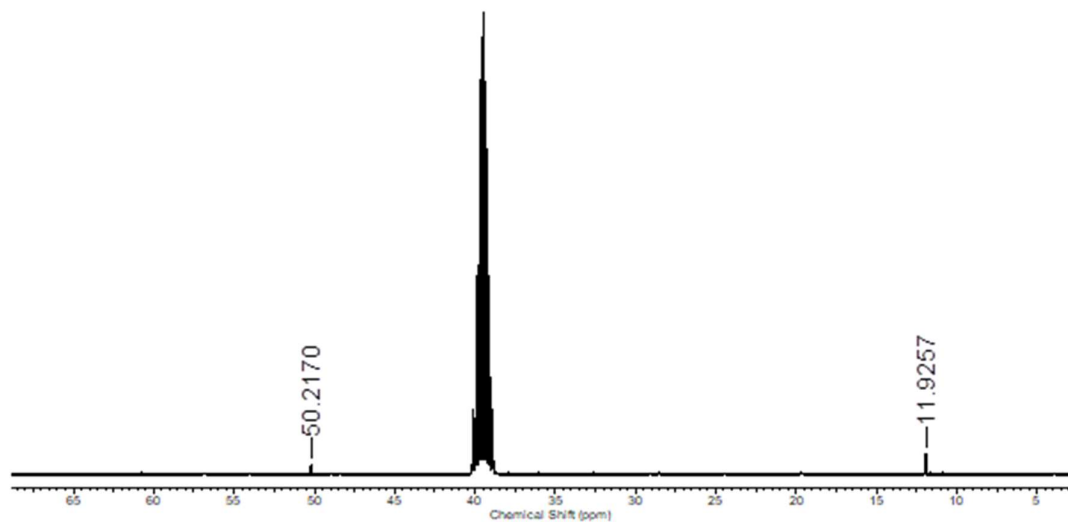


Figure 72 – Enlarged  $^{13}\text{C}$  NMR of Compound 6 in  $\text{DMSO}-d_6$ .

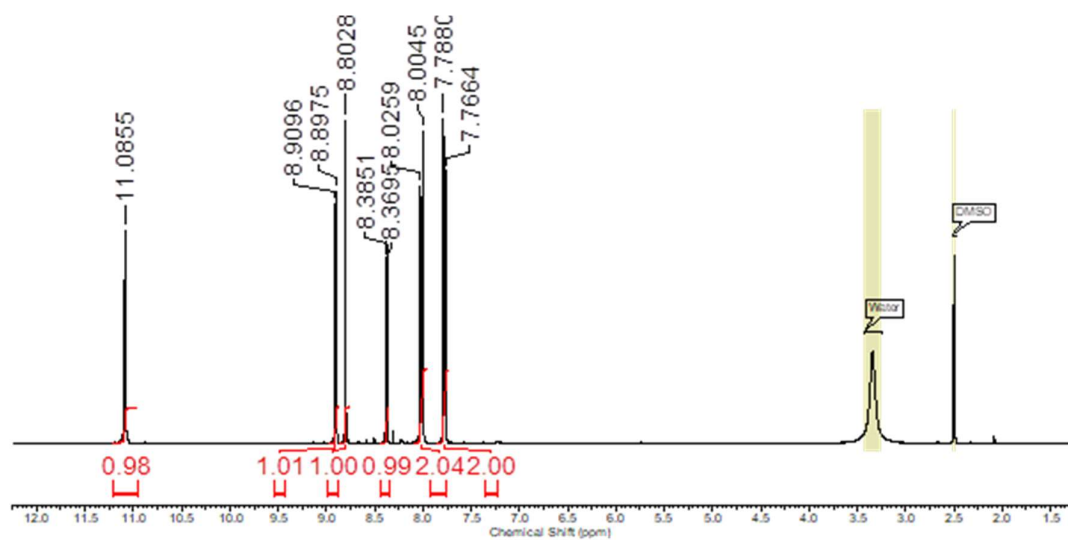


Figure 73 –  $^1\text{H}$  NMR of Compound 7 in  $\text{DMSO}-d_6$ .

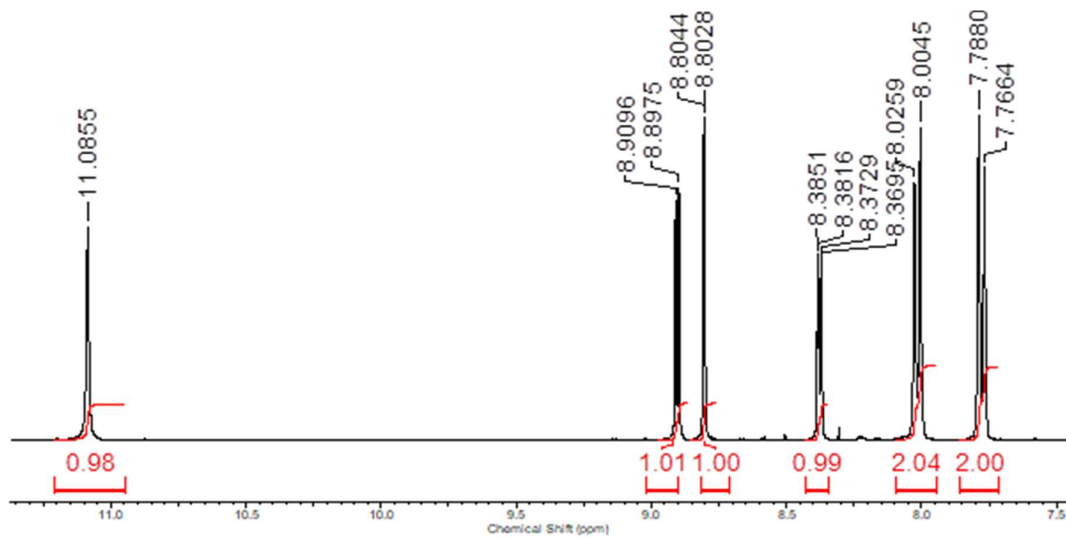


Figure 74 – Enlarged  $^1\text{H}$  NMR of Compound 7 in  $\text{DMSO} - d_6$ .

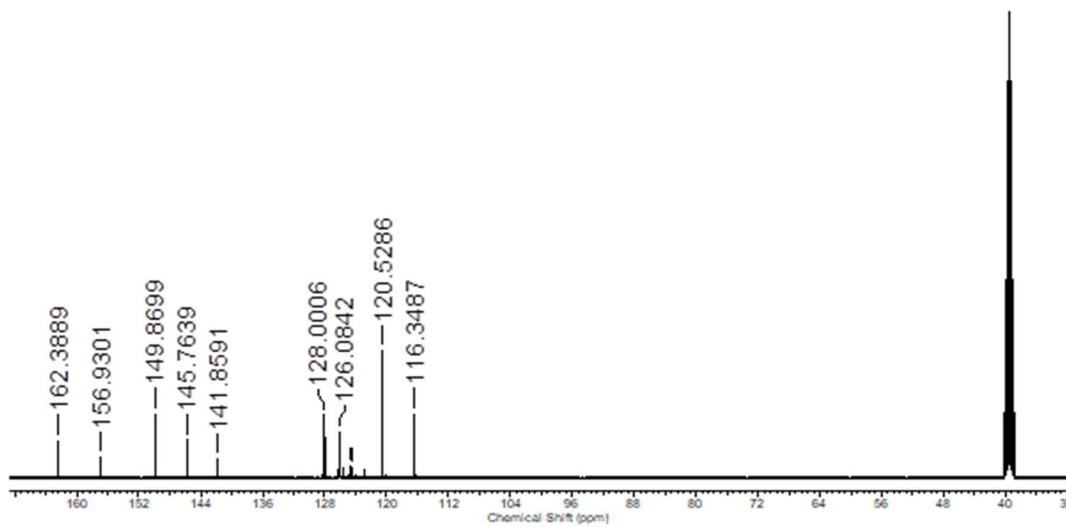


Figure 75 –  $^{13}\text{C}$  NMR of Compound 7 in  $\text{DMSO} - d_6$ .

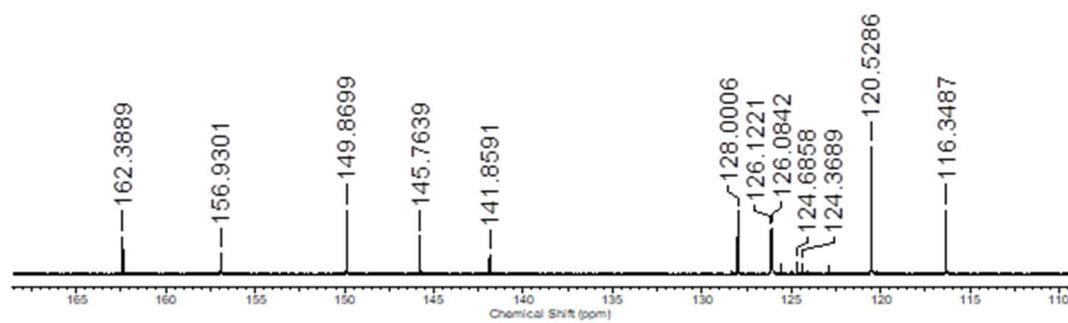


Figure 76 – Enlarged  $^{13}\text{C}$  NMR of Compound **7** in  $\text{DMSO} - d_6$ .

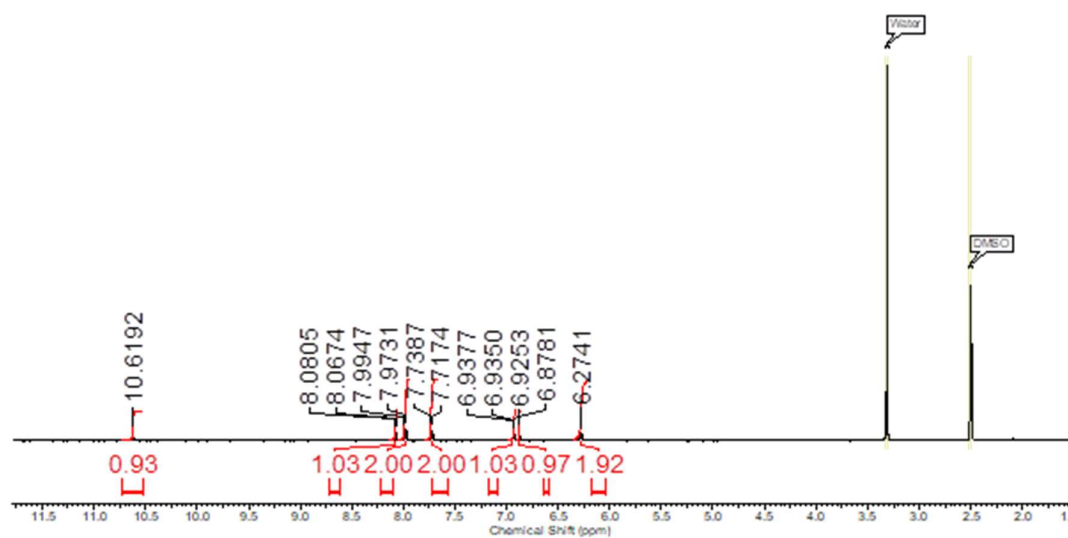


Figure 77 –  $^1\text{H}$  NMR of Compound **8** in  $\text{DMSO} - d_6$ .

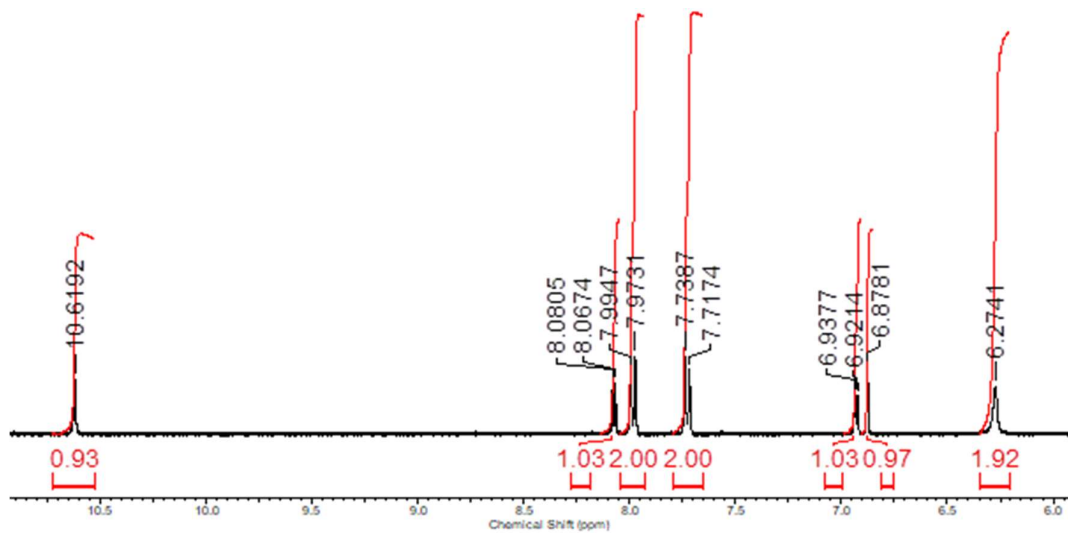


Figure 78 – Enlarged  $^1\text{H}$  NMR of Compound **8** in  $\text{DMSO} - d_6$ .

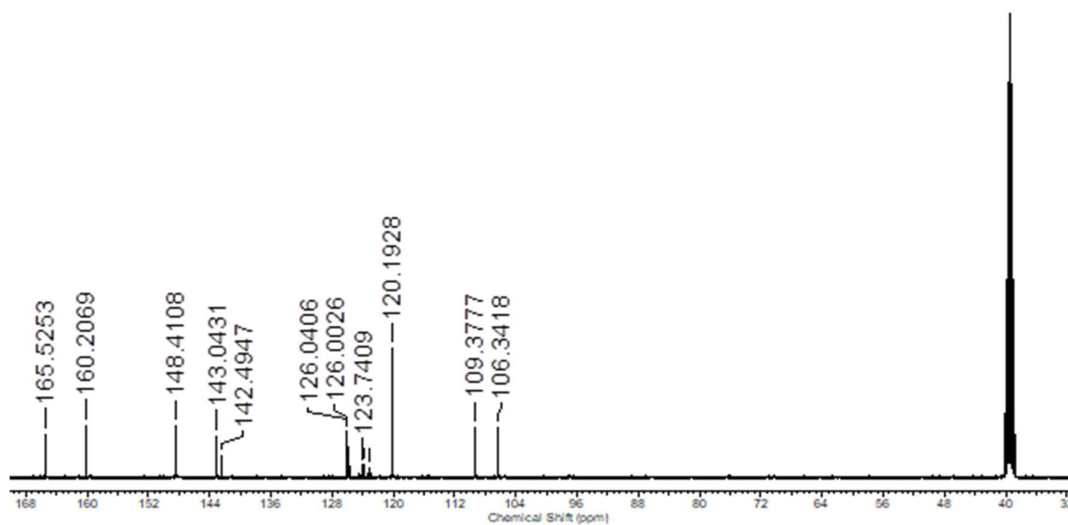


Figure 79 –  $^{13}\text{C}$  NMR of Compound **8** in  $\text{DMSO} - d_6$ .

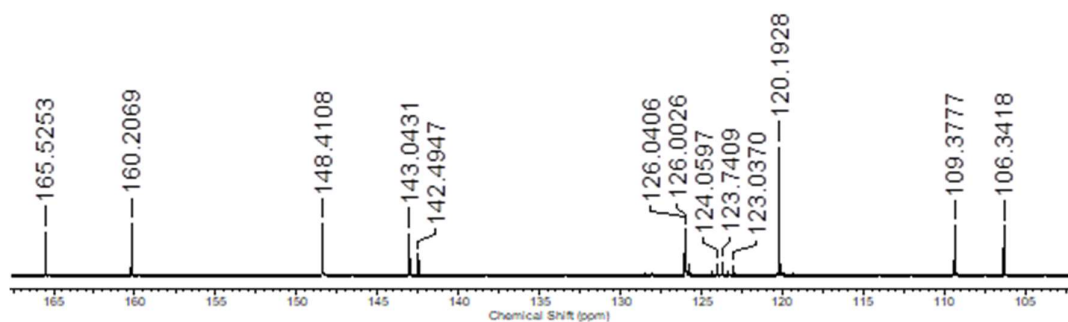


Figure 80 – Enlarged  $^{13}\text{C}$  NMR of Compound **8** in  $\text{DMSO} - d_6$ .

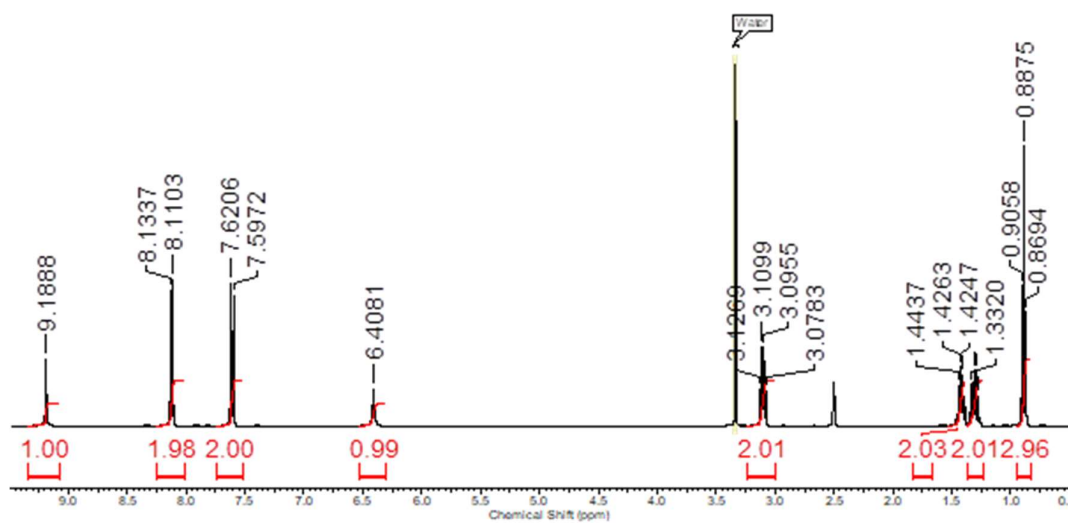


Figure 81 –  $^1\text{H}$  NMR of Compound **9** in  $\text{DMSO} - d_6$ .

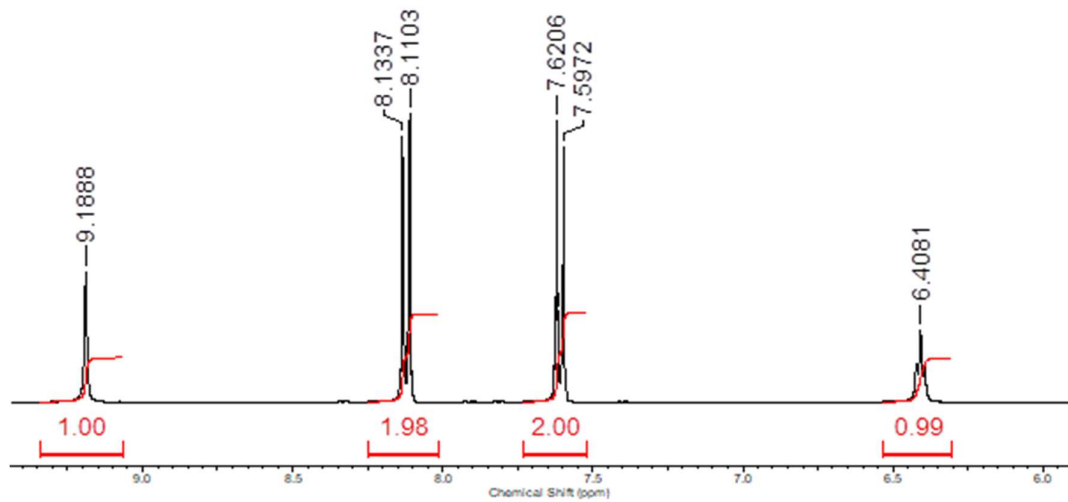


Figure 82 – Enlarged  $^1\text{H}$  NMR of Compound **9** in  $\text{DMSO}-d_6$ .

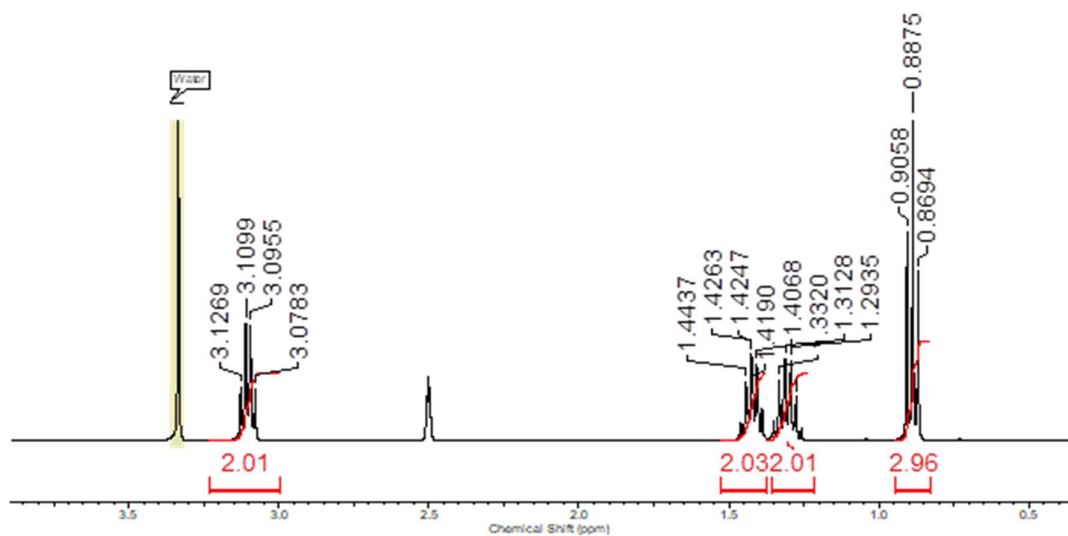


Figure 83 – Enlarged  $^1\text{H}$  NMR of Compound **9** in  $\text{DMSO}-d_6$ .

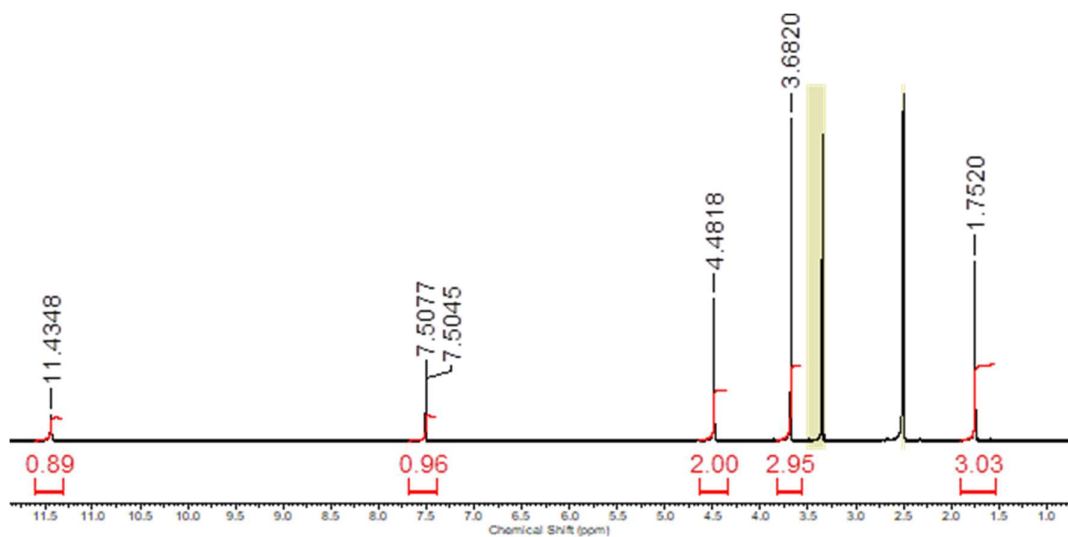


Figure 84 –  $^1\text{H}$  NMR of Compound **10** in  $\text{DMSO}-d_6$ .

## 6.2 Single crystal X-ray structures

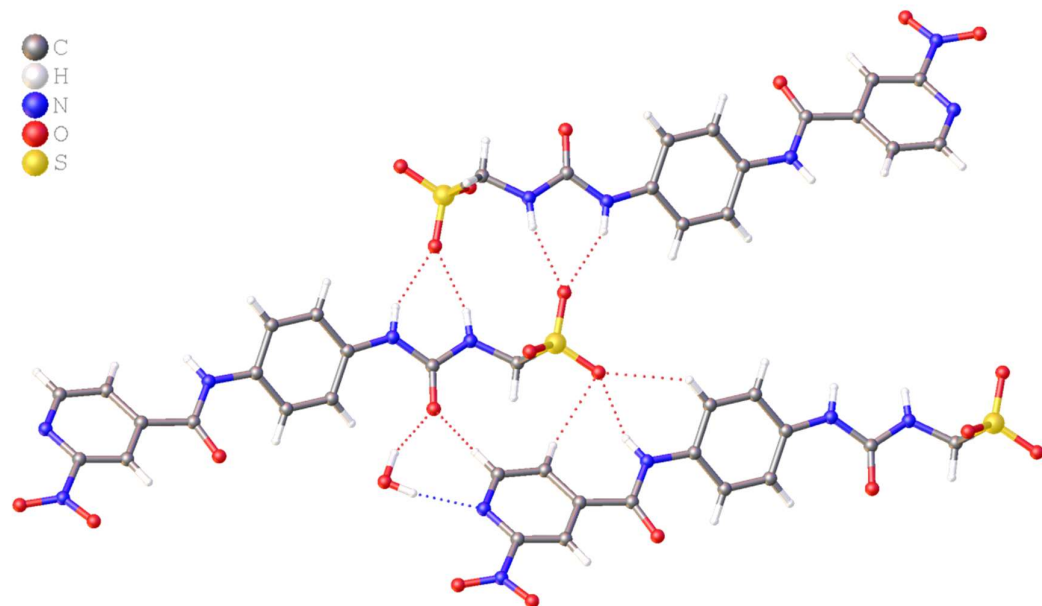


Figure 85 – Single crystal X-ray structure of compound 4.

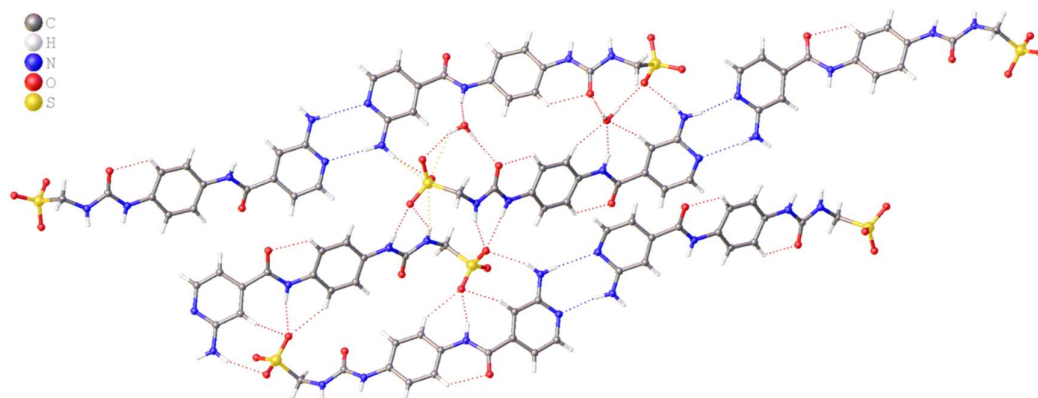


Figure 86 – Single crystal X-ray structure of compound 5.

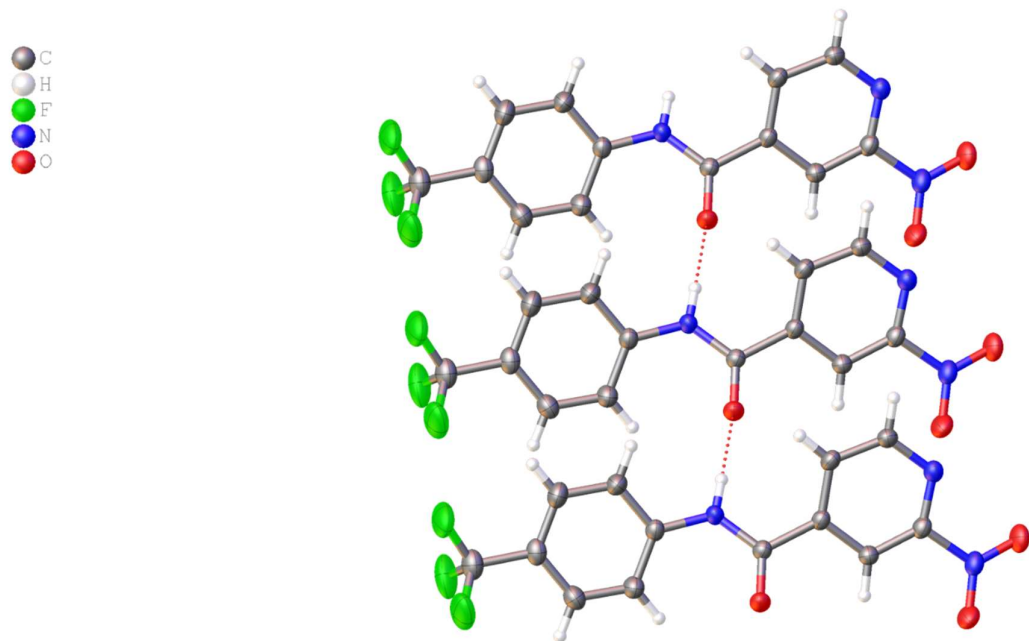


Figure 87 – Single crystal X-ray structure of compound **7**.

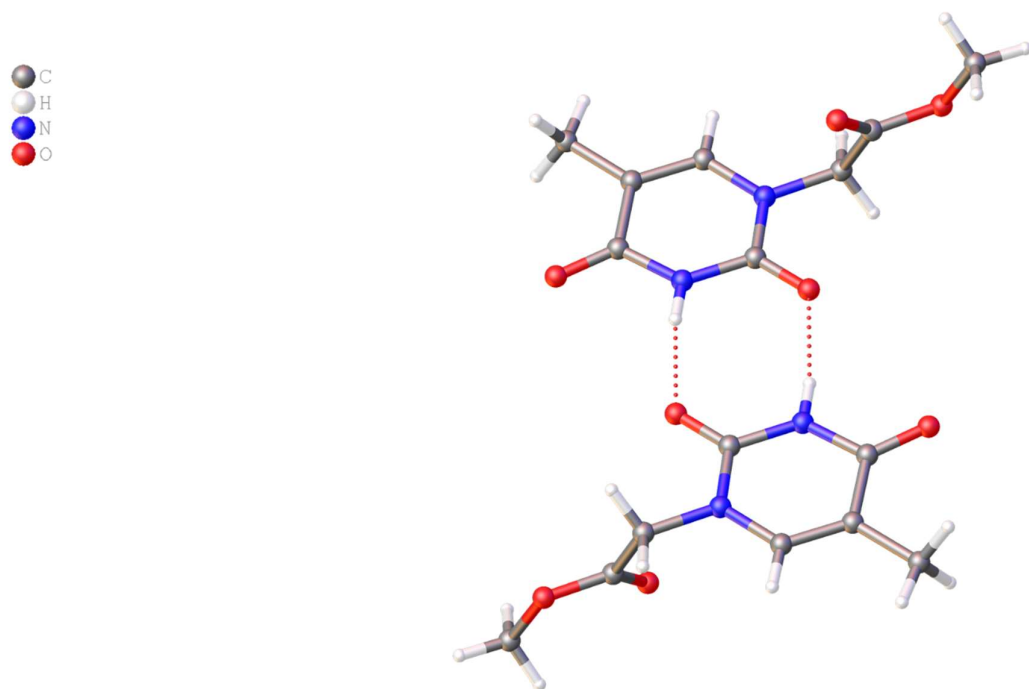


Figure 88 – Single crystal X-ray structure of compound **9**.

### 6.3 Mass spectrum data

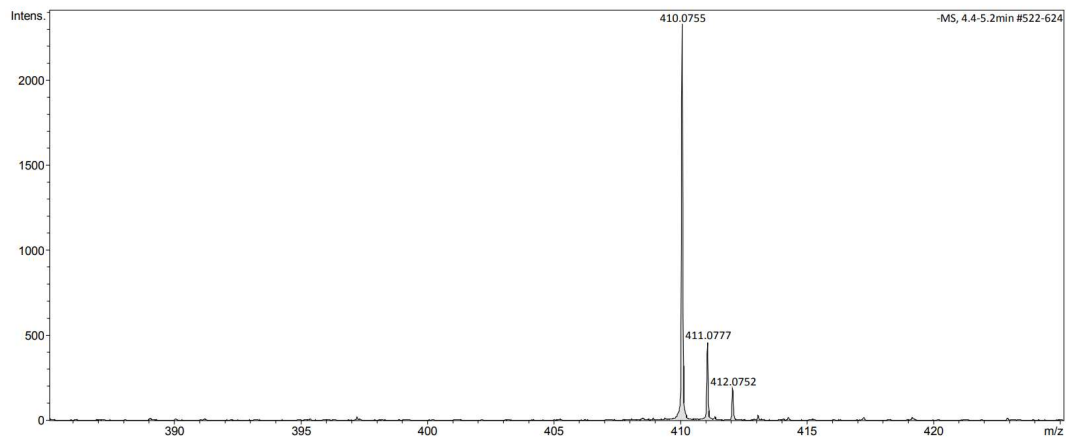


Figure 89 – ESI<sup>+</sup> mass spectrum collected for compound **3**.

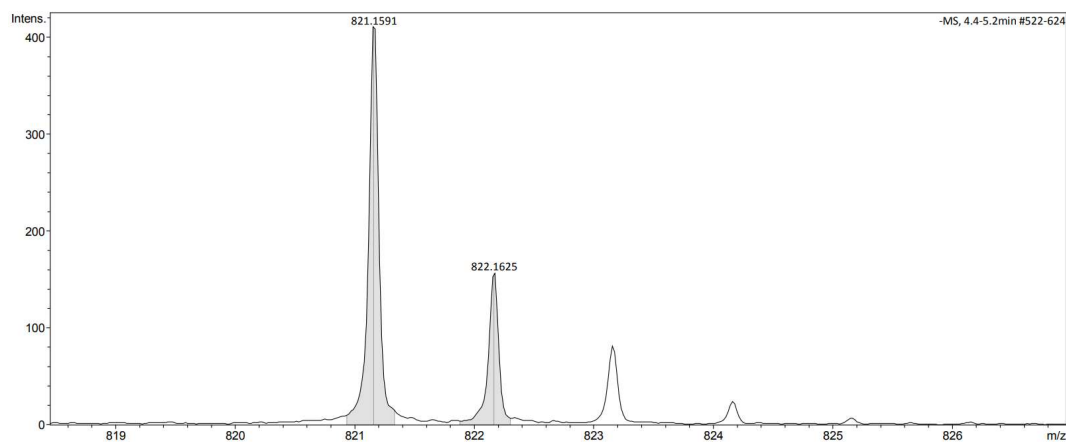


Figure 90 – ESI<sup>+</sup> mass spectrum collected for compound **3**.

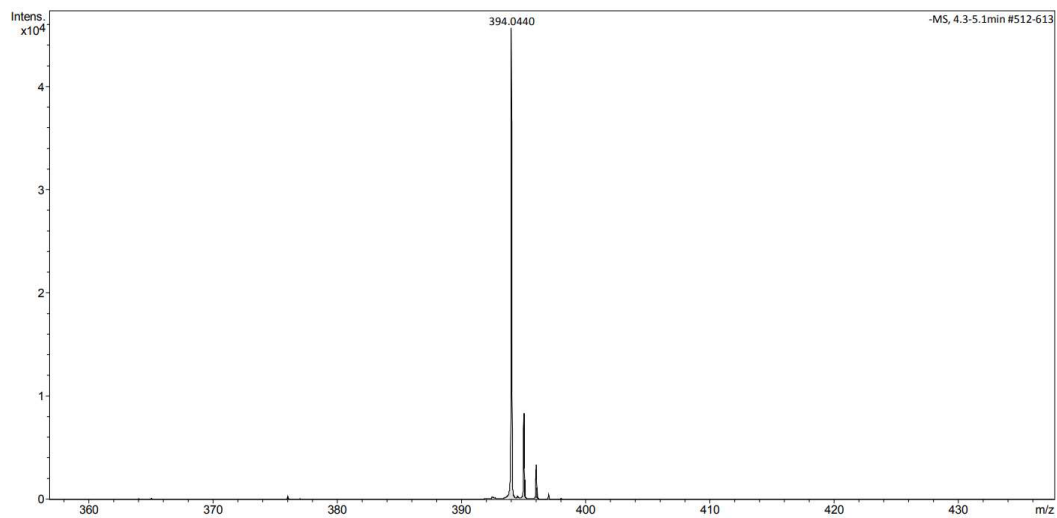


Figure 91 – ESI- mass spectrum collected for compound 4.

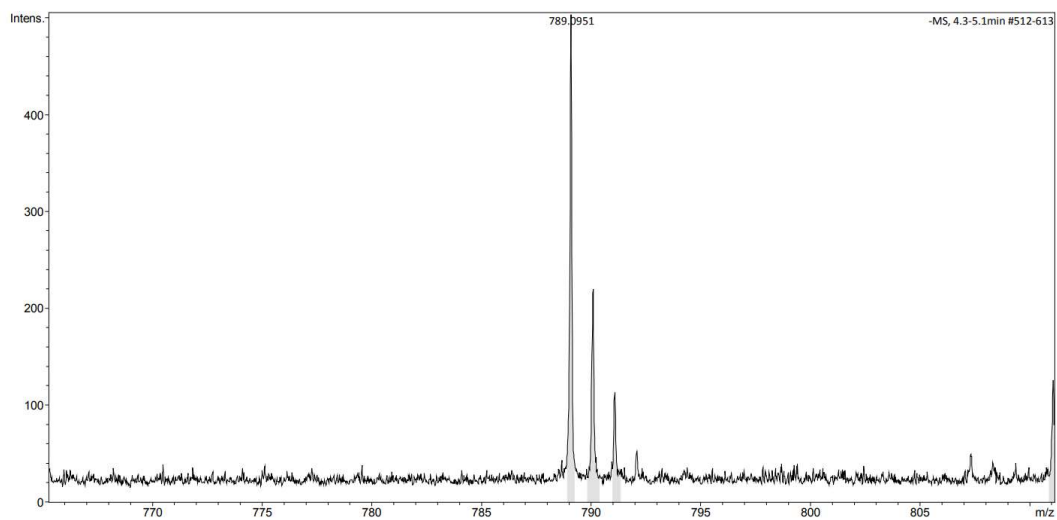


Figure 92 – ESI- mass spectrum collected for compound 4.

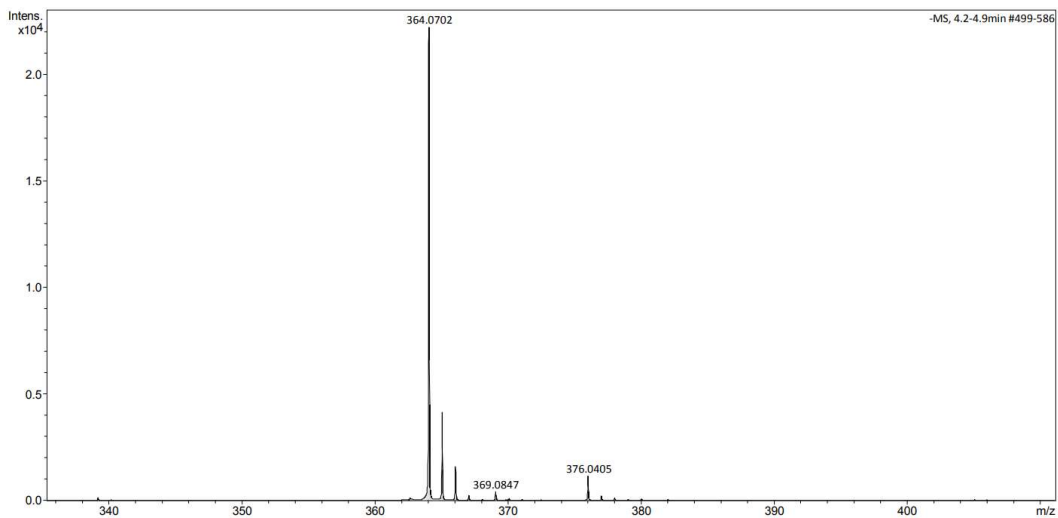


Figure 93 – ESI<sup>-</sup> mass spectrum collected for compound 5.

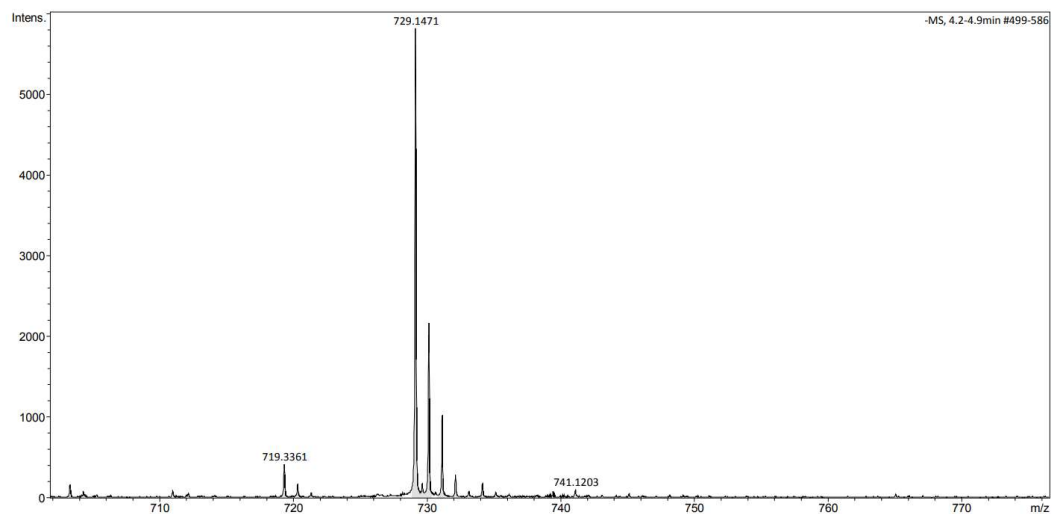


Figure 94 – ESI<sup>-</sup> mass spectrum collected for compound 5.

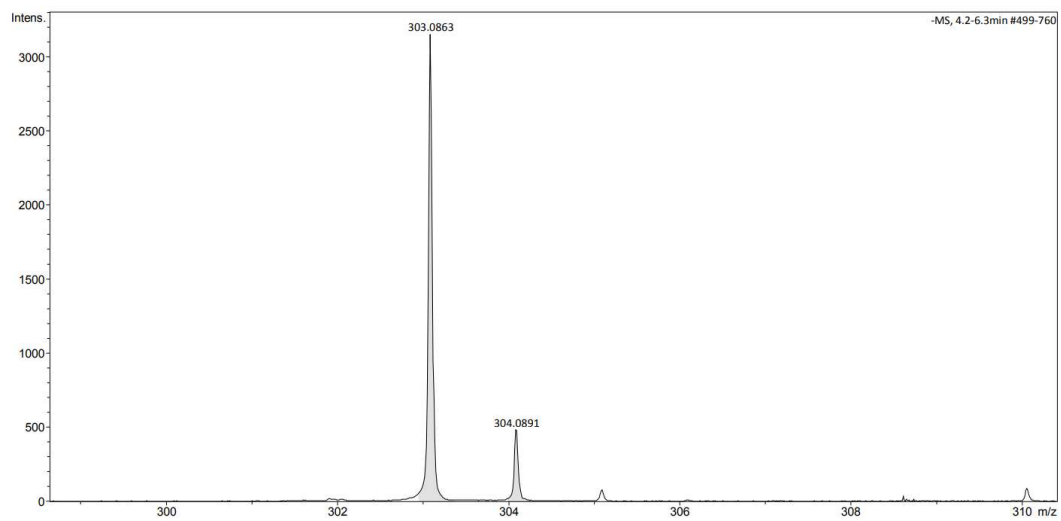


Figure 95 – ESI<sup>-</sup> mass spectrum collected for compound **6**.

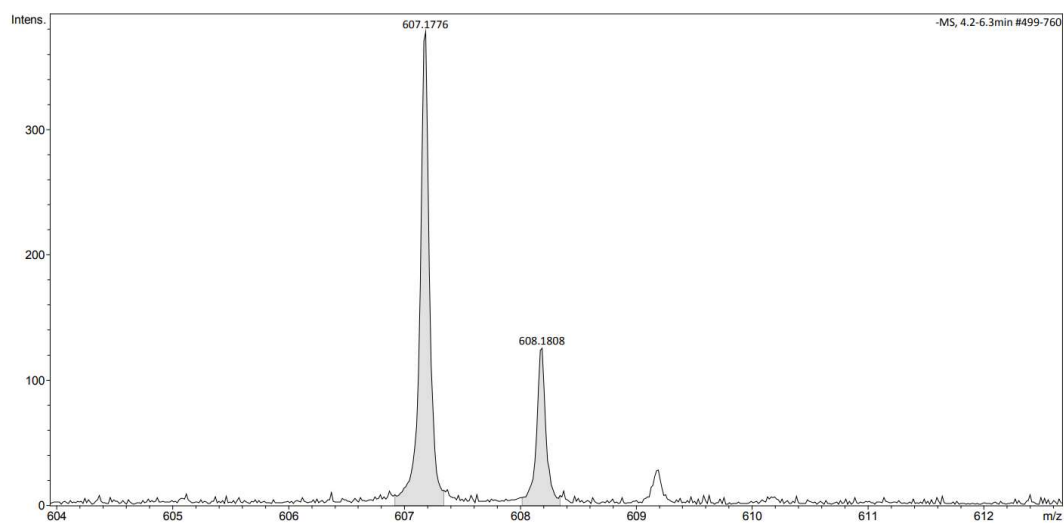


Figure 96 – ESI<sup>-</sup> mass spectrum collected for compound **6**.

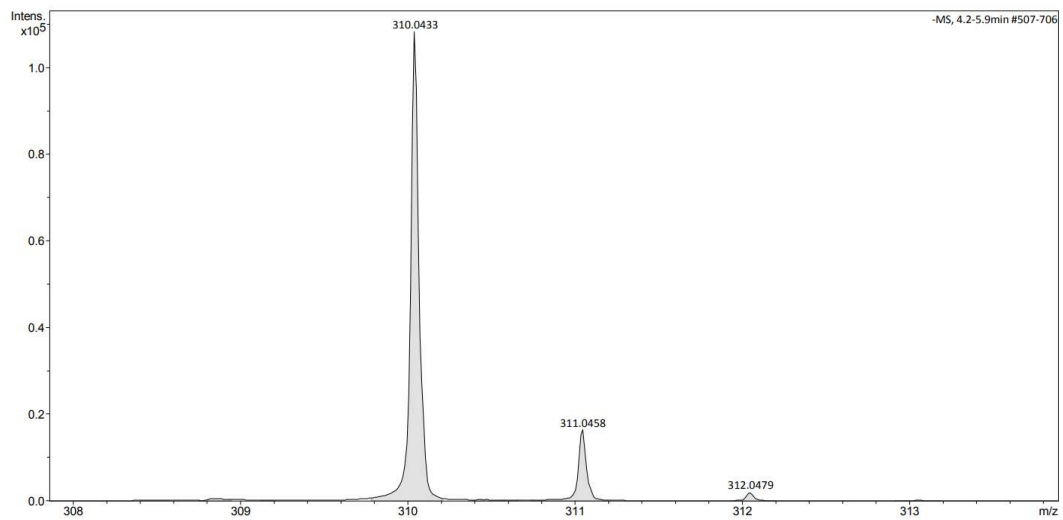


Figure 97 – ESI mass spectrum collected for compound 7.

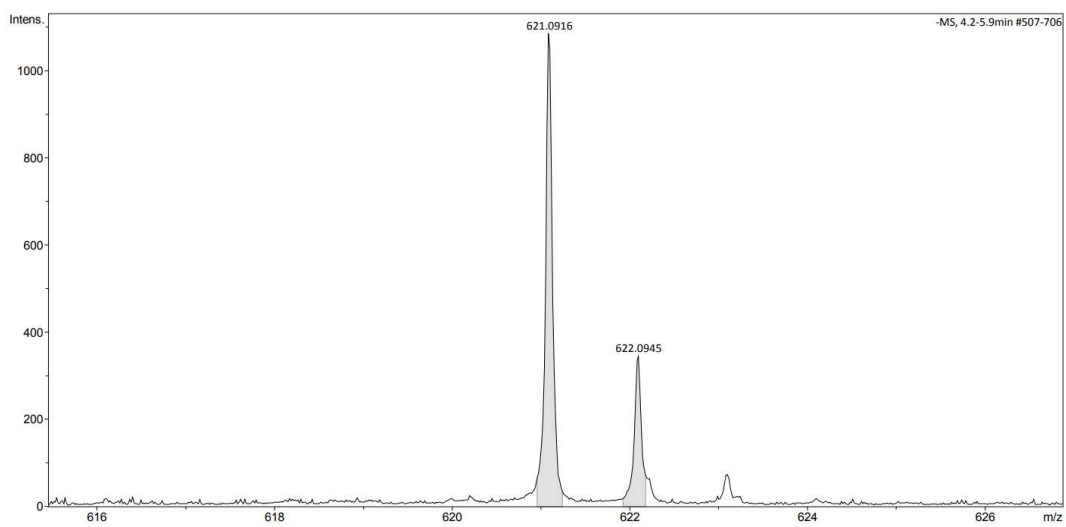


Figure 98 – ESI mass spectrum collected for compound 7.

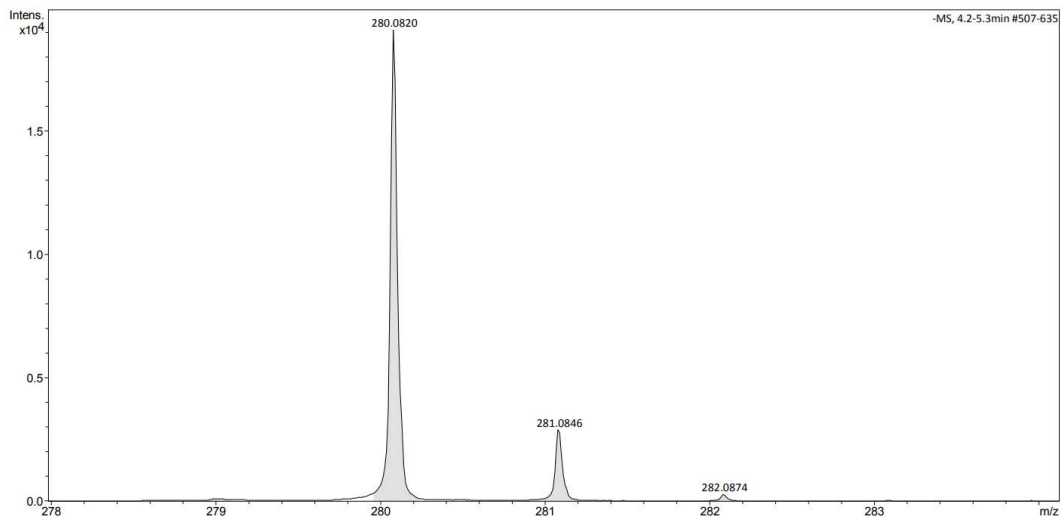


Figure 99 – ESI<sup>-</sup> mass spectrum collected for compound **8**.

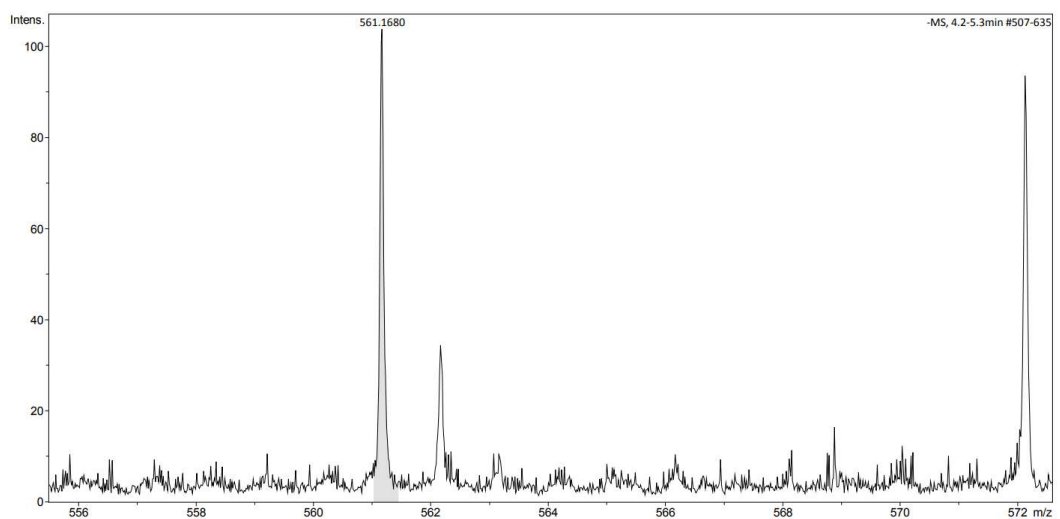


Figure 100 – ESI<sup>-</sup> mass spectrum collected for compound **8**.

Table 10 – High Resolution mass spectrometry theoretical and experimentally derived values for compounds **3-5**.

Compound	$m/z$ [ $M$ ] <sup>-</sup>		$m/z$ [ $M + M + H^+$ ] <sup>-</sup>	
	Theoretical	Actual	Theoretical	Actual
<b>3</b>	410.3815	410.0755	821.7700	821.1591
<b>4</b>	394.3385	394.0440	789.6840	789.0951
<b>5</b>	364.3565	364.0702	729.7200	729.1471

Table 11 – High Resolution mass spectrometry theoretical and experimentally derived values for compounds 6-8.

Compound	m/z [M - H] <sup>+</sup>		m/z [M + M] <sup>-</sup>	
	Theoretical	Actual	Theoretical	Actual
<b>6</b>	303.2550	303.0863	607.5170	607.1776
<b>7</b>	310.2132	310.0433	621.4334	621.0916
<b>8</b>	280.2312	280.0820	561.4694	561.1680

#### 6.4 <sup>1</sup>H NMR quantitative studies

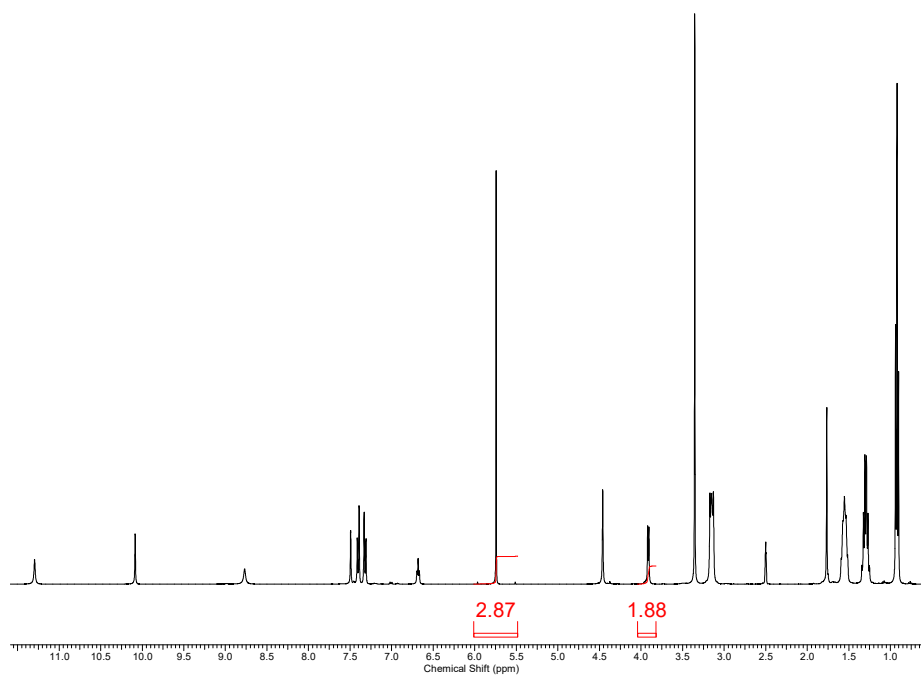


Figure 101 – <sup>1</sup>H NMR spectrum ( $d_1 = 60$  s) of compound **3** (0.0364 g, 111.12 mM) and DCM (5  $\mu$ l, 0.08 mM) in DMSO- $d_6$ . 6% of compound observed upon comparative signal integration.

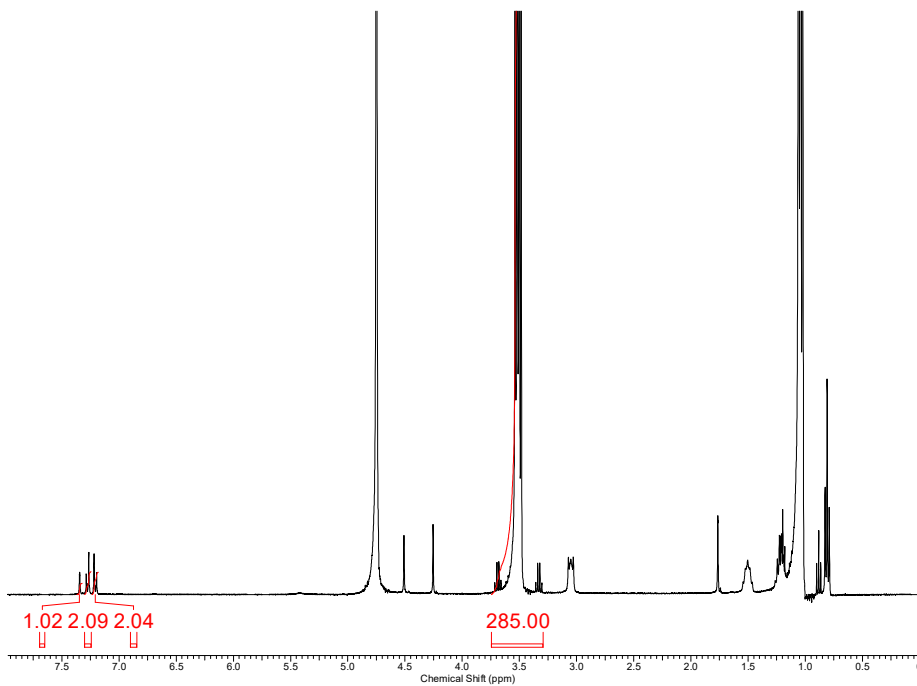


Figure 102 –  $^1\text{H}$  NMR spectrum ( $d_1 = 60$  s) of compound **3** (0.00197 g, 6.00 mM) and EtOH (5  $\mu\text{l}$ , 0.43 mM) in  $\text{D}_2\text{O}$ . No apparent loss of compound observed upon comparative signal integration.

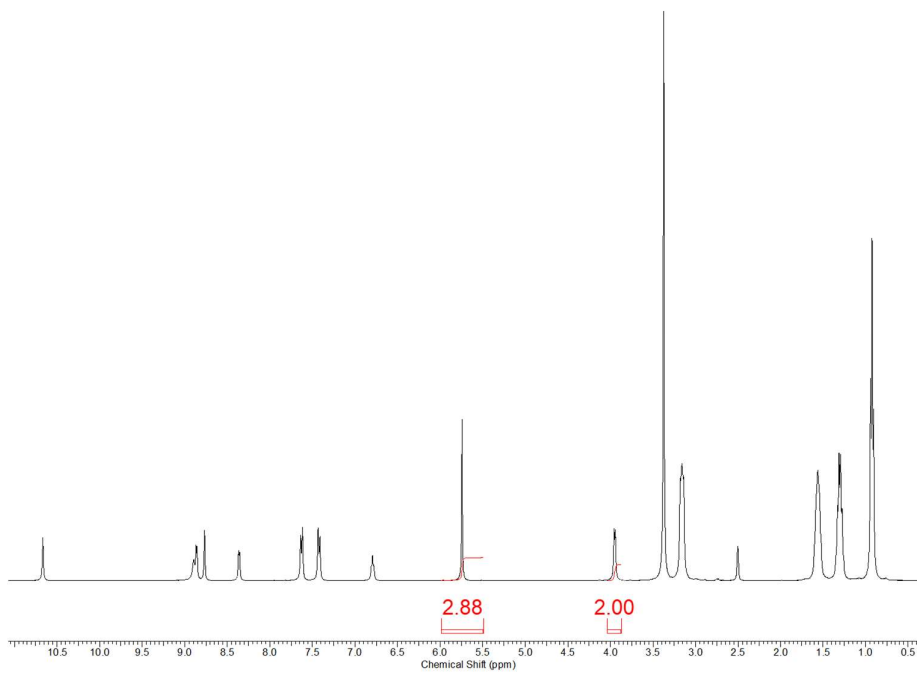


Figure 103 –  $^1\text{H}$  NMR spectrum ( $d_1 = 60$  s) of compound **4** (0.0354 g, 111.12 mM) and DCM (5  $\mu\text{l}$ , 0.08 mM) in  $\text{DMSO}-d_6$ . No apparent loss of compound observed upon comparative signal integration.

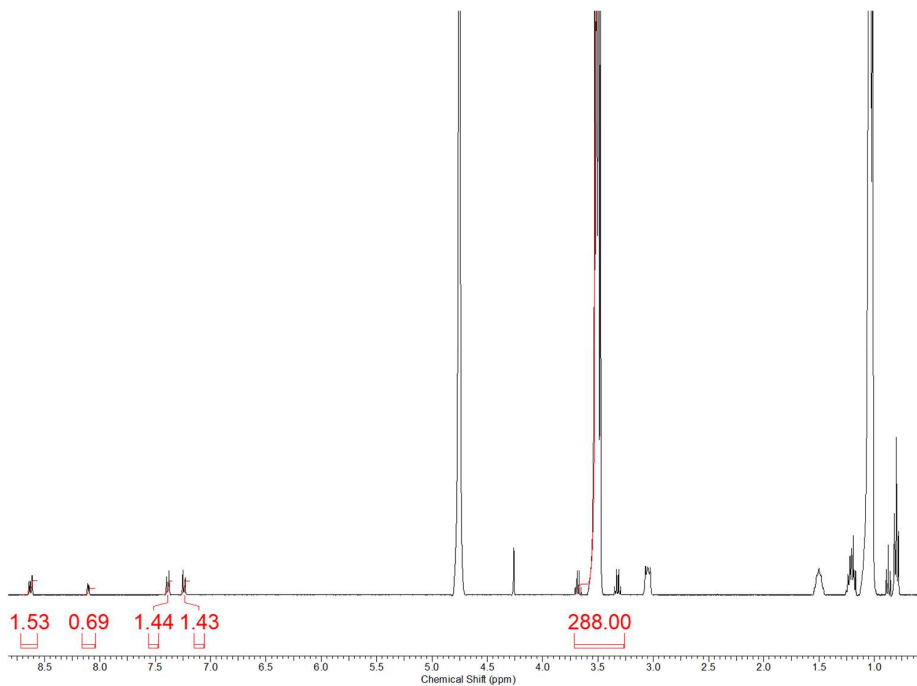


Figure 104 – <sup>1</sup>H NMR spectrum ( $d_1 = 60$  s) of compound **4** (0.00190 g, 6.00 mM) and EtOH (5  $\mu$ l, 0.43 mM) in D<sub>2</sub>O 29% loss of compound observed upon comparative signal integration.

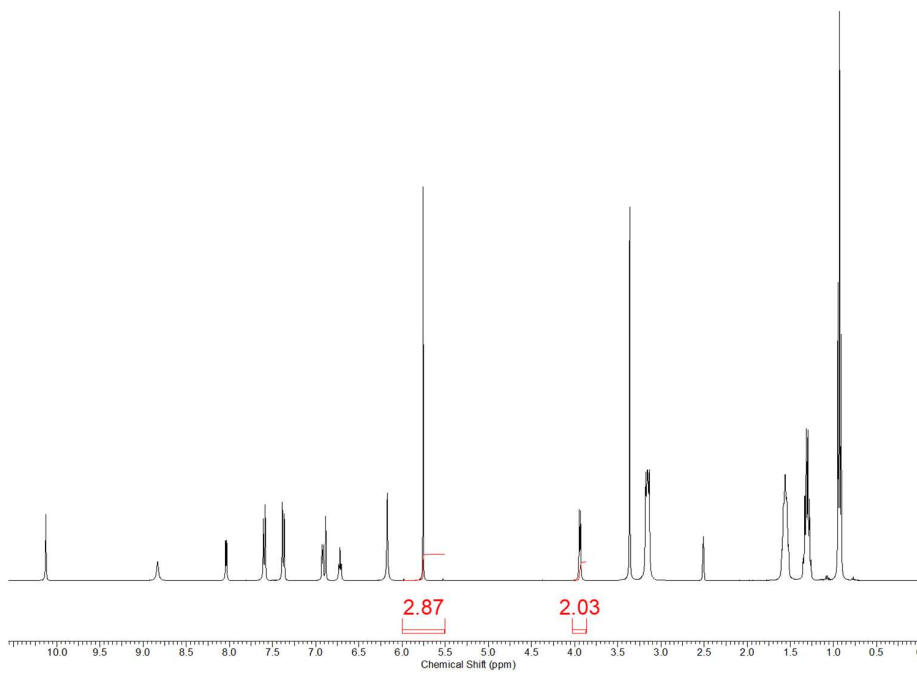


Figure 105 – <sup>1</sup>H NMR spectrum ( $d_1 = 60$  s) of compound **5** (0.0337 g, 111.12 mM) and DCM (5  $\mu$ l, 0.08 mM) in DMSO-*d*<sub>6</sub>. No apparent loss of compound observed upon comparative signal integration.

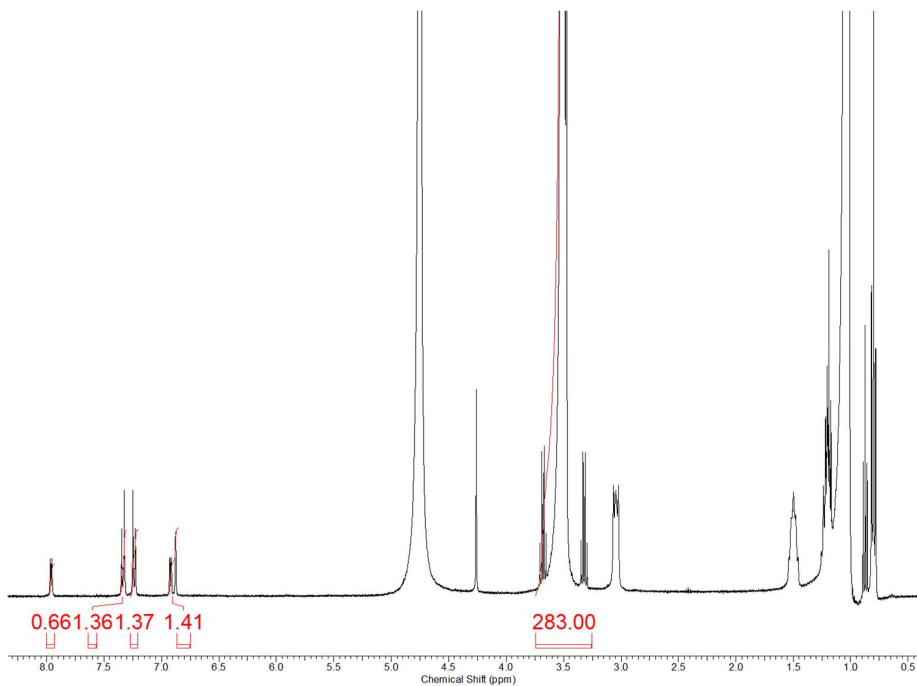


Figure 106 –  $^1\text{H}$  NMR spectrum ( $d_1 = 60$  s) of compound **5** (0.00184 g, 6.00 mM) and EtOH (5  $\mu\text{l}$ , 0.43 mM) in  $\text{D}_2\text{O}$ . 32% loss of compound observed upon comparative signal integration.

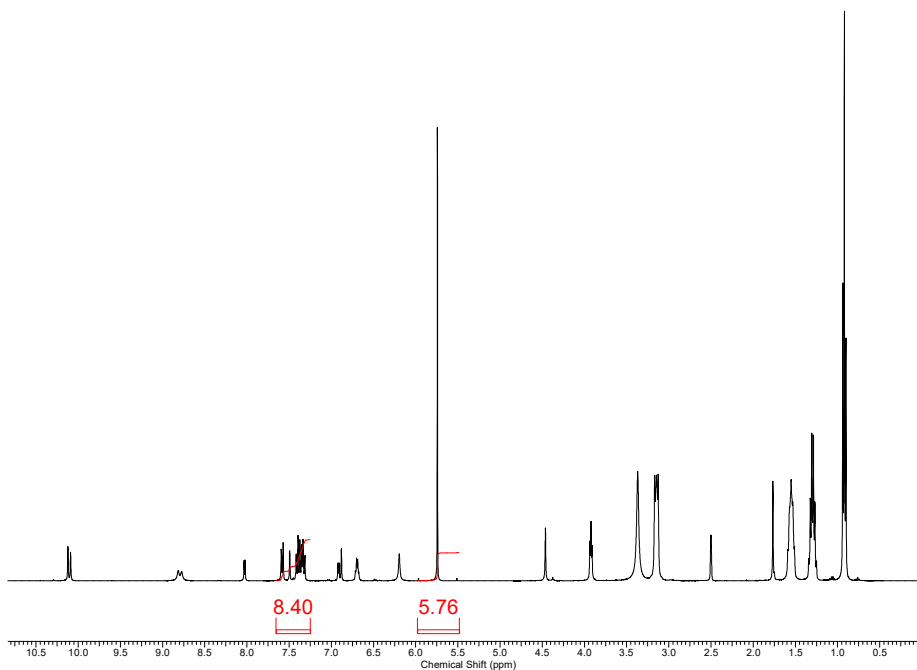


Figure 107 –  $^1\text{H}$  NMR spectrum ( $d_1 = 60$  s) of compound **3** (0.01814 g, 55.56 mM), compound **5** (0.01687 g, 55.56 mM) and DCM (5  $\mu\text{l}$ , 0.08 mM) in  $\text{DMSO}-d_6$ . 7% loss of compound observed upon comparative signal integration.

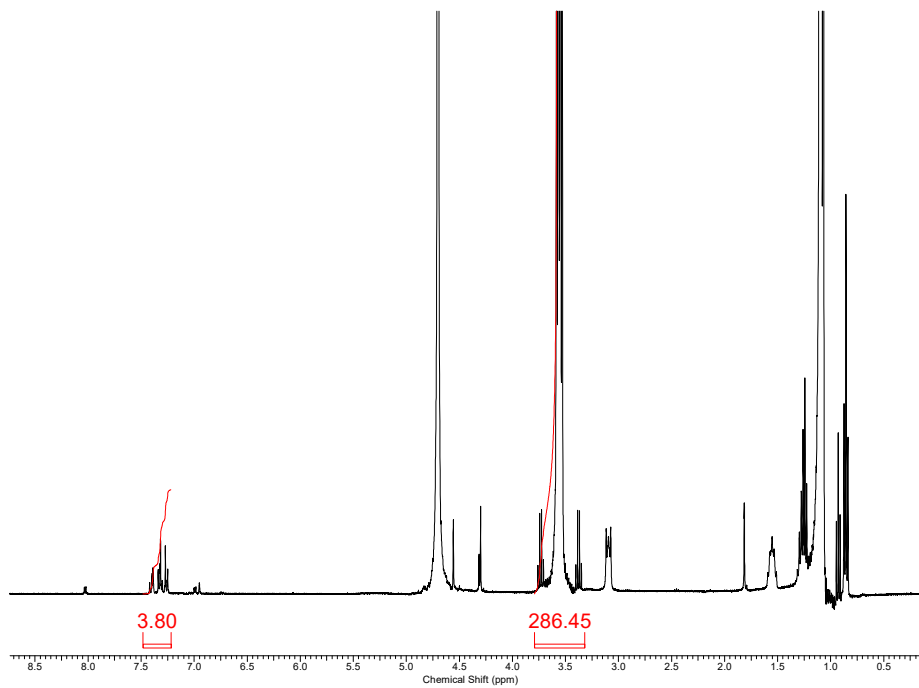


Figure 108 – <sup>1</sup>H NMR spectrum ( $d_1 = 60$  s) of compound **3** (0.00196 g, 3.00 mM), compound **5** (0.00183 g, 3.00 mM) and DCM (5  $\mu$ l, 0.08 mM) in D<sub>2</sub>O. 58 % loss of compound observed upon comparative signal integration.

6.5  $^1\text{H}$  NMR DOSY studies

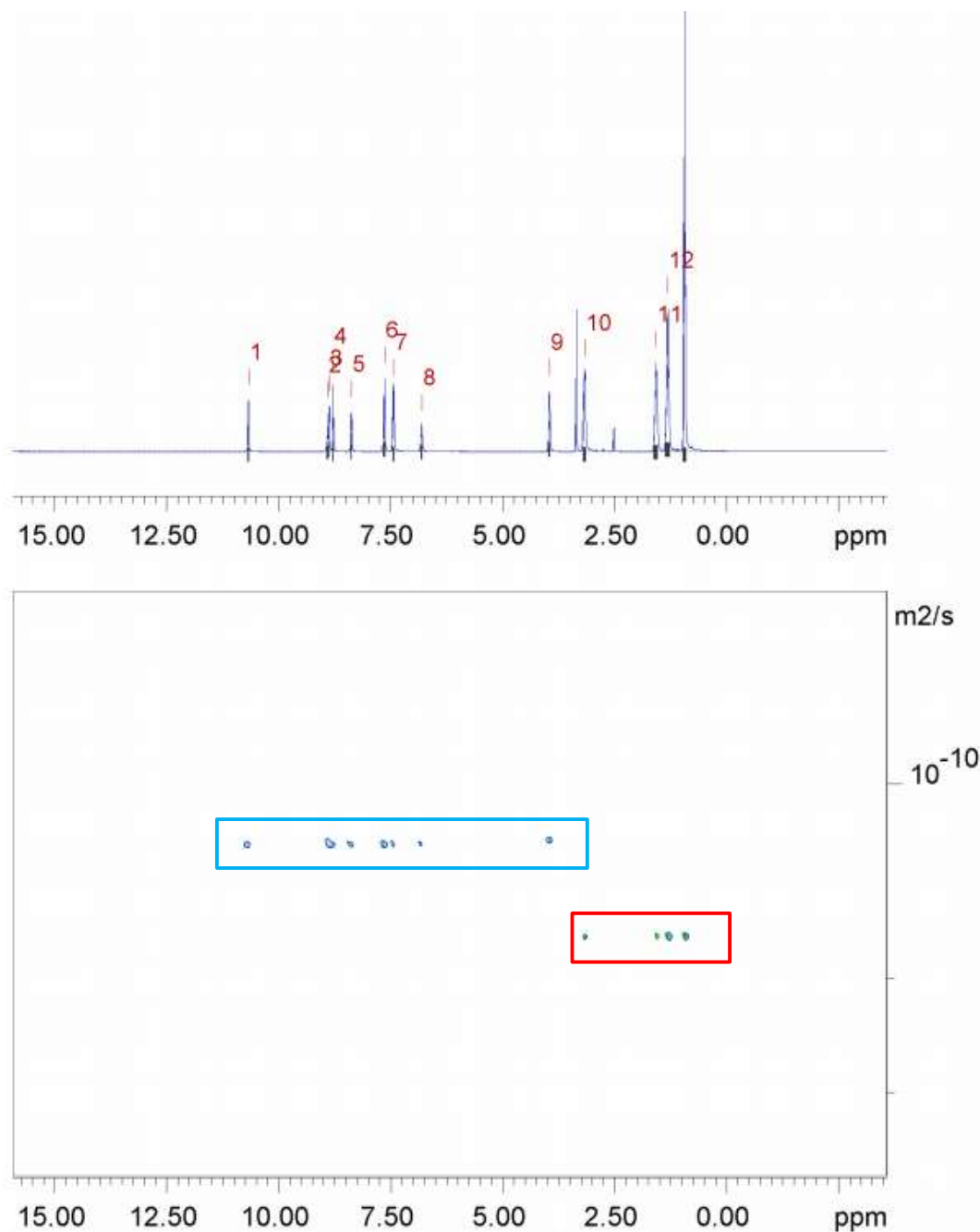


Figure 109 –  $^1\text{H}$  DOSY NMR of compound 4 (111.12 mM) in  $\text{DMSO}-d_6$  conducted at 298.15 K. Anionic component highlighted in blue, TBA counter cation highlighted in red.

Table 12 – Diffusion data obtained from <sup>1</sup>H DOSY NMR of compound **4** (111.12 mM) in DMSO-*d*<sub>6</sub> conducted at 298.15 K.

Peak name	F2 [ppm]	D [m <sup>2</sup> /s]	error
1	10.670	1.23e-10	1.265e-14
2	8.906	1.23e-10	2.190e-14
3	8.871	1.23e-10	9.310e-15
4	8.777	1.23e-10	9.960e-15
5	8.371	1.23e-10	1.037e-14
6	7.634	1.23e-10	5.860e-15
7	7.429	1.24e-10	5.840e-15
8	6.804	1.23e-10	1.461e-14
9	3.948	1.23e-10	6.315e-15
10	3.166	1.71e-10	4.747e-15
11	1.569	1.71e-10	4.661e-15
12	1.309	1.71e-10	3.502e-15
13	0.931	1.71e-10	1.818e-15

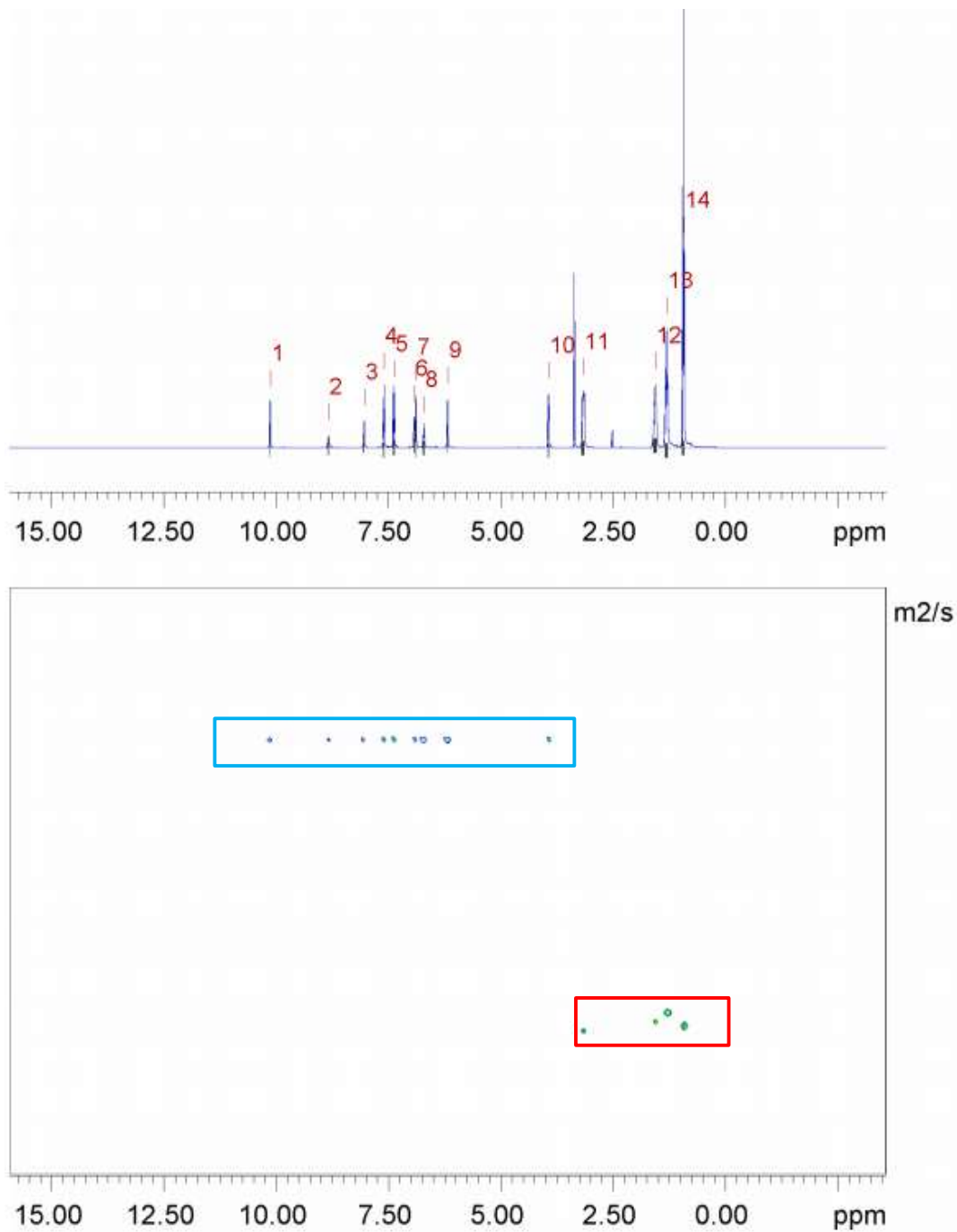


Figure 110 –  $^1\text{H}$  DOSY NMR of compound 5 (111.12 mM) in  $\text{DMSO-}d_6$  conducted at 298.15 K. Anionic component highlighted in blue, TBA counter cation highlighted in red.

Table 13 – Diffusion data obtained from <sup>1</sup>H DOSY NMR of compound **5** (111.12 mM) in DMSO-*d*<sub>6</sub> conducted at 298.15 K.

Peak name	F2 [ppm]	D [m <sup>2</sup> /s]	error
1	10.128	1.13e-10	9.945e-15
2	8.830	1.13e-10	2.220e-14
3	8.037	1.13e-10	1.083e-14
4	7.595	1.13e-10	5.575e-15
5	7.372	1.13e-10	5.491e-15
6	6.918	1.13e-10	9.468e-15
7	6.880	1.13e-10	8.380e-15
8	6.709	1.13e-10	1.383e-14
9	6.175	1.13e-10	7.963e-15
10	3.931	1.12e-10	5.805e-15
11	3.156	1.62e-10	5.040e-15
12	1.557	1.60e-10	4.653e-15
13	1.301	1.58e-10	3.186e-15
14	0.926	1.61e-10	1.630e-15

Table 14 – Calculated hydrodynamic diameter for compounds **4** and **5** in DMSO-*d*<sub>6</sub> conducted at 298.15 K.

Compound	Anion (nm)	Cation (nm)
<b>4</b>	1.78	1.28
<b>5</b>	1.94	1.37

## 6.6 <sup>1</sup>H NMR self-association studies

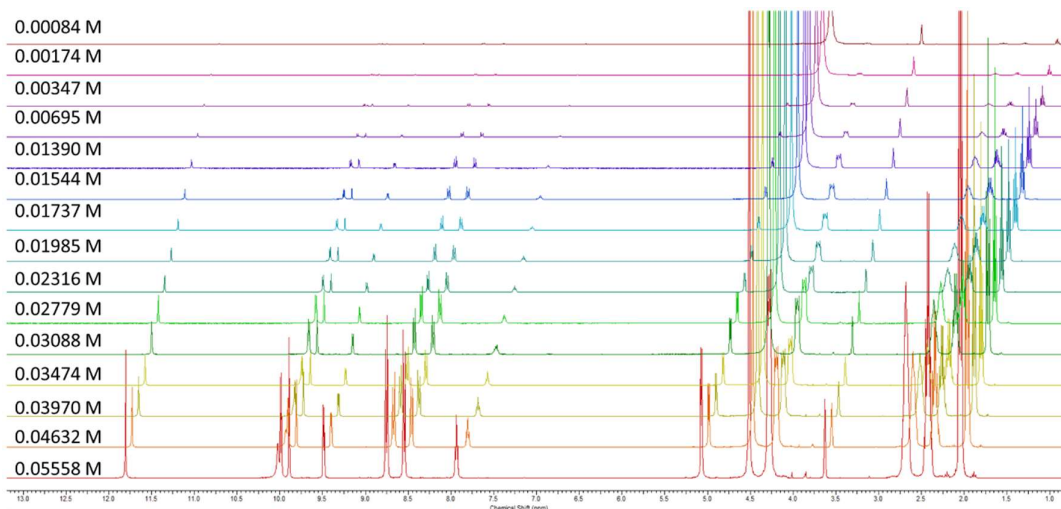


Figure 111 – <sup>1</sup>H NMR stack plot of compound **4** in a DMSO- *d*<sub>6</sub> 0.5 % H<sub>2</sub>O solution. Samples were prepared in series with an aliquot of the most concentrated solution undergoing serial dilution.

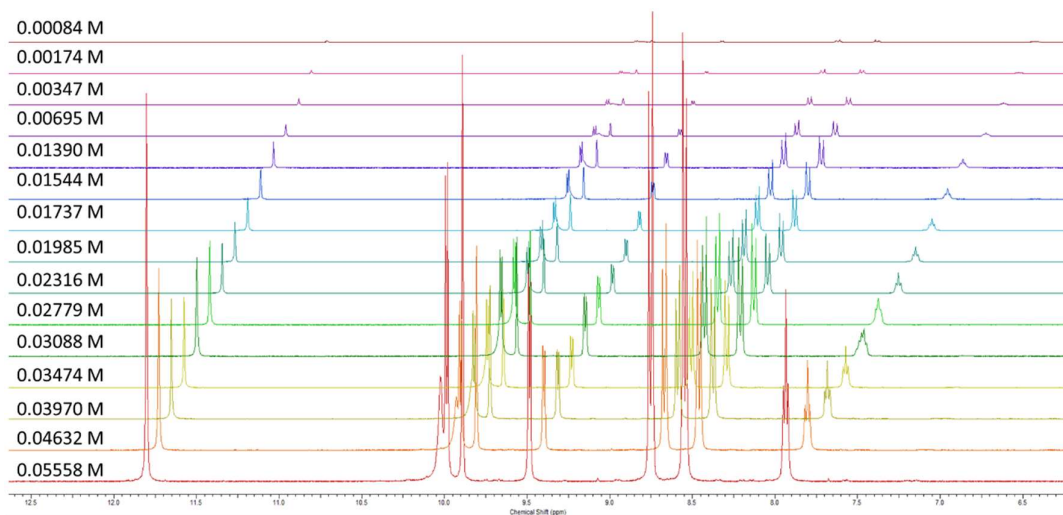


Figure 112 – Enlarged  $^1\text{H}$  NMR stack plot of compound **4** in a  $\text{DMSO-}d_6$  0.5 %  $\text{H}_2\text{O}$  solution. Samples were prepared in series with an aliquot of the most concentrated solution undergoing serial dilution.

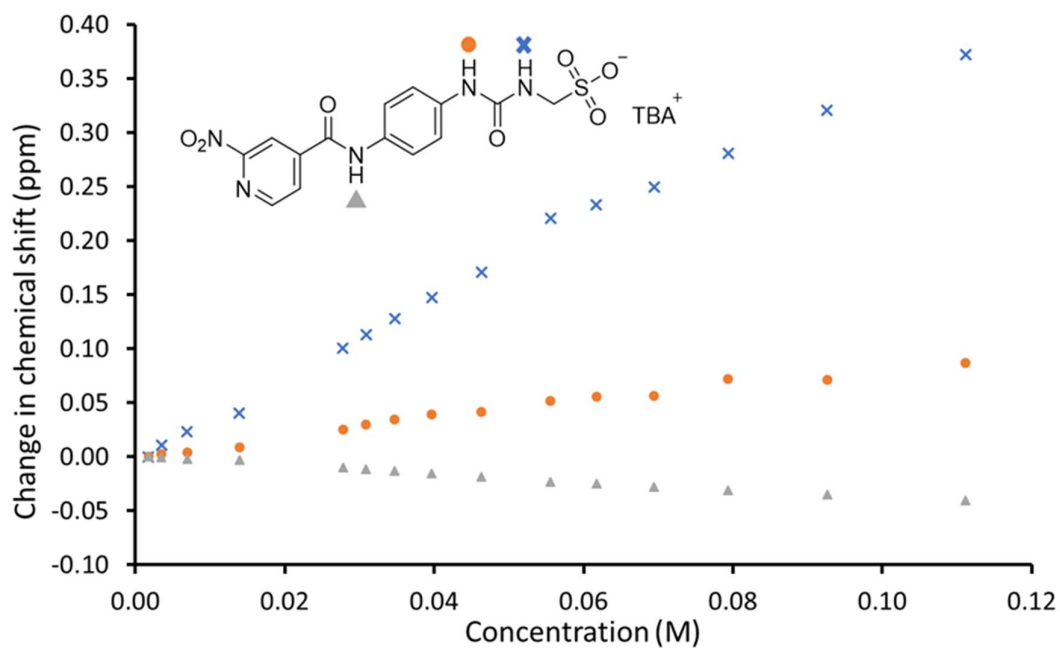


Figure 113 – Graph illustrating the  $^1\text{H}$  NMR down-field change in chemical shift of NH resonances with increasing concentration of compound **4** in  $\text{DMSO-}d_6$  w/ 0.5 %  $\text{H}_2\text{O}$  (298.15 K).

### Self-association constant calculation

Table 15 – Dilution study of compound **4** in DMSO-*d*<sub>6</sub> w/ 0.5 % H<sub>2</sub>O. Values calculated from data gathered from 2 NHs.

Compound	EK Model (M <sup>-1</sup> )		CoEK Model (M <sup>-1</sup> )		
	K <sub>e</sub>	K <sub>dim</sub>	K <sub>e</sub>	K <sub>dim</sub>	ρ
<b>4</b>	1.41 (± 1.5 %)	0.71 (± 0.7 %)	10.91 (± 3.4 %)	5.45 (± 1.7 %)	0.30 (± 10.0 %)
Link for EK	<a href="http://app.supramolecular.org/bindfit/view/090bee18-4a16-4728-9d3a-565b04666500">http://app.supramolecular.org/bindfit/view/090bee18-4a16-4728-9d3a-565b04666500</a>				
Link for CoEK	<a href="http://app.supramolecular.org/bindfit/view/573b0ca3-687a-437f-bff5-3ded4a748198">http://app.supramolecular.org/bindfit/view/573b0ca3-687a-437f-bff5-3ded4a748198</a>				

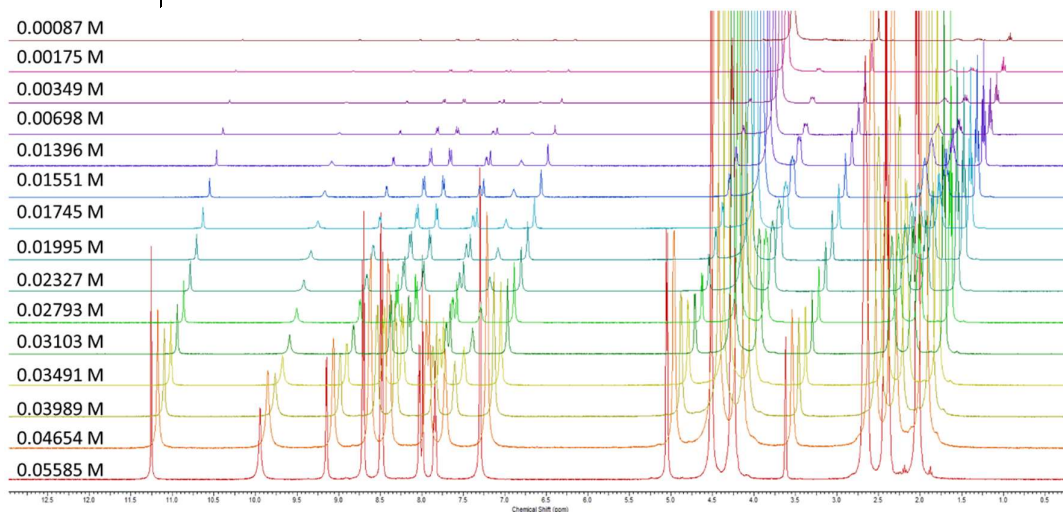


Figure 114 – <sup>1</sup>H NMR stack plot of compound **5** in a DMSO-*d*<sub>6</sub> 0.5 % H<sub>2</sub>O solution. Samples were prepared in series with an aliquot of the most concentrated solution undergoing serial dilution.

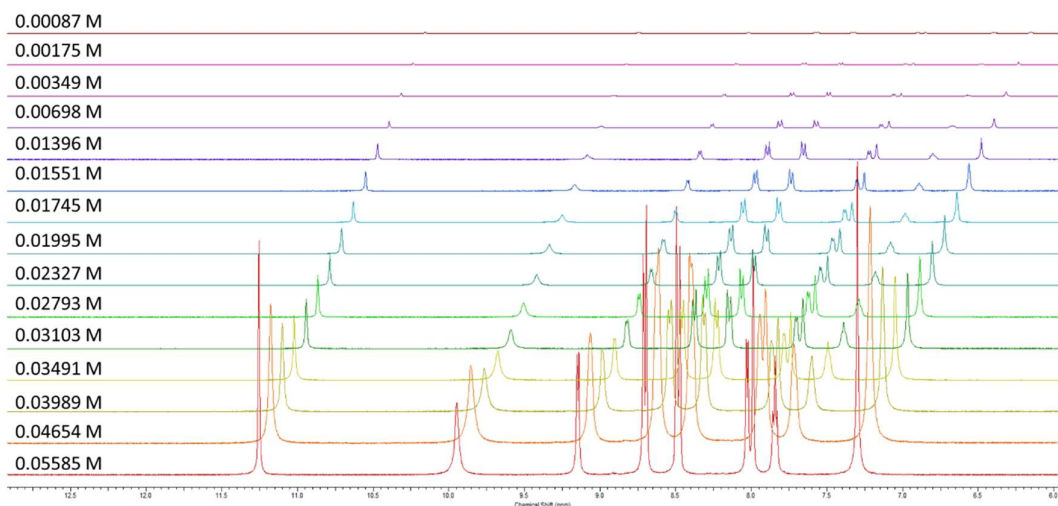


Figure 115 – Enlarged <sup>1</sup>H NMR stack plot of compound **5** in a DMSO-*d*<sub>6</sub> 0.5 % H<sub>2</sub>O solution. Samples were prepared in series with an aliquot of the most concentrated solution undergoing serial dilution.

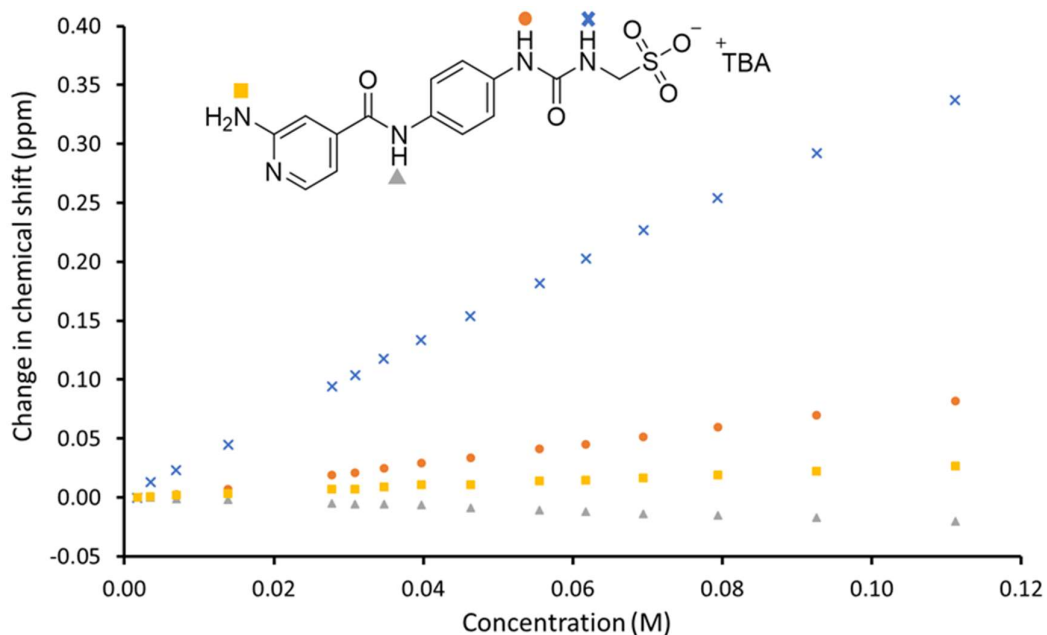


Figure 116 – Graph illustrating the  $^1\text{H}$  NMR down-field change in chemical shift of urea NH resonances with increasing concentration of compound **5** in  $\text{DMSO-}d_6$  0.5 %  $\text{H}_2\text{O}$  (298.15 K).

#### Self-association constant calculation

Table 16 – Dilution study of compound **5** in  $\text{DMSO-}d_6$  5 %  $\text{H}_2\text{O}$ . Values calculated from data gathered from 2 NH.

Compound	EK Model ( $\text{M}^{-1}$ )		CoEK Model ( $\text{M}^{-1}$ )		
	$K_e$	$K_{\text{dim}}$	$K_e$	$K_{\text{dim}}$	$\rho$
<b>5</b>	1.78 ( $\pm 0.6\%$ )	0.89 ( $\pm 0.3\%$ )	8.32 ( $\pm 3.1\%$ )	4.16 ( $\pm 1.6\%$ )	0.50 ( $\pm 5.2\%$ )
Link for EK	<a href="http://app.supramolecular.org/bindfit/view/005255d3-873e-49e1-b066-d6b551ddc6fd">http://app.supramolecular.org/bindfit/view/005255d3-873e-49e1-b066-d6b551ddc6fd</a>				
Link for CoEK	<a href="http://app.supramolecular.org/bindfit/view/96557a3e-c430-4e14-9bc4-11cc00d92277">http://app.supramolecular.org/bindfit/view/96557a3e-c430-4e14-9bc4-11cc00d92277</a>				

## 6.7 $^1\text{H}$ NMR titration studies

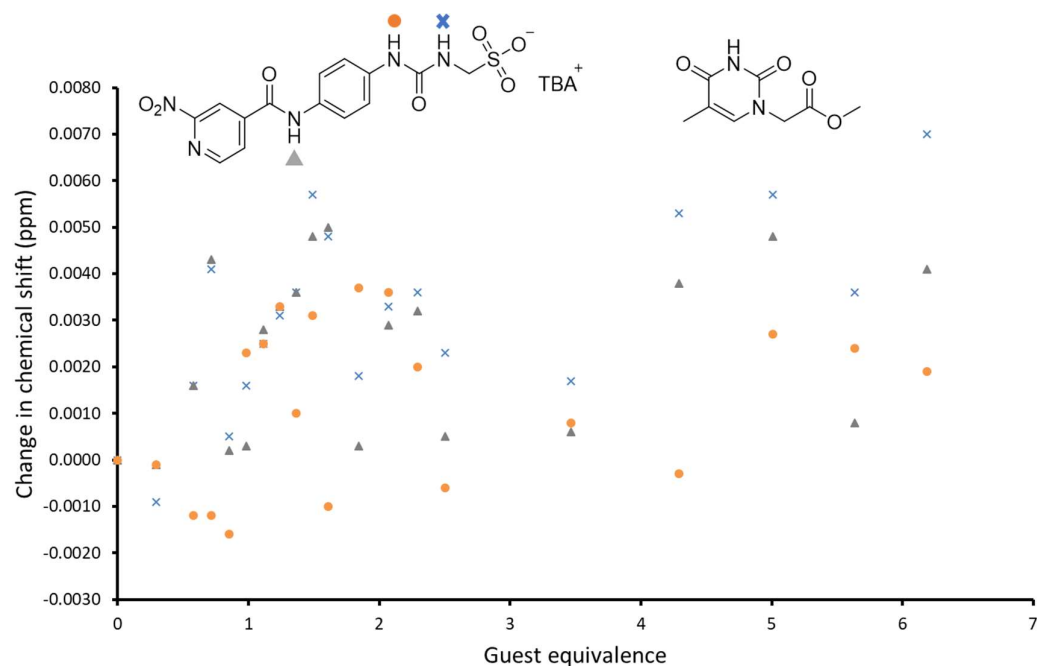


Figure 117 – A graph showing the downfield  $^1\text{H}$  NMR change in chemical shift for the NHs of compound **4** (host) with increasing the concentration of compound **10** (guest) in a  $\text{DMSO-}d_6$  – 0.5%  $\text{H}_2\text{O}$  solution (298 K).

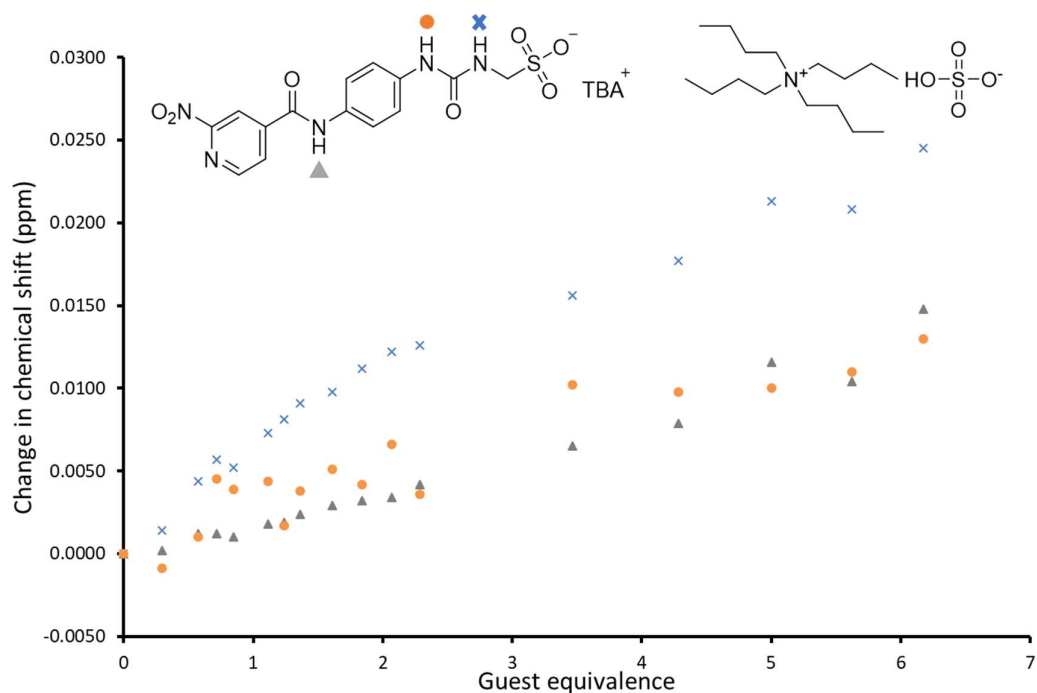


Figure 118 – A graph showing the downfield  $^1\text{H}$  NMR change in chemical shift for the NHs of compound **4** (host) with increasing the concentration of  $\text{TBA}^+ \text{HSO}_4^-$  (guest) in a  $\text{DMSO-}d_6$  – 0.5%  $\text{H}_2\text{O}$  solution (298 K).

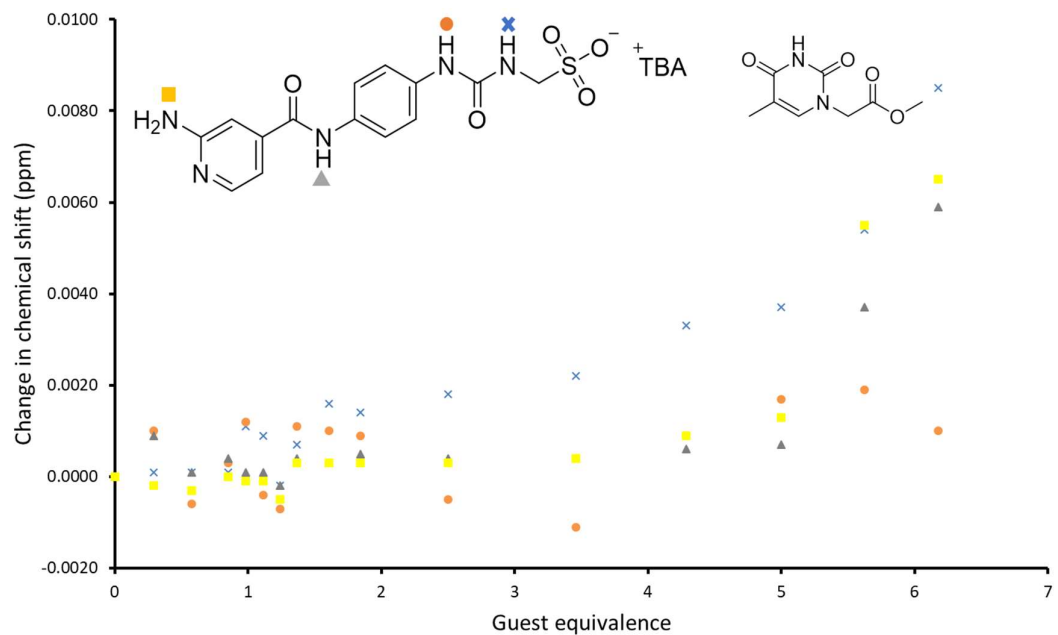


Figure 119 – A graph showing the downfield  $^1\text{H}$  NMR change in chemical shift for the NHs of compound **5** (host) with increasing the concentration of compound **10** (guest) in a  $\text{DMSO-}d_6$  – 0.5%  $\text{H}_2\text{O}$  solution (298 K).

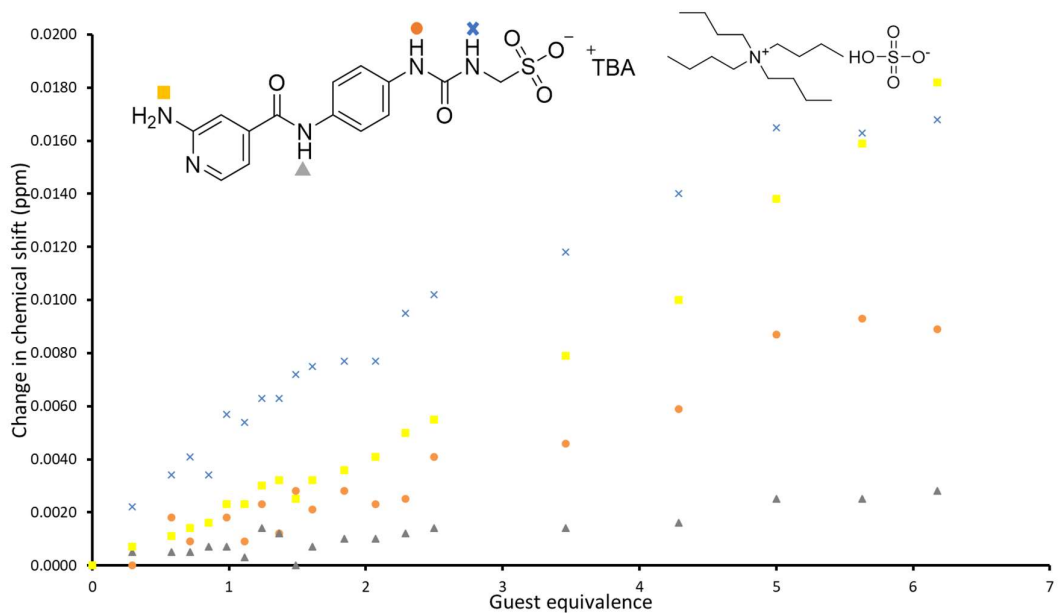


Figure 120 – A graph showing the downfield  $^1\text{H}$  NMR change in chemical shift for the NHs of compound **5** (host) with increasing the concentration of  $\text{TBA}^+ \text{HSO}_4^-$  (guest) in a  $\text{DMSO-}d_6$  – 0.5%  $\text{H}_2\text{O}$  solution (298 K).

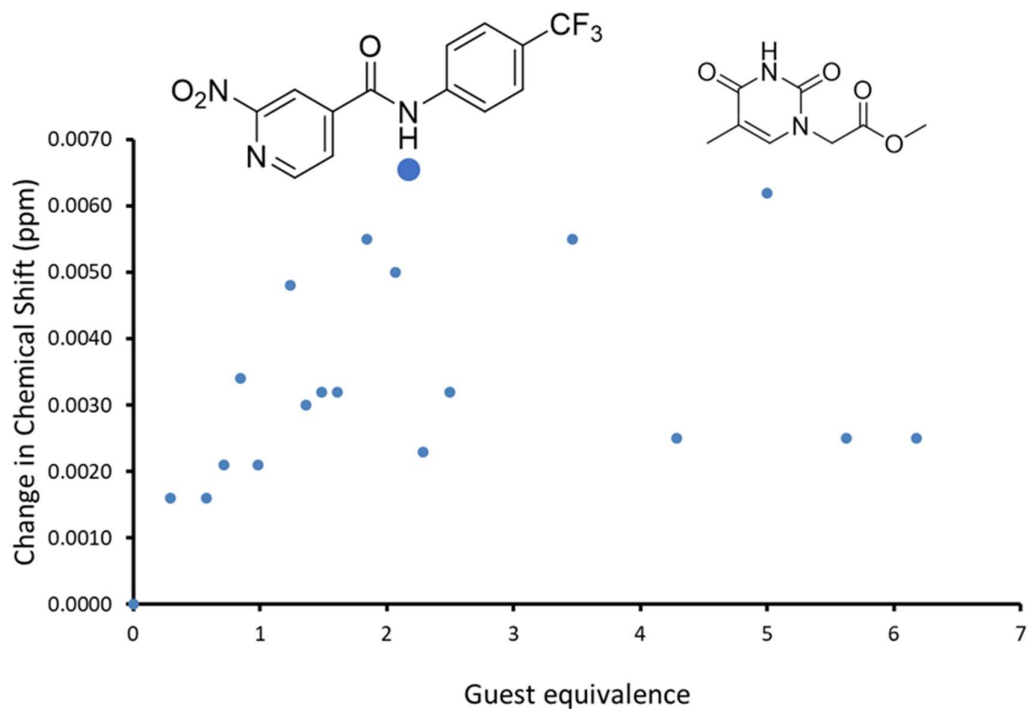


Figure 121 – A graph showing the downfield <sup>1</sup>H NMR change in chemical shift for the NHs of compound **7** (host) with increasing the concentration of compound **10** (guest) in a DMSO-*d*<sub>6</sub> – 0.5% H<sub>2</sub>O solution (298 K).

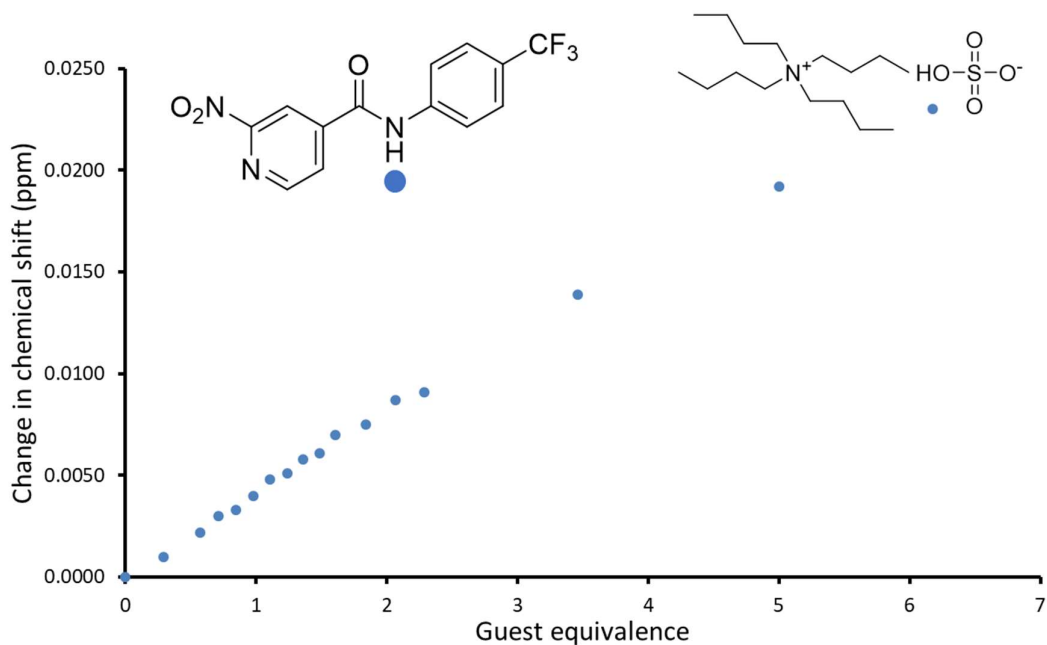


Figure 122 – A graph showing the downfield <sup>1</sup>H NMR change in chemical shift for the NHs of compound **7** (host) with increasing the concentration of TBA<sup>+</sup> HSO<sub>4</sub><sup>-</sup> (guest) in a DMSO-*d*<sub>6</sub> – 0.5% H<sub>2</sub>O solution (298 K).

Table 17 – Association constants ( $M^{-1}$ ) calculated for each NH in compound **7** (host) titrated against  $TBA^+ HSO_4^-$  (guest) in a  $DMSO-d_6 - 0.5\% H_2O$  solution (298 K).

Host: Guest	1: 1	1: 2		2: 1	
NH	K	$K_{11}$	$K_{12}$	$K_{11}$	$K_{21}$
Circle	3.35 ( $\pm 1.1\%$ )	436846684486 ( $\pm 8309238\%$ )	3.49 ( $\pm 1.8\%$ )	-48.9 ( $\pm 9.0\%$ )	-24.69 ( $\pm 8.1\%$ )
Link to 1:1	<a href="http://app.supramolecular.org/bindfit/view/f66937c8-9eab-4632-a8ff-b4085f79f1fc">http://app.supramolecular.org/bindfit/view/f66937c8-9eab-4632-a8ff-b4085f79f1fc</a>				
Link to 1:2	<a href="http://app.supramolecular.org/bindfit/view/0c7d2b13-9028-4787-a84c-f145c7f474d3">http://app.supramolecular.org/bindfit/view/0c7d2b13-9028-4787-a84c-f145c7f474d3</a>				
Link to 2:1	<a href="http://app.supramolecular.org/bindfit/view/06b6b7a0-a00e-417f-bcf3-c8dec846d20d">http://app.supramolecular.org/bindfit/view/06b6b7a0-a00e-417f-bcf3-c8dec846d20d</a>				

*a* – association constant too large ( $> 10^5 M^{-1}$ ) *b* – negative association constant.

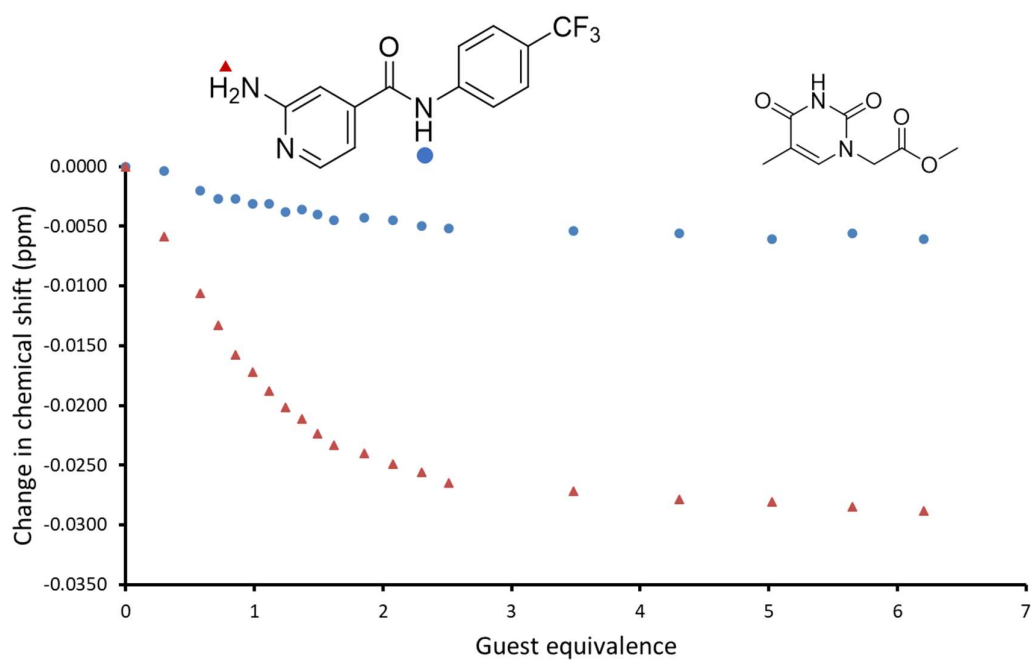


Figure 123 – A graph showing the downfield  $^1H$  NMR change in chemical shift for the NHs of compound **8** (host) with increasing the concentration of compound **10** (guest) in a  $DMSO-d_6 - 0.5\% H_2O$  solution (298 K).

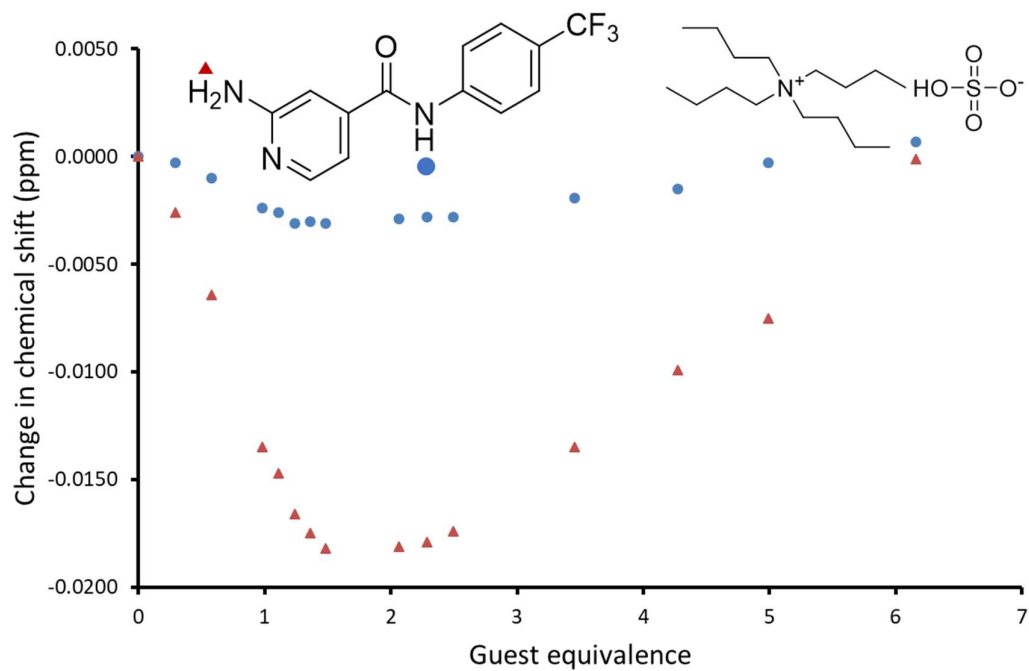


Figure 124 – A graph showing the downfield <sup>1</sup>H NMR change in chemical shift for the NHs of compound **8** (host) with increasing the concentration of TBA<sup>+</sup> HSO<sub>4</sub><sup>-</sup> (guest) in a DMSO-*d*<sub>6</sub> – 0.5% H<sub>2</sub>O solution (298 K)..

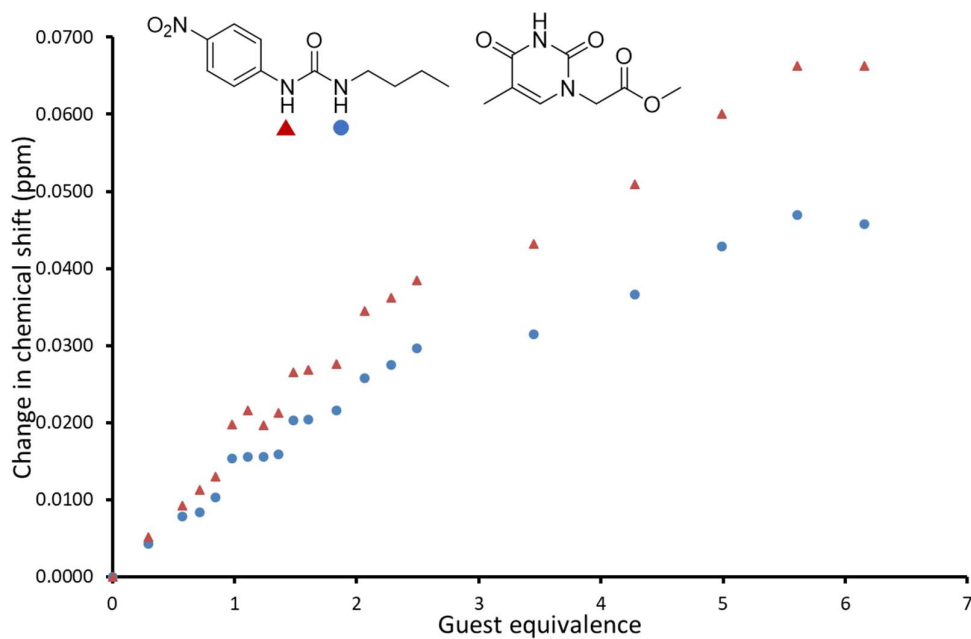


Figure 125 – A graph showing the downfield <sup>1</sup>H NMR change in chemical shift for the NHs of compound **9** (host) with increasing the concentration of compound **10** (guest) in a DMSO-*d*<sub>6</sub> – 0.5% H<sub>2</sub>O solution (298 K).

Table 18 – Association constants ( $M^{-1}$ ) calculated for each NH in compound **9** (host) titrated against compound **10** (guest) in a DMSO- $d_6$  – 0.5% H<sub>2</sub>O solution (298 K).

Host:	1: 1		1: 2		2: 1	
Guest						
NH	K	K <sub>11</sub>	K <sub>12</sub>	K <sub>11</sub>	K <sub>21</sub>	
<b>Circle</b>	25.92 (± 5.7 %)	2010437381651813 (± 169434405 %)	20.46 (± 9.7 %)	56.18 (± 97.5 %)	639.76 (± 112.9 %)	
Link to 1:1	<a href="http://app.supramolecular.org/bindfit/view/b5b7f1f9-f026-4ac7-a3ff-349589218af0">http://app.supramolecular.org/bindfit/view/b5b7f1f9-f026-4ac7-a3ff-349589218af0</a>					
Link to 1:2	<a href="http://app.supramolecular.org/bindfit/view/c423c643-5207-4222-bd8f-9932be63f86f">http://app.supramolecular.org/bindfit/view/c423c643-5207-4222-bd8f-9932be63f86f</a>					
Link to 2:1	<a href="http://app.supramolecular.org/bindfit/view/cd5c2e7e-4eb6-4786-a37e-f6c106443e77">http://app.supramolecular.org/bindfit/view/cd5c2e7e-4eb6-4786-a37e-f6c106443e77</a>					
<b>Triangle</b>	17.33 (± 4.8 %)	38.31 (± 9.3 %)	-5.25 (± -24.1 %)	0.00881 (± 104.1 %)	5400616 (± 115.3 %)	
Link to 1:1	<a href="http://app.supramolecular.org/bindfit/view/2346a76b-c509-42ab-9a0c-df612552486e">http://app.supramolecular.org/bindfit/view/2346a76b-c509-42ab-9a0c-df612552486e</a>					
Link to 1:2	<a href="http://app.supramolecular.org/bindfit/view/b9d513ac-beb9-4d35-a767-24cdafe748d7">http://app.supramolecular.org/bindfit/view/b9d513ac-beb9-4d35-a767-24cdafe748d7</a>					
Link to 2:1	<a href="http://app.supramolecular.org/bindfit/view/27939811-fa26-4a78-896f-bd0b27b0e951">http://app.supramolecular.org/bindfit/view/27939811-fa26-4a78-896f-bd0b27b0e951</a>					

## 6.8 DLS data

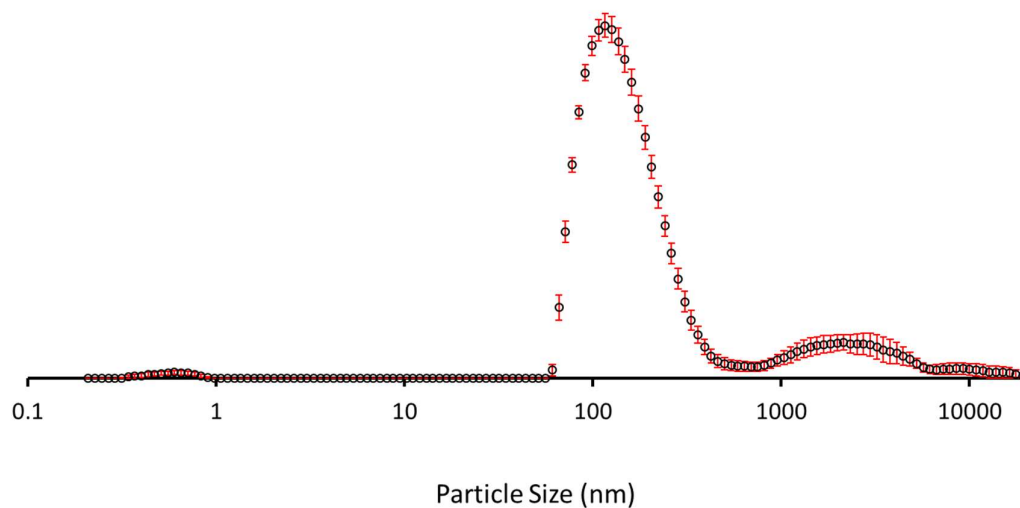


Figure 126 – Average intensity particle size distribution, calculated from 9 DLS runs, of aggregates formed by dissolving compound **3** at a concentration of 3.00 mM in a solution of EtOH: H<sub>2</sub>O 1:19, after heating to 40 °C and cooling to 25 °C.

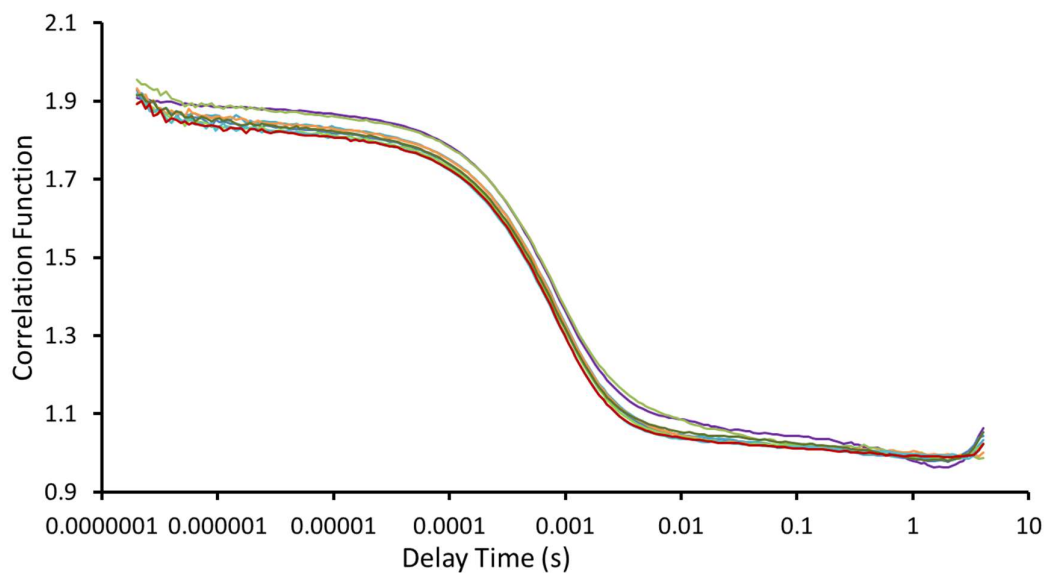


Figure 127 – Correlation function data for 9 DLS runs of compound **3** at a concentration of 3.00 mM in a solution of EtOH: H<sub>2</sub>O 1:19, after heating to 40 °C and cooling to 25 °C.

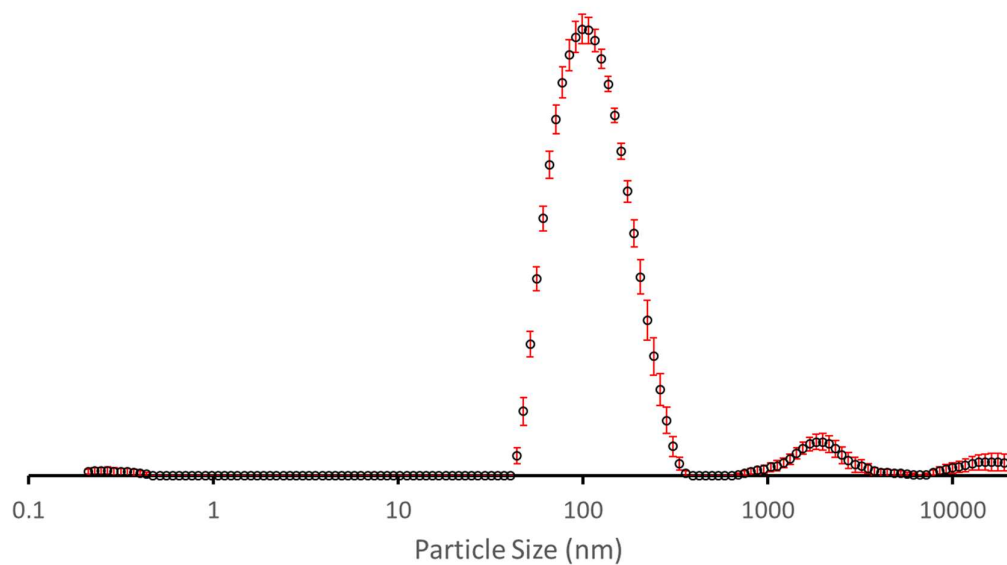


Figure 128 – Average intensity particle size distribution, calculated from 10 DLS runs, of aggregates formed by dissolving compound **3** at a concentration of 0.30 mM in a solution of EtOH: H<sub>2</sub>O 1:19, after heating to 40 °C and cooling to 25 °C.

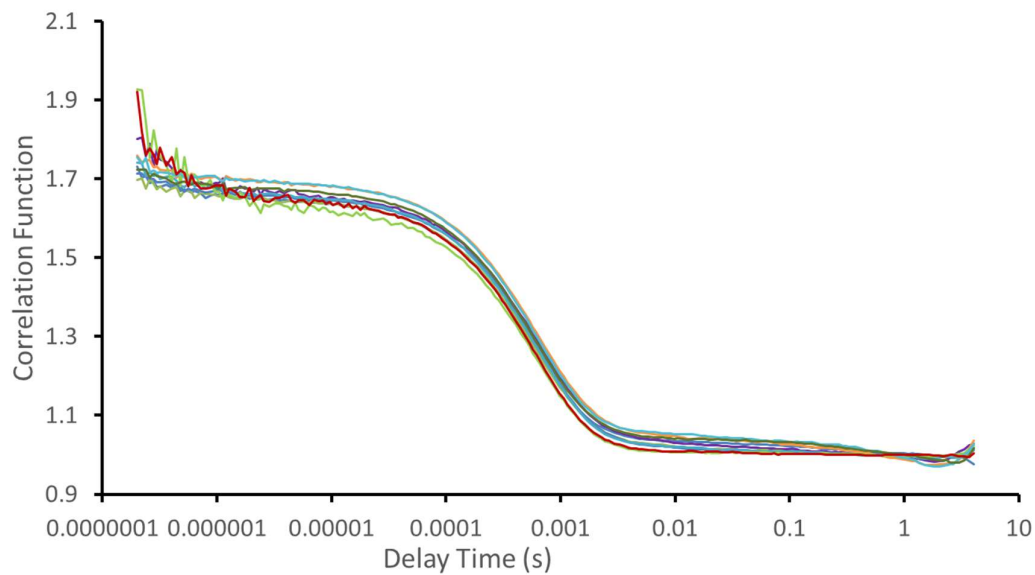


Figure 129 – Correlation function data for 10 DLS runs of compound **3** at a concentration of 0.30 mM in a solution of EtOH: H<sub>2</sub>O 1:19, after heating to 40 °C and cooling to 25 °C.

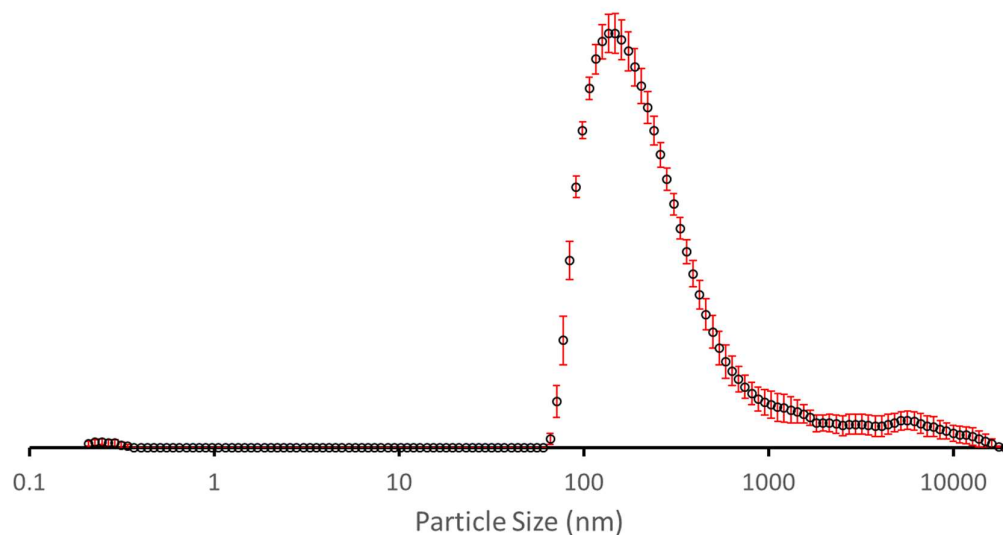


Figure 130 – Average intensity particle size distribution, calculated from 10 DLS runs, of aggregates formed by dissolving compound **4** at a concentration of 3.00 mM in a solution of EtOH: H<sub>2</sub>O 1:19, after heating to 40 °C and cooling to 25 °C.

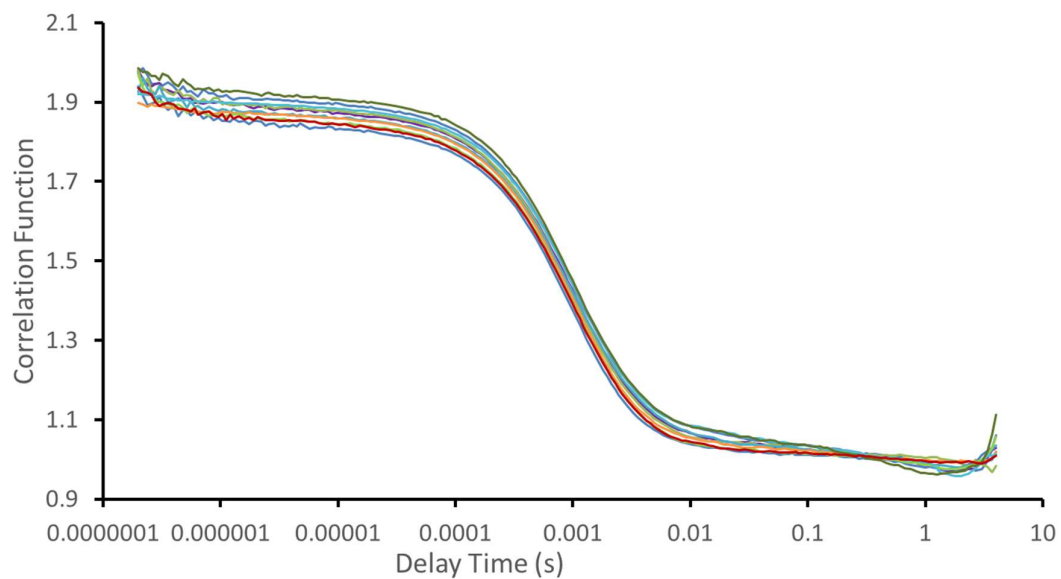


Figure 131 – Correlation function data for 10 DLS runs of compound **4** at a concentration of 3.00 mM in a solution of EtOH: H<sub>2</sub>O 1:19, after heating to 40 °C and cooling to 25 °C.

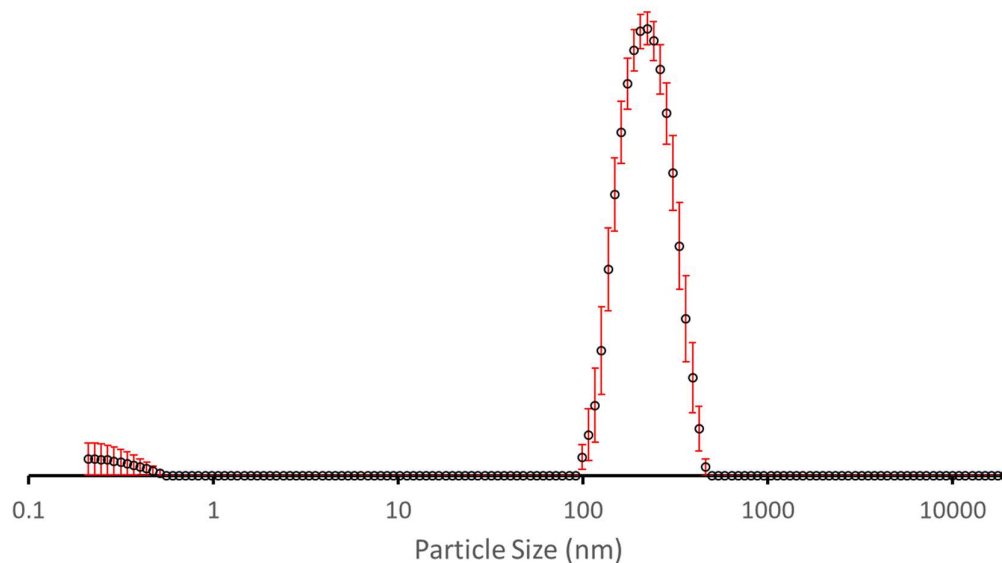


Figure 132 – Average intensity particle size distribution, calculated from 10 DLS runs, of aggregates formed by dissolving compound **4** at a concentration of 0.30 mM in a solution of EtOH: H<sub>2</sub>O 1:19, after heating to 40 °C and cooling to 25 °C.

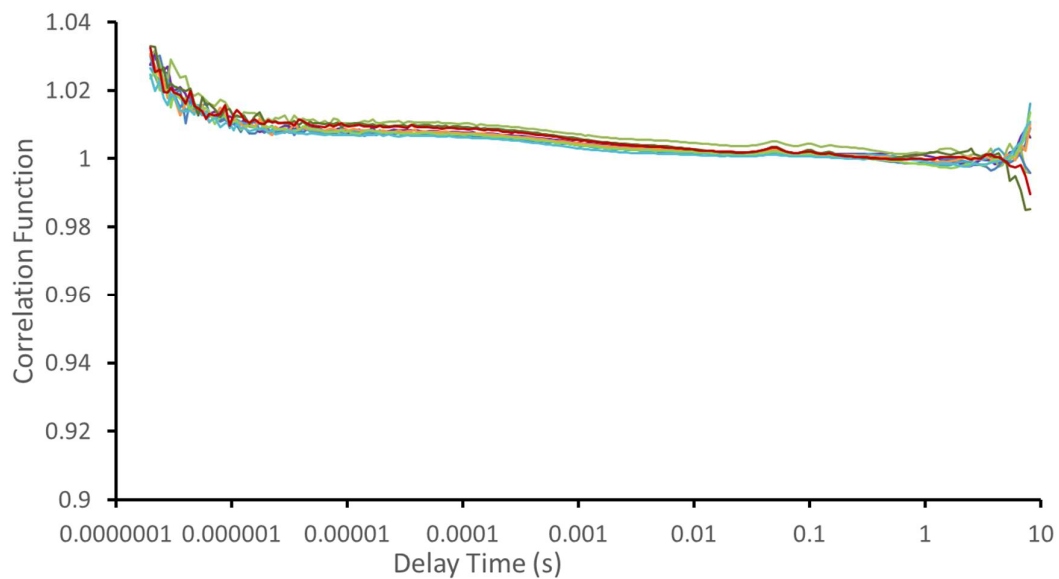


Figure 133 – Correlation function data for 10 DLS runs of compounds **4** at a concentration of 0.30 mM in a solution of EtOH: H<sub>2</sub>O 1:19, after heating to 40 °C and cooling to 25 °C.

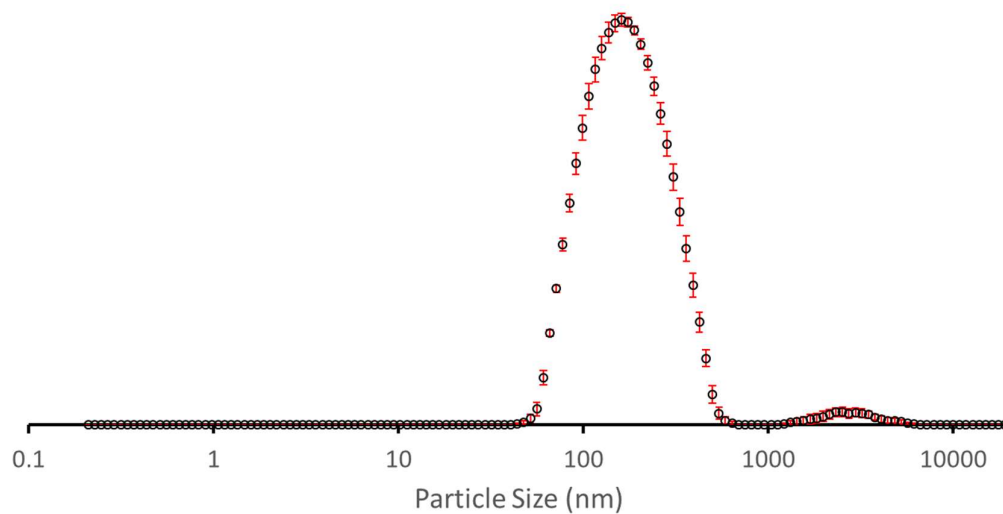


Figure 134 – Average intensity particle size distribution, calculated from 10 DLS runs, of aggregates formed by dissolving compound **5** at a concentration of 3.00 mM in a solution of EtOH: H<sub>2</sub>O 1:19, after heating to 40 °C and cooling to 25 °C.

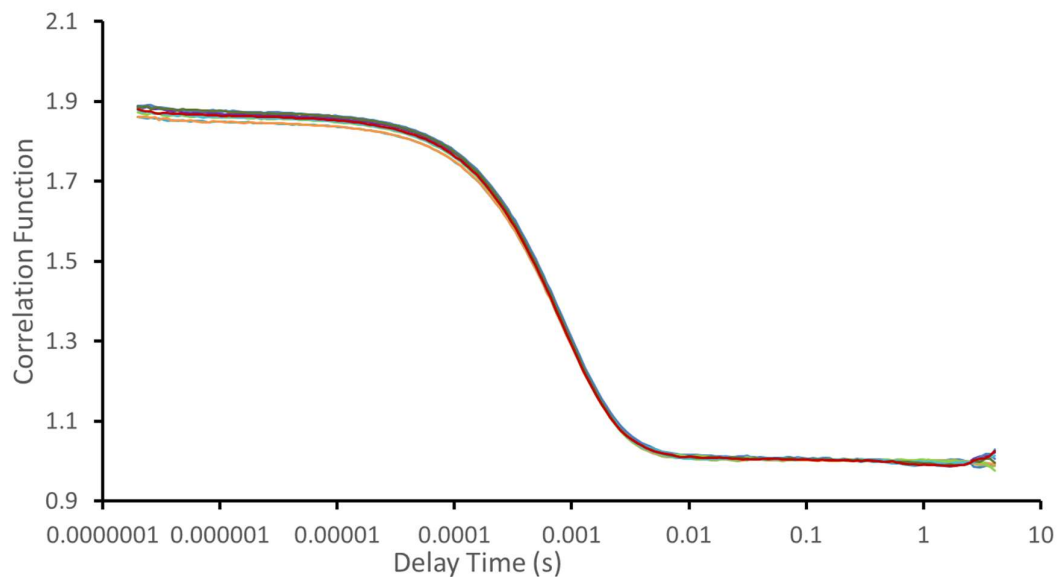


Figure 135 – Correlation function data for 10 DLS runs of compounds **5** at a concentration of 3.00 mM in a solution of EtOH: H<sub>2</sub>O 1:19, after heating to 40 °C and cooling to 25 °C.

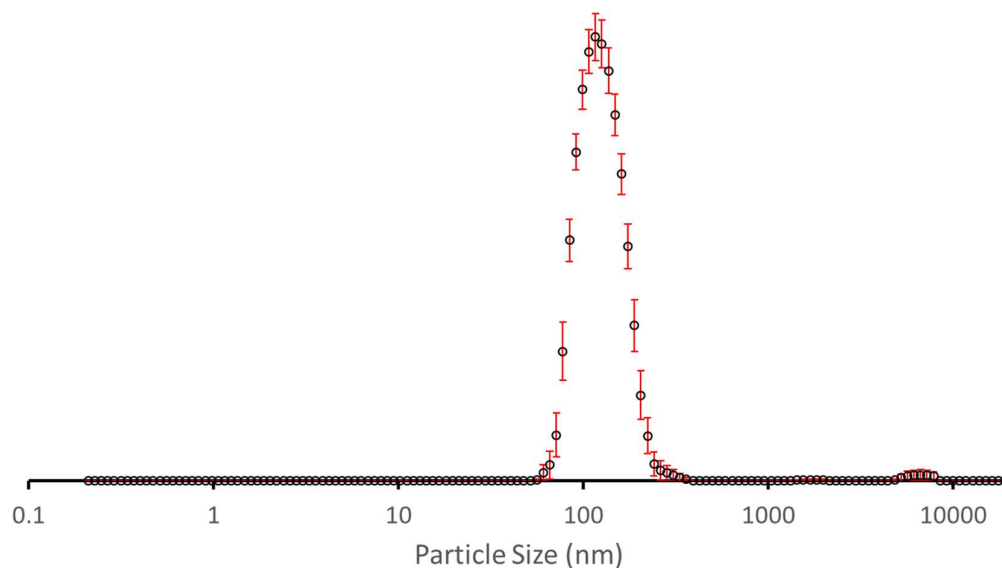


Figure 136 – Average intensity particle size distribution, calculated from 10 DLS runs, of aggregates formed by dissolving compound **5** at a concentration of 0.30 mM in a solution of EtOH: H<sub>2</sub>O 1:19, after heating to 40 °C and cooling to 25 °C.

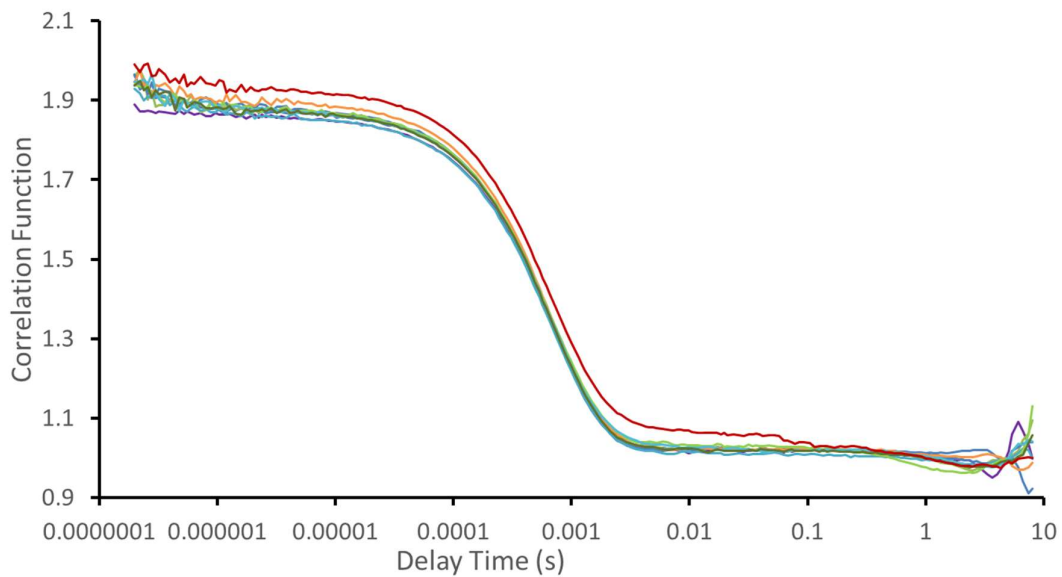


Figure 137 – Correlation function data for 10 DLS runs of compound **5** at a concentration of 0.30 mM in a solution of EtOH: H<sub>2</sub>O 1:19, after heating to 40 °C and cooling to 25 °C.

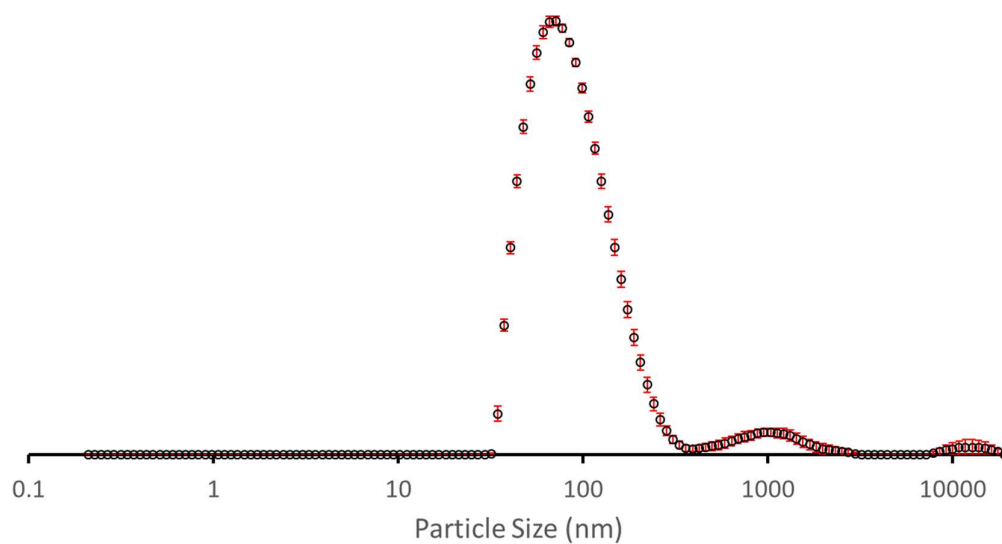


Figure 138 – Average intensity particle size distribution, calculated from 8 DLS runs, of aggregates formed by dissolving compounds **3** and **5** at a concentration of 3.00 mM in a solution of EtOH: H<sub>2</sub>O 1:19, after heating to 40 °C and cooling to 25 °C.

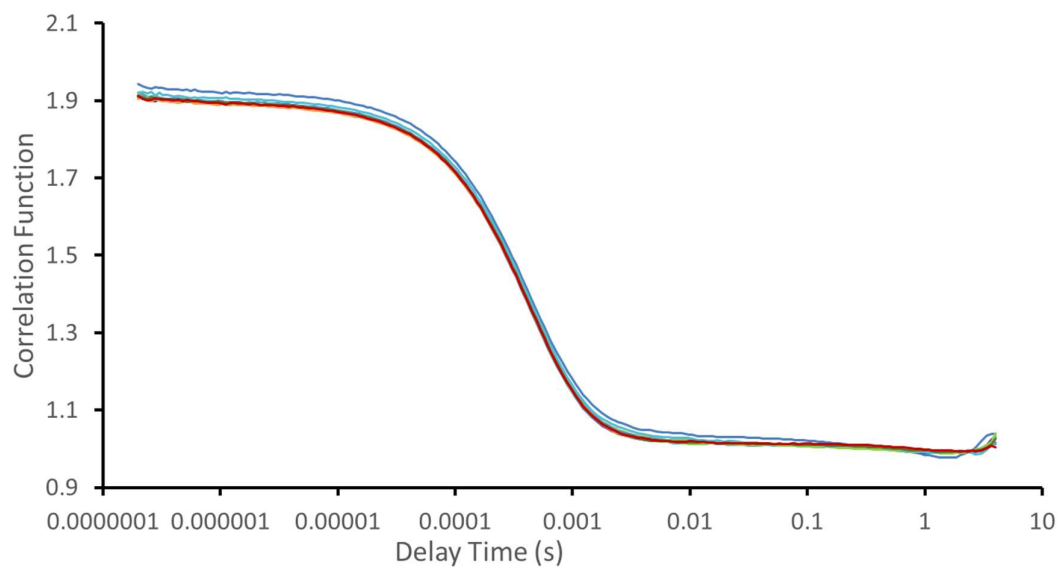


Figure 139 – Correlation function data for 10 DLS runs of a mixture of compounds **3** and **5** at a total concentration of 3.00 mM in a solution of EtOH: H<sub>2</sub>O 1:19, after heating to 40 °C and cooling to 25 °C

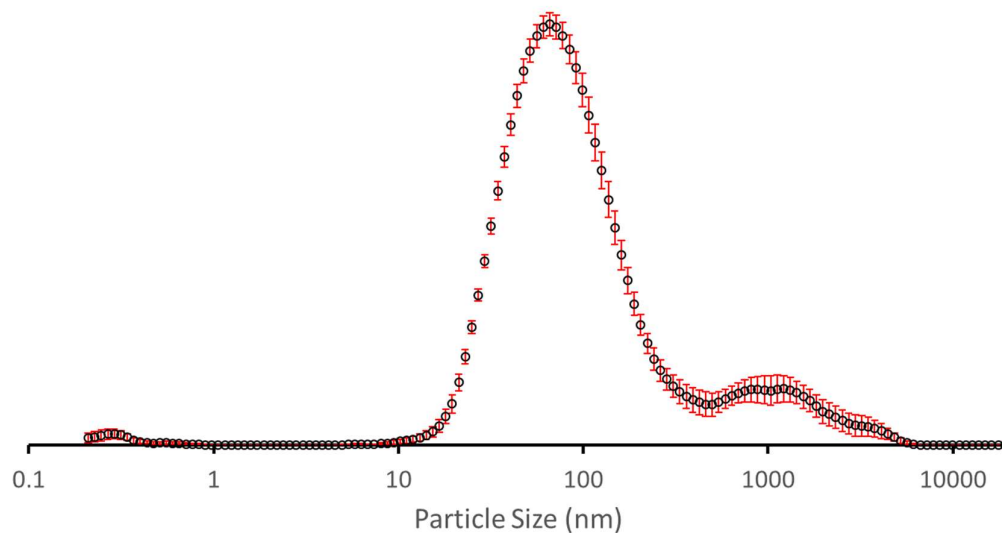


Figure 140 – Average intensity particle size distribution, calculated from 10 DLS runs, of aggregates formed by dissolving compounds **3** and **5** at a concentration of 0.30 mM in a solution of EtOH: H<sub>2</sub>O 1:19, after heating to 40 °C and cooling to 25 °C.

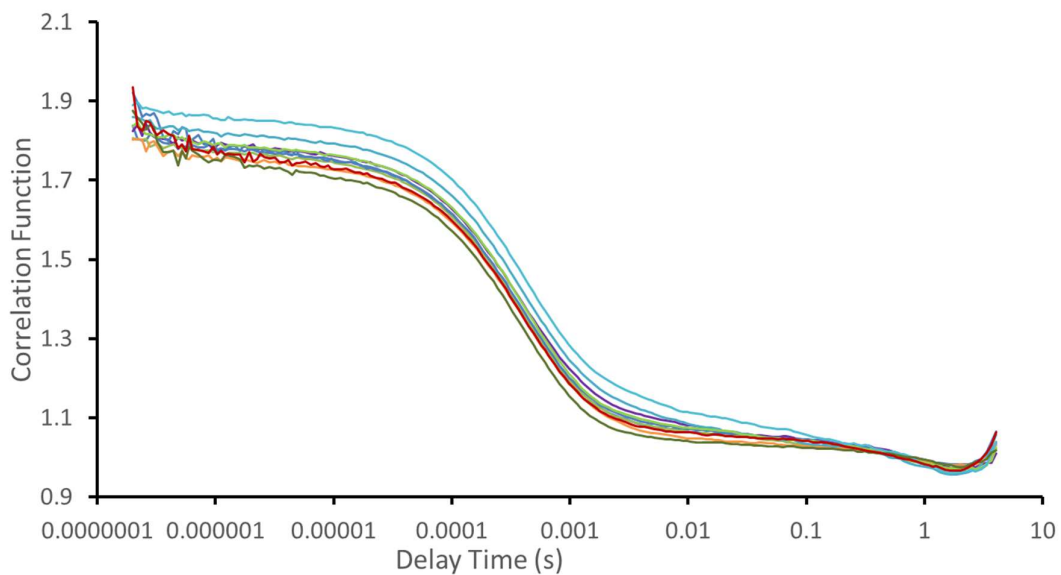


Figure 141 – Correlation function data for 10 DLS runs of a mixture of compounds **3** and **5** at a total concentration of 0.30 mM in a solution of EtOH: H<sub>2</sub>O 1:19, after heating to 40 °C and cooling to 25 °C

Table 19 – Average intensity particle size distribution for compounds **4**, **5** and a mixture of compounds **3** and **5**, calculated from 10 DLS runs at 3.00 mM and 0.3 mM. Samples were prepared in series, with an aliquot of the most concentrated solution undergoing serial dilution and measured after heating to 40 °C and cooling to 25 °C.

Compound	Peak maxima (nm)		PDI (%)	
	3 mM	0.3 mM	3 mM	0.3 mM
<b>3</b>	147.23 (± 7.4)	126.23 (± 2.85)	25.02 (± 0.7)	21.79 (± 0.3)
<b>4</b>	230.97 (± 12.81)	222.45 (± 9.70)	26.13 (± 0.78)	96.25 (± 3.23)
<b>5</b>	189.30 (± 2.96)	128.41 (± 2.66)	23.56 (± 0.41)	14.20 (± 2.52)
<b>3 and 5</b>	94.47 (± 2.0)	88.61 (± 3.9)	24.69 (± 0.4)	25.68 (± 0.8)

### 6.9 Zeta potential

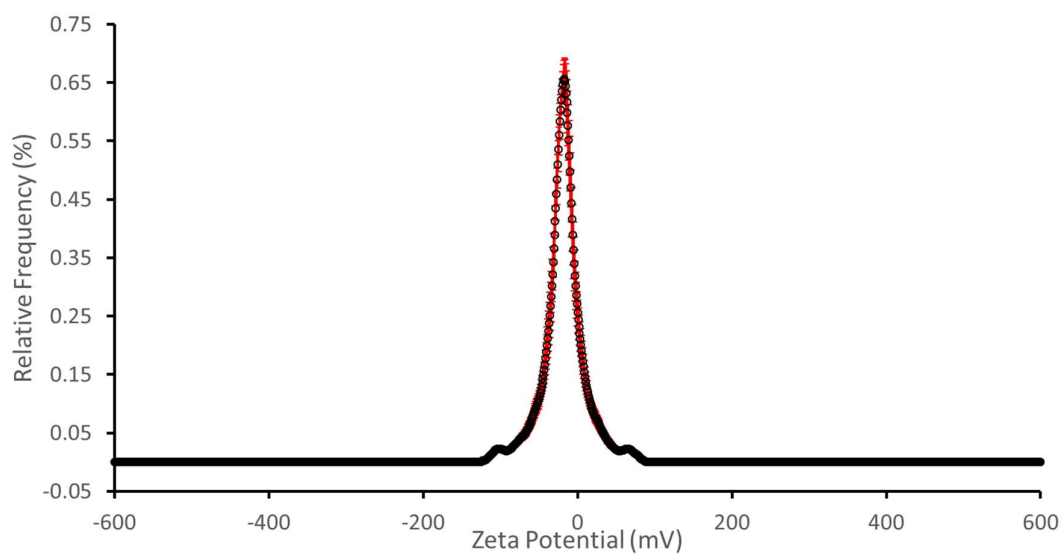


Figure 142 – The average zeta potential distribution calculated using 10 runs for compound **3** (3 mM) in an EtOH: H<sub>2</sub>O (1:19) solution at 298K.

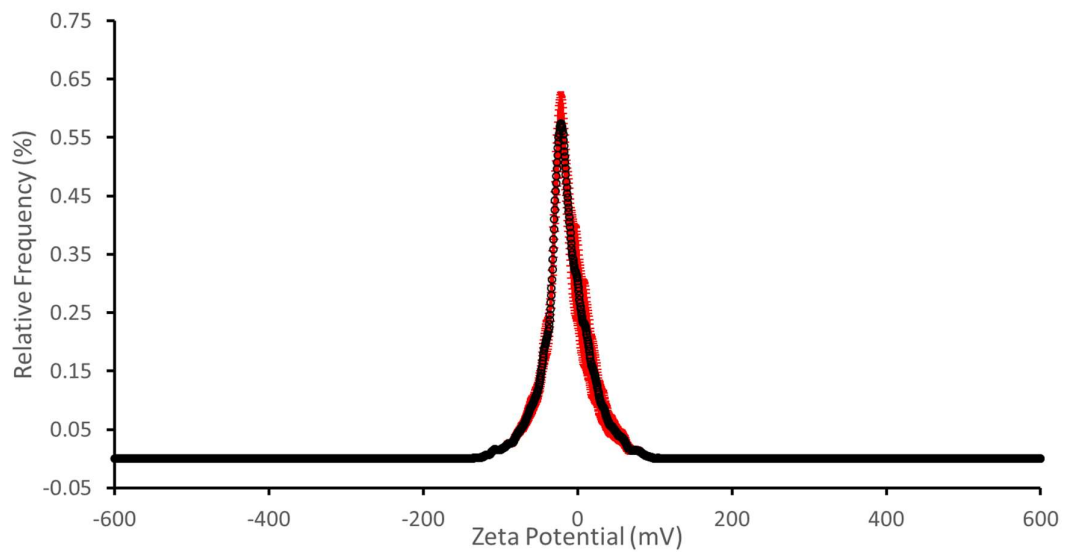


Figure 143 – The average zeta potential distribution calculated using 10 runs for compound 4 (3 mM) in an EtOH: H<sub>2</sub>O (1:19) solution at 298K.

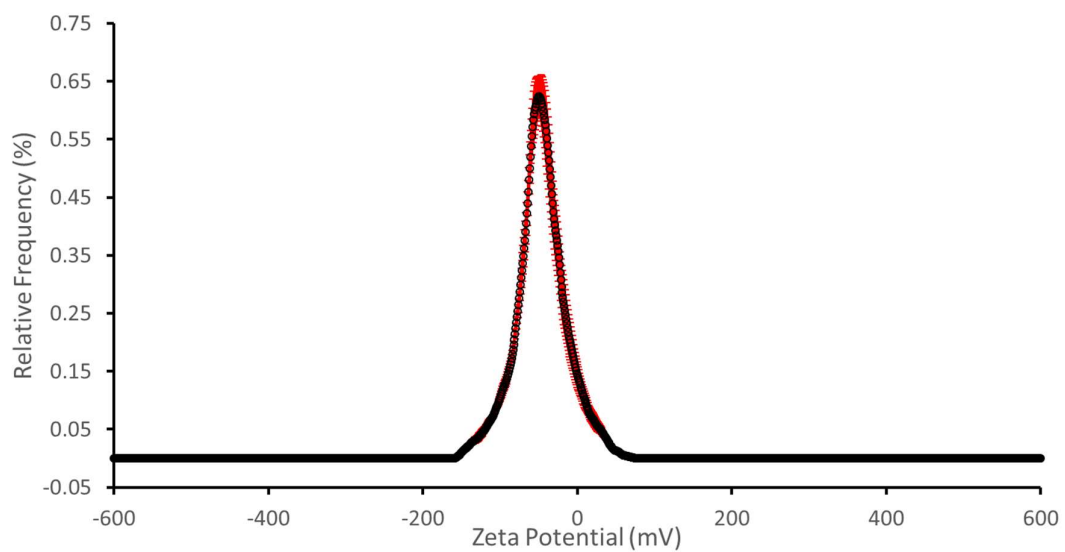


Figure 144 – The average zeta potential distribution calculated using 10 runs for compound 5 (3 mM) in an EtOH: H<sub>2</sub>O (1:19) solution at 298K.

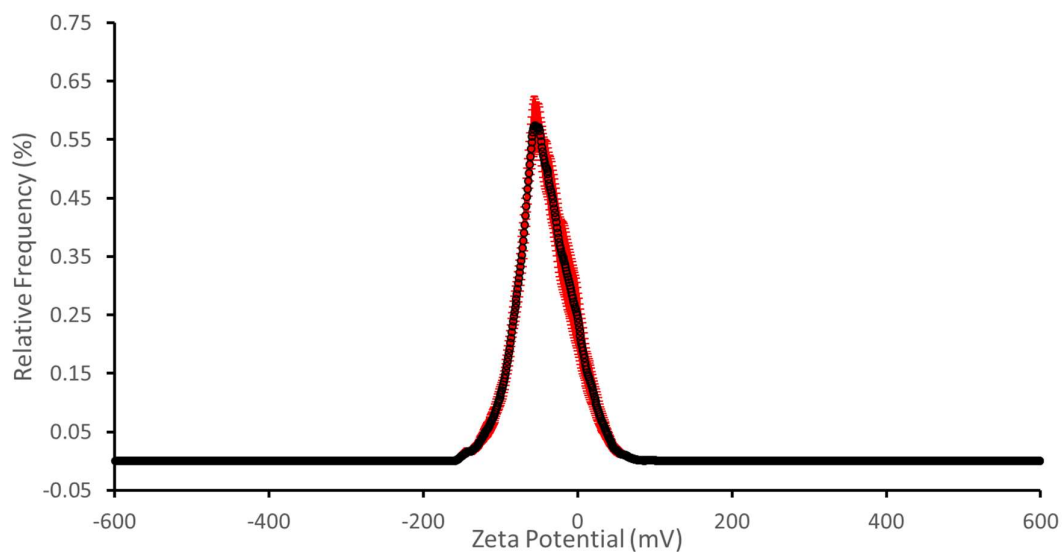


Figure 145 – The average zeta potential distribution calculated using 10 runs for a 1:1 mixture of compound **3** and **5** (total 3 mM) in an EtOH: H<sub>2</sub>O (1:19) solution at 298K.

Table 20 – The average zeta potential distribution calculated using 10 runs for compounds **4**, **5** and a mixture of **3** and **5** at 3 mM, in an EtOH: H<sub>2</sub>O (1:19) solution at 298K.

Compound	Mean Zeta Potential (mV)
<b>3</b>	-14.40
<b>4</b>	- 32.05
<b>5</b>	- 53.75
<b>3 and 5</b>	- 43.00

## 6.10 Critical micelle concentration

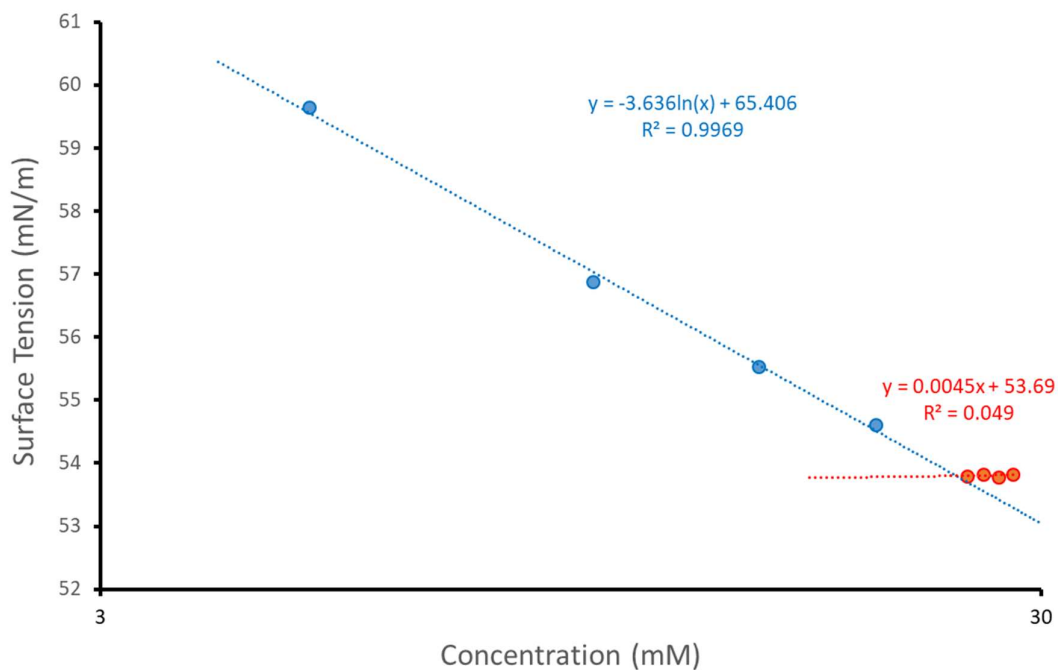


Figure 146 – Calculation of CMC for compound **3** in an EtOH: H<sub>2</sub>O 1:19 mixture using surface tension measurements.

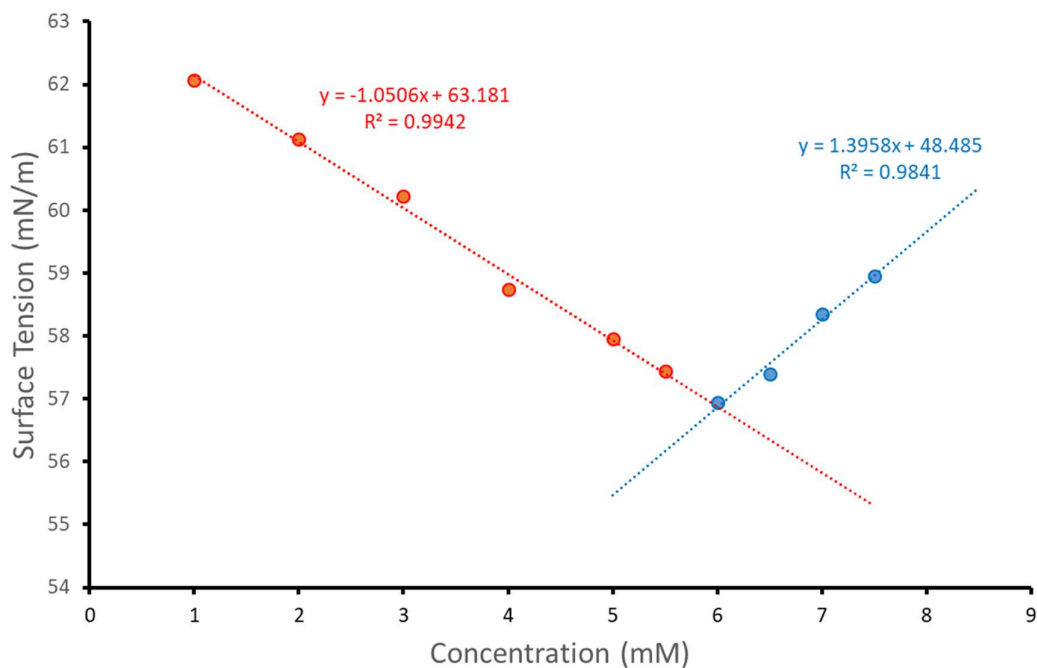


Figure 147 – Calculation of CMC for compound **4** in an EtOH: H<sub>2</sub>O 1:19 mixture using surface tension measurements.

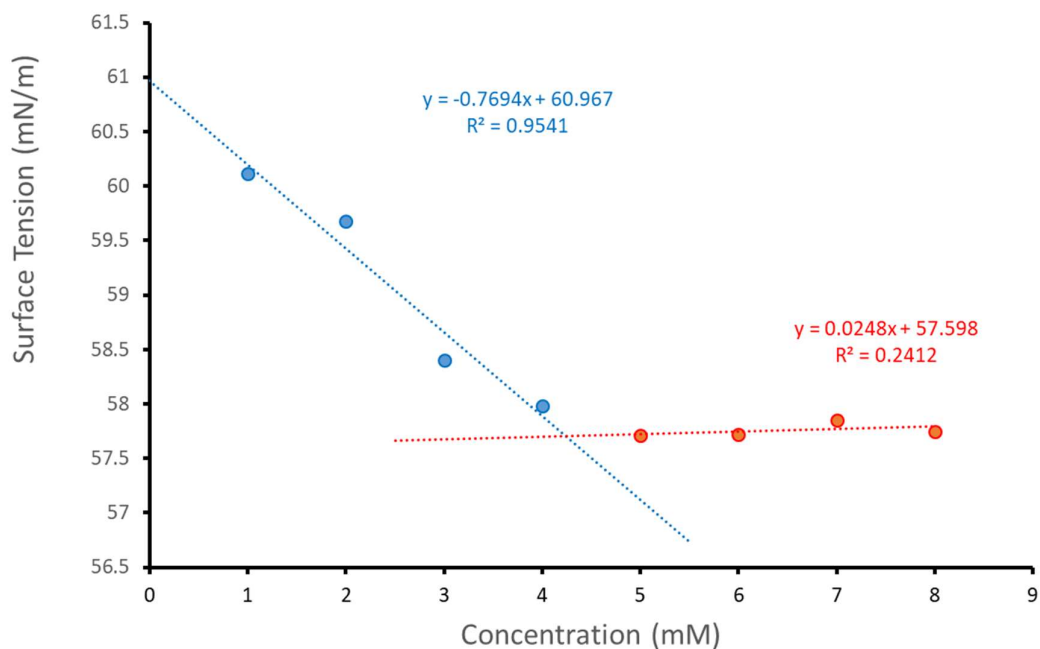


Figure 148 – Calculation of CMC for compound **5** in an EtOH: H<sub>2</sub>O 1:19 mixture using surface tension measurements.

Table 21 – Overview of CMC and surface tension (obtained at CMC) measurements for compounds **3-5** at 25°C

Compound	CMC (mM)	Surface tension at CMC (mN/m)
<b>3</b>	24.98	53.70
<b>4</b>	6.00	56.87
<b>5</b>	4.24	57.70

## 6.11 Low level in-silico modelling

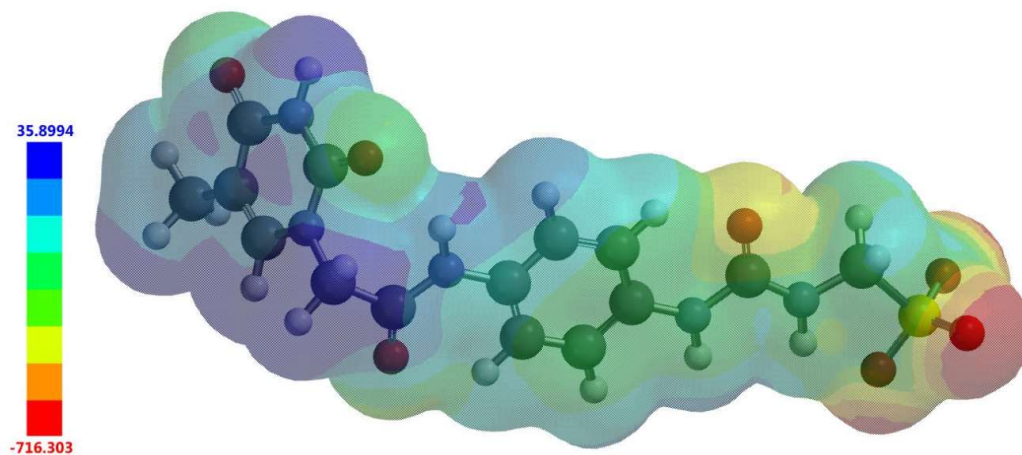


Figure 149 – Electrostatic potential map calculated for the anionic component of **3**.  $E_{\max}$  and  $E_{\min}$  values depicted in the Figure legends are given in kJ/mol.

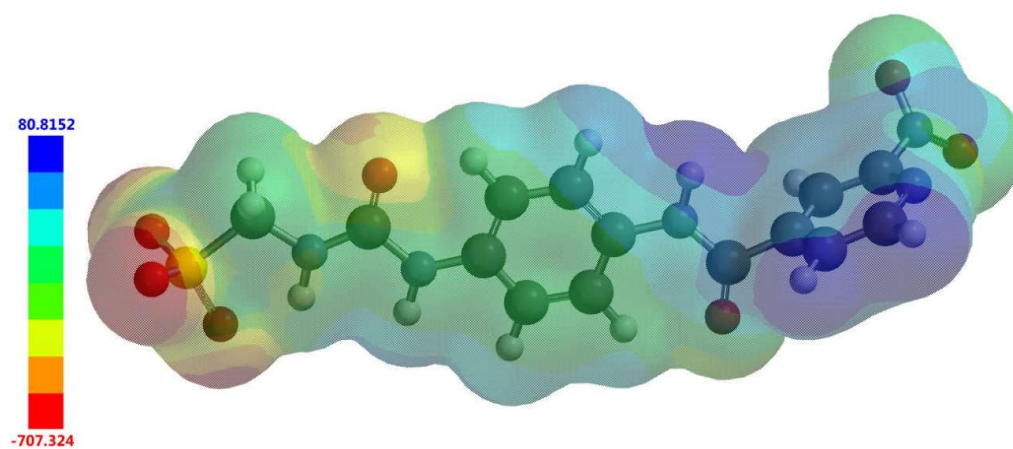


Figure 150 – Electrostatic potential map calculated for the anionic component of **4**.  $E_{\max}$  and  $E_{\min}$  values depicted in the Figure legends are given in kJ/mol.

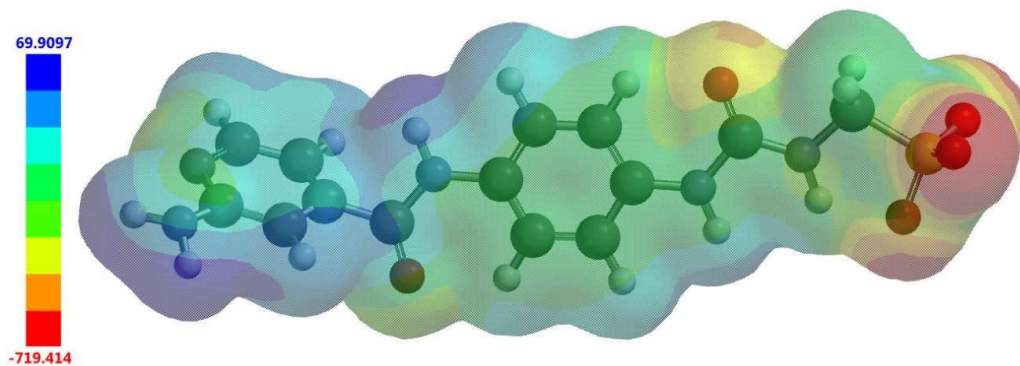


Figure 151 – Electrostatic potential map calculated for the anionic component of **5**.  $E_{\max}$  and  $E_{\min}$  values depicted in the Figure legends are given in kJ/mol.

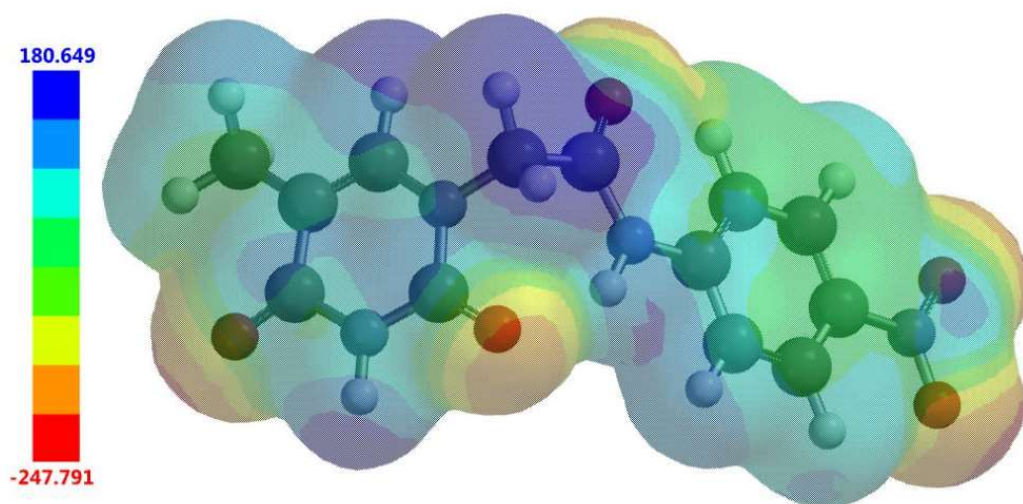


Figure 152 – Electrostatic potential map calculated for compound **6**.  $E_{\max}$  and  $E_{\min}$  values depicted in the Figure legends are given in kJ/mol.

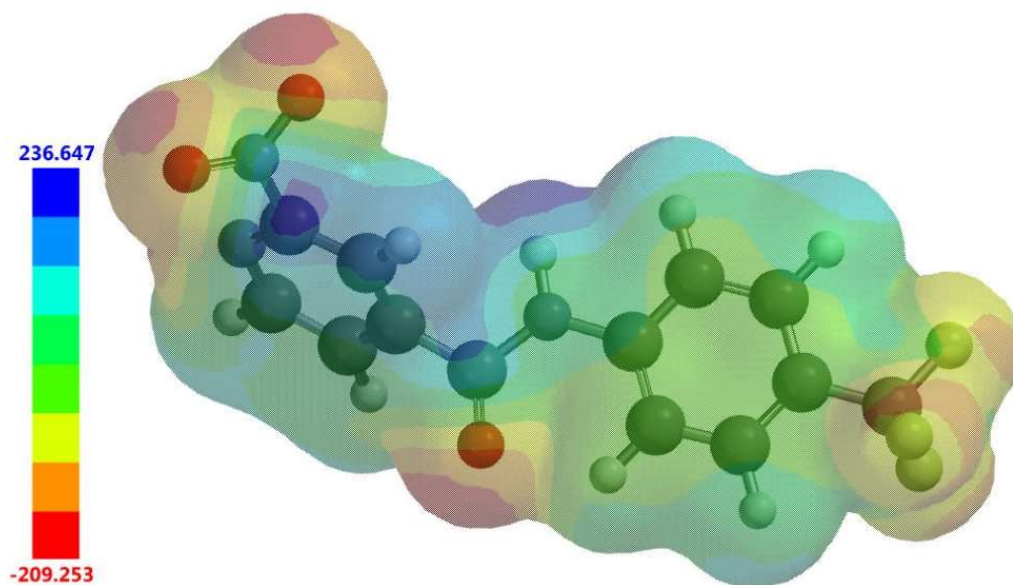


Figure 153 – Electrostatic potential map calculated for compound **7**.  $E_{\max}$  and  $E_{\min}$  values depicted in the Figure legends are given in kJ/mol.

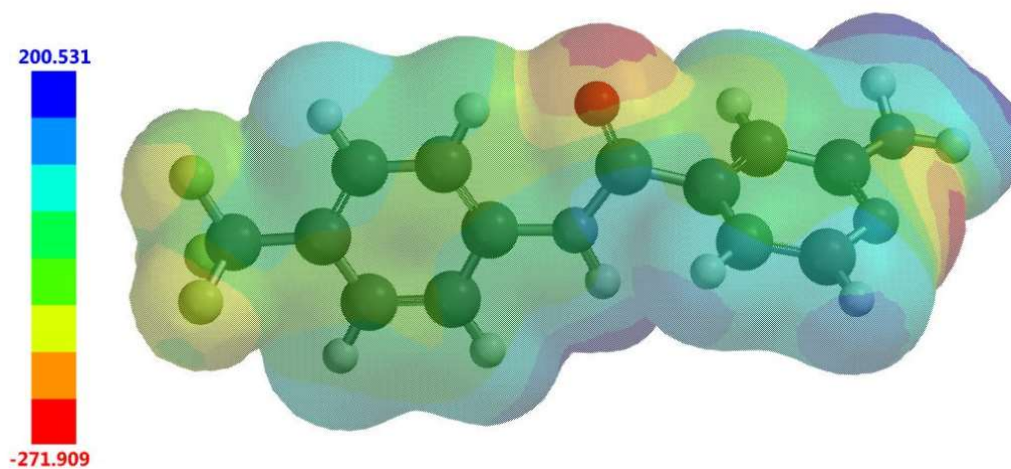


Figure 154 – Electrostatic potential map calculated for compound **8**.  $E_{\max}$  and  $E_{\min}$  values depicted in the Figure legends are given in kJ/mol.

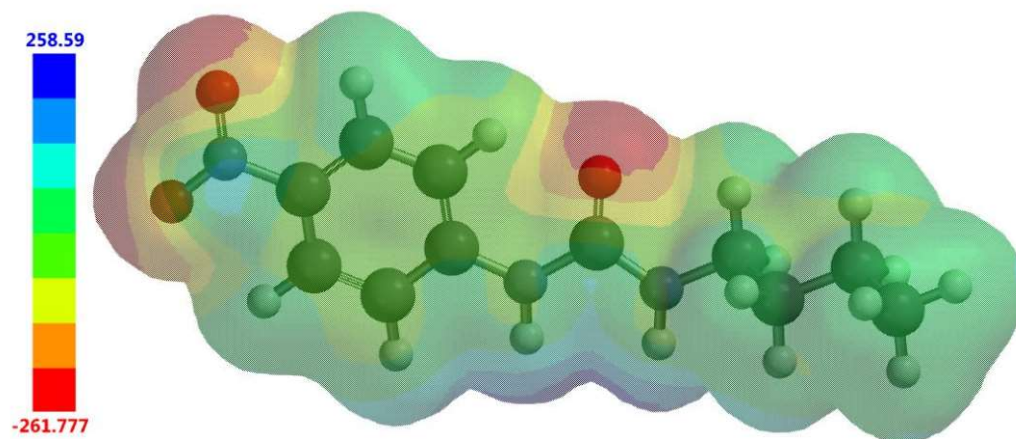


Figure 155 – Electrostatic potential map calculated for compound **9**.  $E_{\max}$  and  $E_{\min}$  values depicted in the Figure legends are given in kJ/mol.

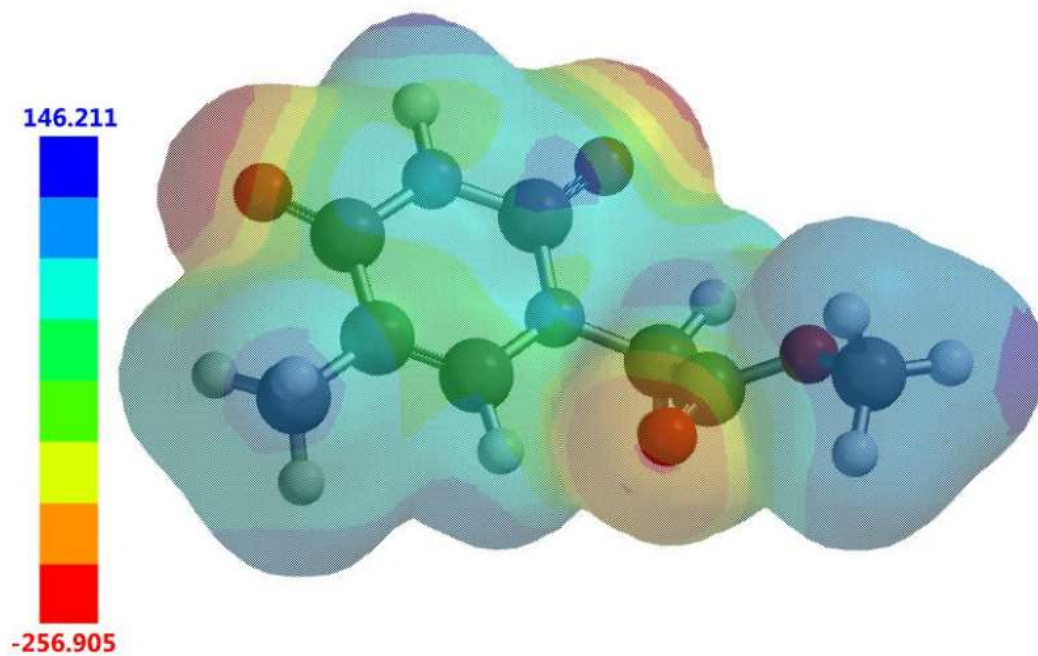


Figure 156 – Electrostatic potential map calculated for compound **10**.  $E_{\max}$  and  $E_{\min}$  values depicted in the Figure legends are given in kJ/mol.

Table 22 – Electrostatic potential calculated for compounds **3-10**.

Compound	$E_{\max}$ (kJ/mol)	$E_{\min}$ (kJ/mol)
<b>3</b>	35.8994	-716.3030
<b>4</b>	80.8152	-707.3240
<b>5</b>	69.9097	-719.4140
<b>6</b>	180.6490	-247.7910
<b>7</b>	236.6470	-209.2530
<b>8</b>	200.5310	-271.9090
<b>9</b>	258.5900	-261.7770
<b>10</b>	146.2110	-256.9050